Characterization of a pig model of Usher syndrome

von Sophia Grotz

Inaugural-Dissertation zur Erlangung der Doktorwürde
der Tierärztlichen Fakultät der Ludwig-Maximilians-Universität München

Characterization of a pig model of Usher syndrome

von Sophia Grotz

aus Schongau

München 2021

Aus dem Veterinärwissenschaftlichen Department der Tierärztlichen
Fakultät der Ludwig-Maximilians-Universität München

Lehrstuhl für Molekulare Tierzucht und Biotechnologie

Arbeit angefertigt unter der Leitung von: Univ.-Prof. Dr. Nikolai Klymiuk

Gedruckt mit Genehmigung der Tierärztlichen Fakultät

der Ludwig-Maximilians-Universität München

Dekan: Univ.-Prof. Dr. Reinhard K. Straubinger, Ph.D.

Berichterstatter: Univ.-Prof. Dr. Nikolai Klymiuk

Korreferent: Univ.-Prof. Dr. Laurent Frantz

Tag der Promotion: 17.07.2021

Für meine Berabeira Oma

TABLE OF CONTENTS

INDEX OF ABBREVIATIONS

AAV	Adeno-associated virus
ABR	Auditory brainstem response
aq. bidest	Bidistilled water
aq. dest.	Distilled water
ASO	Antisense oligonucleotide
BAC	Bacterial artificial chromosome
bp	Base pair
Ca^{2+}	Calcium
Cas	CRISPR associated protein
CC	Coiled-coil region
CCi	Connecting cilium
cDNA	Complementary DNA
CiMM	Center for Innovative Medical Models
CP	Calyceal process
CRISPR	Clustered regularly interspaced short palindromic repeats
dB	Decibel
DFNB	Nonsyndromic autosomal recessive deafness
DNA	Deoxyribonucleic acid
DNase	Deoxyribonuclease
dATP	Deoxyadenosine triphosphate
dCTP	Deoxycytidine triphosphate
dGTP	Deoxyguanosine triphosphate
dNTP	Deoxynucleoside triphosphate
dTTP	Deoxythymidine triphosphate
DTT	Dithiothreitol
EDTA	Ethylenediaminetetraacetic acid
eGFP	Enhanced green fluorescent protein
ET	Embryo transfer
EtOH	Ethanol
ERG	Electroretinography
ffERG	Full field electroretinography

gDNA	Genomic DNA
gRNA	Guide RNA
h	Hour
HCL	Hydrochloric acid
IAA	Iodoacetic acid
IAPG	Institute of Animal Physiology and Genetics
IHC	Inner hair cells
i.m.	Intramuscular
i.v.	Intravenous
IS	Inner segment
ISCEV	International Society for Clinical Electrophysiology of Vision
kb	Kilobase
KD	Knockdown
L	Liter
LMU	Ludwig Maximilian University of Munich
lx	Lux
M	Mole
mfERG	Multifocal electroretinography
mg	Milligram
min	Minute
mL	Milliliter
mM	Millimolar
mRNA	Messenger RNA
mv	Mean value
n.a.	Not analyzed
n.d.	Not determined
NaCl	Sodium chloride
$NaIO_3$	Sodium iodate
NaOH	Sodium hydroxide
NC	Negative control
nm	Nanometer
nt	Nucleotide
OCT	Optical coherence tomography

OHC	Outer hair cells
ONL	Outer nuclear layer
OS	Outer segment
PCR	Polymerase chain reaction
PR	Photoreceptor
PST	Proline-serine-threonine rich region
RHO	Rhodopsin
RNA	Ribonucleic acid
RNase	Ribonuclease
RP	Retinitis pigmentosa
RPE	Retinal pigment epithelium
rpm	Revolutions per minute
s	Second
SCNT	Somatic cell nuclear transfer
sd	Standard deviation
SD-OCT	Spectral domain optical coherence tomography
se	Standard error
SEM	Scanning electron microscopy
SNP	Single nucleotide polymorphism
SPL	Sound pressure level
STGD	Stargardt disease
TEM	Transmission electron microscopy
TRID	Translational read-through inducing drug
TRIS	Tris (hydroxymethyl)-aminomethane
U	Unit
USH	Usher syndrome
USH1	Usher syndrome type 1
USH2	Usher syndrome type 2
USH3	Usher syndrome type 3
UTLD	Upper tip link density
UV	Ultraviolet
WT	Wild type
µL	Microliter

I. INTRODUCTION

Usher syndrome (USH) is the most common form of inherited deaf-blindness. It is divided into three groups, depending on severity of hearing loss, beginning of vision loss, and existence of vestibular dysfunction. To date, 13 genes have been confirmed to cause USH (reviewed in TOMS et al., 2020a). In the subgroup USH1C, the scaffold protein harmonin is defective, causing onset of retinitis pigmentosa in the first decade of life, congenital deafness, and vestibular hypofunction (REINERS et al., 2005). Pathogenesis of the audiovestibular phenotype is relatively well understood, here, harmonin plays an important role in mechanoelectrical transduction (MICHALSKI et al., 2009). Deafness can also be treated successfully with cochlear implants (JATANA et al., 2013). Less knowledge exists about the pathophysiology of vision loss, due to the fact that USH mouse models exhibit - if any - only a mild retinal phenotype, as there are structural differences in murine and human photoreceptor cells. Furthermore, no therapy is available for retinitis pigmentosa so far (reviewed in EL-AMRAOUI & PETIT, 2014). As human and porcine eyes have a similar morphology, pigs are often used in vision research (reviewed in SANCHEZ et al., 2011). Hence, an USH1C pig model was generated using CRISPR/Cas technology at the Chair of Molecular Animal Breeding and Biotechnology, LMU. The porcine exon 2 and surrounding regions were replaced with the orthologous human fragment carrying the R31X mutation, which leads to a premature translational stop that results in lack of harmonin protein.

I started working on the USH1C pig project when first founder animals had been generated by somatic cell nuclear transfer. Aim of this thesis was the expansion of animals by setting up a breeding herd and to characterize the phenotype and genotype of this novel USH1C pig model. Molecular biological analyses were performed to see whether pigs correctly express USH1C transcripts including the humanized exon 2 and the stop mutation. Moreover, visual capacity, hearing ability and vestibular function of USH1C pigs were assessed to compare the pigs' phenotype to the phenotype found in USH patients. Therefore, I designed and conducted behavioral tests. USH1C and wildtype pigs were evaluated in two different obstacle courses to test their vision. Additionally, pigs were clinically examined with ERG, OCT, and ABR with collaboration partners.

Large parts of this thesis were integrated in a manuscript describing the generation and the phenotypical characterization of the USH1C pig model (Grotz & Schäfer et al., submitted).

II. LITERATURE REVIEW

1. Usher syndrome

Albrecht von Graefe was the first to describe the coincidence of blind- and deafness in 1858 (V. GRAEFE, 1858). The hereditary nature of this syndrome was discovered by Charles Usher in 1914 (USHER, 1914). USH is inherited in an autosomal recessive manner. The worldwide prevalence is estimated between 4 -17 per 100.000 people (reviewed in TOMS et al., 2020a).

Dependent on disease onset, severity of hearing loss, and occurrence of vestibular dysfunction, USH is divided into three clinical groups (Table 1). With prepubertal onset of retinitis pigmentosa (RP), deafness from birth on, and vestibular areflexia, USH1 is the most severe subgroup.

Table 1: Classification of Usher syndrome based on clinical symptoms. (Adapted by TOMS et al., 2020a).

	Vision loss	**Hearing loss**	**Vestibular dysfunction**
USH1	Onset of RP in first decade of life	Severe to profound deafness, congenital	Vestibular hypofunction, delayed motor development
USH2	Onset of RP in second decade of life	Moderate to severe, congenital	No vestibular dysfunction
USH3	Variable, onset of RP normally in second decade	Variable, progressive, post-lingual onset	Variable, abnormalities in 50% of patients

1.1. Genetics of Usher Syndrome

So far, mutations at 13 different loci (Table 2) have been confirmed to cause USH, nine are causative for USH1, three for USH2 and one for USH3 (reviewed in TOMS et al., 2020a). Next generation sequencing replaced Sanger sequencing as method of choice for molecular diagnosis, identifying up to 80% of mutated alleles by gene panel testing (APARISI et al., 2014; KRAWITZ et al., 2014). Between 25% and 44% of all USH patients suffer from USH1, mostly USH1B; 56% to 75% are affected by USH2, with USH2A being the most frequent USH

subtype and only about 2% of all cases are associated with USH3, which can be mainly found in Finnish USH patients (reviewed in REINERS et al., 2006).

Table 2: USH loci, genes and predicted protein functions.
(Adapted by TOMS et al., 2015).

Locus	Gene	Chromosome	Protein	Function
USH1B	*MYO7A*	11q13.5	Myosin VIIa	Motor protein
USH1C	*USH1C*	11p15.1	Harmonin	PDZ scaffold protein
USH1D	*CDH23*	10q21-q22	Cadherin 23	Cell adhesion protein
USH1E	Unknown	21q21	Unknown	Unknown
USH1F	*PCDH15*	10q21-q22	Protocadherin 15	Cell adhesion protein
USH1G	*USH1G*	17q24-q25	SANS	Scaffold protein
USH1H	Unknown	15q22-23	Unknown	Unknown
USH1J	*CIB2*	15q23-q25.1	CIB2	Ca^{2+} and integrin binding protein
USH1K	Unknown	10p11.21-q21.1	Unknown	Unknown
USH2A	*USH2A*	1q41	Usherin	Cell adhesion protein
USH2C	*GPR98*	5q14-q21	GRP81 / VLGR1 / MASS1	G-protein coupled receptor
USH2D	*WHRN*	9q32-q34	Whirlin	PDZ scaffold protein
USH3A	*CLRN1*	3q21-q25	Clarin-1	Transmembrane protein

USH1C is caused by mutations in the harmonin encoding *USH1C* gene. The gene consists of 29 exons. For the human gene, the three main splice variants a, b, and c (Figure 1) have been described, but according to GenBank by NCBI, numerous additional transcripts might exist. Functional segments have been defined in the harmonin protein, including the characteristic harmonin-N domain as well as

several PDZ, coiled-coil (CC), and proline-serine-threonine rich (PST) domains (VERPY et al., 2000; NCBI, Conserved Domain Database). As all those domains take part in protein – protein interactions, the function of harmonin has been deciphered as a scaffold protein (reviewed in REINERS et al., 2006). *USH1C* transcripts and the protein harmonin are expressed in numerous organs, albeit at relatively low levels (SCANLAN et al., 1999; NCBI, GenBank).

Multiple defects have been identified in the human *USH1C* gene, causing either USH or DFNB18, a nonsyndromic autosomal recessive deafness (OMIM JOHNS HOPKINS UNIVERSITY; AHMED et al., 2002). Most of the mutations result in a loss of function of harmonin due to frameshift, nonsense, and splice site mutations, leading to the typical USH1C clinical manifestation. Some leaky splice site and missense mutations, however, have been associated with DFNB18 (reviewed in MATHUR & YANG, 2015; TOMS et al., 2020a).

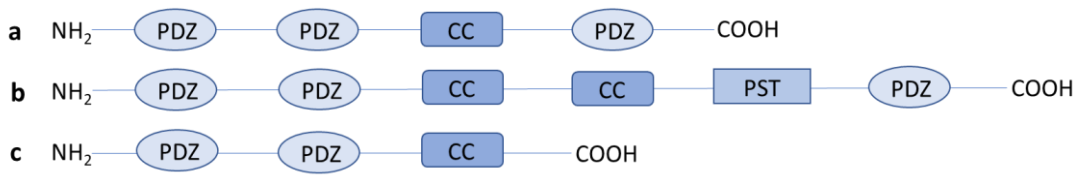

Figure 1: Harmonin isoforms. The abundance and localization of the characteristic protein domains in the distinct harmonin isoforms are shown according to VERPY et al. (2000).

1.2. Pathophysiology

1.2.1. Hair cells

Hair cells in the inner ear are responsible for mechanoelectrical transduction by transforming mechanical stimuli of sound or head movement into electrical responses, which is the basis of the sense of hearing and balance. In the organ of Corti, they are arranged into one row of inner hair cells (IHC) and three rows of outer hair cells (OHC). Hair cells comprise so-called hair bundles on their apex (Figure 2a). Mature hair bundles consist of rows of stereocilia in different lengths, which are, inter alia, connected by tip links. Those are anchored at the longer stereocilium at the upper tip link density (UTLD) and at the shorter stereocilium at the lower tip link density. Deflection of cilia on hair cells leads to the opening

of ion channels, resulting in a depolarization of the hair cell and to following signal transmission to the brain (reviewed in LEMASURIER & GILLESPIE, 2005; reviewed in GILLESPIE & MÜLLER, 2009; reviewed in MATHUR & YANG, 2015).

At the apex of hair cells, USH proteins harmonin, SANS, and myosin VIIA can be found in the UTLD; cadherin 23 and protocadherin 15 are localized in tip links themselves (reviewed in COSGROVE & ZALLOCCHI, 2014). Based on examinations in animal models, defective harmonin impairs mechanoelectrical transduction. Independent of their respective mutation, mouse models are entirely deaf (see 1.5.1.). USH1C$^{dfcr\text{-}2J/dfcr\text{-}2J}$ mice showed reduced transduction currents and slower adaptation in response to hair bundle deflections (MICHALSKI et al., 2009). Furthermore, UTLD were not detectable in USH1C$^{dfcr/dfcr}$ mice (GRILLET et al., 2009). Harmonin-PDZ2$^{AAA/AAA}$ mice exhibit disturbed hair bundle morphogenesis and abnormally localized harmonin (GRILLET et al., 2009).

In addition to their role in mechanistic sensing, USH proteins harmonin, cadherin 23, clarin-1, protocadherin 15, usherin, VLGR1, and whirlin may be relevant for signal transduction, as they are also localized in the hair cells' synapses (reviewed in MATHUR & YANG, 2015). Over its PDZ domain, harmonin interacts with $Ca_v1.3Ca^{2+}$ channels, which regulate calcium influx and exocytosis at the synapses of inner hair cells (GREGORY et al., 2011). USH1C$^{dfcr/dfcr}$ mice expressing harmonin that cannot bind to $Ca_v1.3Ca^{2+}$ channels showed hampered Ca^{2+} release and altered voltage-dependent facilitation (GREGORY et al., 2013).

1.2.2. Retina

In contrast to the detailed understanding of USH protein function in the ear, much less is known about USH pathogenesis in the eye. Main reason for this is the lacking or, at best, mild retinal phenotype in USH mouse models (see 1.5.1.). In human photoreceptors (PRs) (Figure 2b), USH proteins can be found in the outer segment (OS), the connecting cilium (CCi), the periciliary membrane complex, the calyceal processes (CPs), the inner segment (IS), and the synapse (reviewed in MATHUR & YANG, 2015). Best studied is the role of myosin VIIA, which is crucial for transport of melanosomes, phagosomes, and enzymes in PRs as well as in retinal pigment epithelium cells (RPE) (LIU et al., 1998; GIBBS et al., 2003; LOPES et al., 2011). Harmonin has been detected in the OS, CP, and synapse of

PRs, but not in RPE (reviewed in MATHUR & YANG, 2015). Studies with *USH1C* zebrafish morphants show that depletion of harmonin in Müller glial cells leads to a reduced function of PR ribbon synapses (PHILLIPS et al., 2011). However, the general function of harmonin is still unclear.

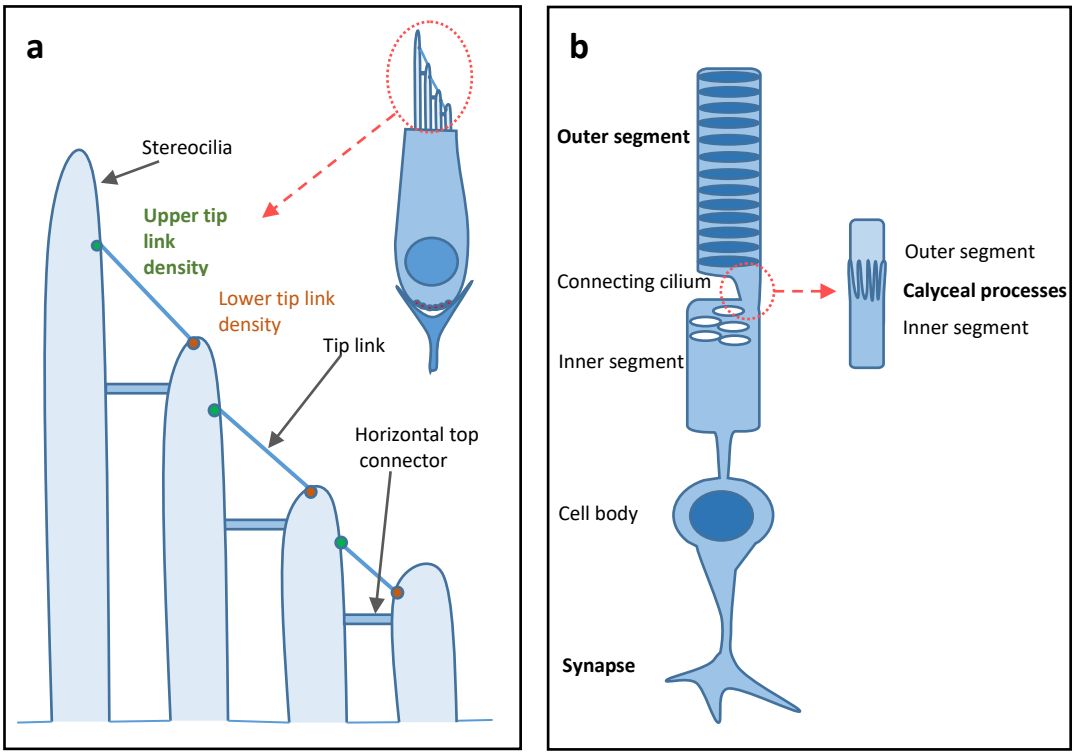

Figure 2: Schematic illustrations of a hair cell, enlarged a mature hair bundle (a) and a photoreceptor cell with enlarged CPs (b). Bold captions show localization of harmonin (adapted by MATHUR & YANG, 2015).

1.3. Clinical phenotype

1.3.1. Audiovestibular phenotype

All USH patients are first diagnosed with audiological symptoms: congenital deafness in case of USH1, innate moderate to severe hearing loss in USH2 and a progressive hearing loss in USH3. USH1 patients have a pure-tone average of 100 dB or greater, USH2 patients between 40 and 90 dB (EDWARDS et al., 1998). USH1 and some USH3 patients also show vestibular dysfunction. USH1 children show delayed childhood motor milestones and usually do not walk before an age of 22 months, later their gait is often shaky. Furthermore, some USH patients manifest a nystagmus (MOLLER et al., 1989).

1.3.2. Ocular phenotype

Although USH patients may not show symptoms of vision loss at birth, changes in electroretinography can be detected already at an age of 17 months (FLORES-GUEVARA et al., 2009). Therefore, USH should be considered in children showing hearing deficits and additionally, eye examination should be included in etiological diagnosis of bilateral sensorineural hearing loss (reviewed in TOMS et al., 2020a). Eventually, retinitis pigmentosa develops in all USH subgroups. The first clinical symptom of vision loss is usually night blindness, followed by loss of peripheral vision resulting in tunnel vision due to rod degeneration. Later, degeneration of cones leads to loss of color and central vision (HARTONG et al., 2006). Onset of RP differs between USH types, in USH1 it normally begins in the first decade and in USH2 and USH3 in the second decade of life (reviewed in TOMS et al., 2020a). Patients have individual rates of degree and progression of visual acuity loss, but total vision loss before 60 years of age is not common (SADEGHI et al., 2006). In two different studies, 12% - 17% in USH1 and USH2 patients have been designated as legally blind (EDWARDS et al., 1998; SADEGHI et al., 2006). 59% of USH1 patients and 67% of USH2 patients had at least in one eye a concentric central visual field greater than 20°. 51% of USH1 patients and 71% of USH2 patients had a visual acuity of 0.5 (20/40) or better (EDWARDS et al., 1998).

Fundus assessment reveals narrowing of arterial vessels, abnormal retinal pigmentation with bone spicules, and optic disc pallor. Cataract and macular edema can also be seen in patients. Electroretinography (ERG, see 3.1.1.) measurements display delay and reduction of a- and b-wave amplitudes. Optical coherence tomography (OCT, see 3.1.2.) shows thinning of the outer nuclear layer (ONL), the layer where nuclei of PRs can be found (reviewed in HARTONG et al., 2006; SEELIGER et al., 2009; reviewed in TOMS et al., 2015; reviewed in TOMS et al., 2020a).

Furthermore, the psychological component of living with USH needs consideration. USH patients report difficulties in everyday life like fear of tripping over things, communication with others, acceptance in society, career choice, and of course worry of symptom progression (LONBORG-MOLLER et al., 2020; ROBOREL DE CLIMENS et al., 2020).

1.4. Therapy

1.4.1. Hearing loss

Cochlear implants are used to treat deafness in USH1 and USH3 patients. Most children treated with those implants develop open-set speech perception and learn to communicate orally (PIETOLA et al., 2012; JATANA et al., 2013). USH2 patients benefit from hearing aids, as they do have residual hearing (reviewed in TOMS et al., 2015).

Novel therapeutic approaches are intensively tested in animal models. Neonatal injections of adeno-associated virus (AAV) vectors in the inner ear have been able to improve hearing and vestibular function in USH1C, USH1G, USH2D, and USH3 mice models (EMPTOZ et al., 2017; ISGRIG et al., 2017; PAN et al., 2017; GYÖRGY et al., 2019). However, it has to be considered that the inner ears of mice are still immature at time of birth, whereas human hearing is already mature at birth. Therefore, treatment in humans might be necessary in the fetal stage (HASTINGS & BRIGANDE, 2020; reviewed in TOMS et al., 2020a). Furthermore, prenatal treatment with antisense oligonucleotides, which influence pre-mRNA splicing by binding RNA, ameliorated hearing and vestibular function in USH1C mice (WANG et al., 2020).

1.4.2. Vision loss

At the moment, no cure is available for RP, but many treatment options are being tested. As the eye has an immune privileged status, is easily accessible, and the vision loss in USH is not congenital but developing over time, allowing enough time for intervention, it is an interesting target for therapies (reviewed in TOMS et al., 2020a).

Gene therapy via subretinal injections of AAVs or lentiviral based vectors was able to restore correct expression of prior dysfunctional USH genes in USH1B, USH2D, and USH3A mouse models (ZOU et al., 2011; LOPES et al., 2013; ZALLOCCHI et al., 2014; DINCULESCU et al., 2016). UshStat, a lentiviral vector carrying *MYO7A* cDNA, has been tested for treating patients with USH1B, but the clinical trial was terminated prematurely due to priorities and reviews of clinical development plans (reviewed in TOMS et al., 2020a).

In contrast to gene therapy, gene editing aims at repairing the genetic defect. Zinc-finger nucleases restored expression of harmonin in HEK293 cells comprising

USH1C^{R31X} (OVERLACK et al., 2012). Similarly, CRISPR/Cas system achieved repair of the c.2299delG mutation in USH2A fibroblasts, albeit at a low efficacy (FUSTER-GARCÍA et al., 2017).

Furthermore, translational read-through inducing drugs (TRIDs) like Ataluren (PTC124) and NB54, which enable read-through of nonsense mutations by inserting an amino acid at the premature stop codon site, are examined for their potential to heal USH1C, USH1F, and USH2A (reviewed in TOMS et al., 2020a). For example, both PTC124 and NB54 were able to induce expression of full-length harmonin in mice retinal explants electroporated with R31X reporter constructs *in vivo* (GOLDMANN et al., 2012).

Effort has also been made in retinal implants, but so far, they are not as successful as cochlear implants (reviewed in CHUANG et al., 2014). Likewise, the intensive investigation in stem cell transplantation did not gain success in treating inherited retinal diseases (reviewed in TERRELL & COMANDER, 2019).

1.5. USH animal models

1.5.1. Mouse models

Mutant mouse models are existing for USH1B, USH1C (Table 3), USH1D, USH1F, USH1G, USH2A, USH2C, USH2D, and USH3A. All models correctly imitate the hearing impairment and vestibular dysfunction found in the corresponding human USH subtype. Generally, hair bundles are disorganized and mechanoelectrical transduction is abnormal in these animals (reviewed in WILLIAMS, 2008; EL-AMRAOUI & PETIT, 2014).

The situation is different for the retinal phenotype, which mouse models do not mimic accurately. USH1C$^{216AAA/216AAA}$ and USH2A$^{-/-}$ mouse models are the only ones that show mild vision loss and retinal degeneration (LIU et al., 2007; LENTZ et al., 2010). Attempts of explanations for the lacking retinal phenotype in mice are differences in exposure to light, a shorter life expectancy, and a different PR architecture with functional redundancy of Usher proteins in mice. Particularly, USH1 proteins seem to be crucial in connecting the PRs' OS to the CPs, which are absent in rodents. CPs are microvilli-like structures that extend from the IS to the OS and are required for the normal growth and shaping of the OS (reviewed in SAHLY et al., 2012; EL-AMRAOUI & PETIT, 2014; reviewed in TOMS et al., 2015; SCHIETROMA et al., 2017).

Table 3: USH1C animal models.

(Adapted by EL-AMRAOUI & PETIT, 2014; TOMS et al., 2015).

	Animal model	Genetic mutation	Auditory phenotype	Retinal phenotype
Mouse models	**USH1C$^{dfcr/dfcr}$** (deaf circler) **USH1C$^{dfcr\text{-}2J/dfcr\text{-}2J}$** (deaf circler 2 Jackson) (JOHNSON et al., 2003)	Large deletion of *USH1C* 1 bp deletion in exon 3	Congenital deafness; vestibular dysfunction	No retinal degeneration
	USH1C$^{-/-}$ (LEFÈVRE et al., 2008)	Deletion of exon 1	Congenital deafness; vestibular dysfunction	No retinal degeneration
	Harmonin-PDZ2$^{AAA/AAA}$ (GRILLET et al., 2009)	AAA mutation in exon 2	Congenital deafness; vestibular dysfunction	No retinal degeneration
	USH1C$^{216AAA/216AAA}$ (LENTZ et al., 2010)	Cryptic splice site in exon 3	Congenital deafness; vestibular dysfunction	A- and b-wave reduced between 16% and 34%; reduced ONL thickness
	USH1C knockout mouse (TIAN et al., 2010)	Replacement of exon 1-4 with lacZ reporter and neomycin resistance genes	Congenital deafness; vestibular dysfunction	No retinal degeneration up to an age of 12 months
Zebrafish	**USH1C^{fh298}** (PHILLIPS et al., 2011)	Nonsense mutation in exon 5	Hearing and balance defects	Retinal architecture unaffected, visual function defects

1.5.2. Other USH animal models

Zebrafish models exist for USH1B, USH1C (Table 3), USH1D, and USH1F. They all show altered hair bundle morphology resulting in hearing and balance defects. USH1B, USH1C, and USH1F zebrafish models also display mild retinal

degeneration and reduced ERG responses. Knockdowns (KD) of USH2A, USH2D, and USH3A show abnormal development of hair bundles; USH2A KDs also present enhanced PR death (reviewed in TOMS et al., 2015).

Furthermore, USH1D and USH1F claw frog models were developed by partial KD of cadherin-23 and protocadherin-15, respectively. In contrast to mice, Xenopus tropicalis PRs do comprise CPs and indeed, these models exhibited impaired architecture of CPs and disks in OSs showed a pronounced outgrowth (SCHIETROMA et al., 2017).

Over all, existing animal models for USH, and for USH1C in particular, did not substantially promote our understanding of the harmonin deficiency in the eye. While the translational potential of non-mammalian species such as zebrafish or frog are often put into question for their distant relationship to humans, mouse models do not convincingly show a retinal phenotype. The most ideal model species are, evidently, primates, as their eye architecture is very similar to the human one (reviewed in MCGILL et al., 2018). However, using primates in experiments is problematic due to low accessibility, limited breeding capacity, ethical concerns, and their potential for genetic modification is not well established (BRITT, 2006). For this reason, interest in alternative model species has grown in the recent past.

2. Pig models for retinal degeneration

2.1. Suitability of pigs in translational vision research

Human and pig eyes have a similar morphology (MIDDLETON, 2010; SANCHEZ et al., 2011). Both the human and the porcine eyeball are about 24 mm in diameter and the intraocular pressure of porcine eyes with ~ 15 mmHg is equivalent to human pressure of 15 - 18 mmHg (RUIZ-EDERRA et al., 2005; SANCHEZ et al., 2011; BERGUA, 2017). Moreover, they have a comparable rod-cone ratio. The pig retina also has a cone-rich region, referred to as visual streak, reminding of the human macula, although the peak cone density in the pig retina is lower than in the human one (CHANDLER et al., 1999; HENDRICKSON & HICKS, 2002). Furthermore, like humans, pigs lack a tapetum lucidum (OLLIVIER et al., 2004). Important for USH research, porcine

PRs have calyceal processes (SAHLY et al., 2012). Therefore, the pig is often used in research about ocular diseases like cataract, glaucoma, choroidal neovascularization, RP or retinal detachment (GARCÍA-LAYANA et al., 1997; PETTERS et al., 1997; SUGIURA et al., 1999; RUIZ-EDERRA et al., 2005; LASSOTA et al., 2007). Pig eyes are also applied for the development of drugs and of novel surgical tools or techniques (TRAN et al., 2017; PATEL et al., 2019).

2.2. Pig models induced by chemicals or light

Retinal degeneration in pigs can be induced by chemicals or light. DUREAU et al. (1996) exposed minipigs to light with an intensity of 2500 lx for 24 hours a day over a period of one to three months. Those pigs showed a 20% reduced ONL thickness, but no changes in ERG. Prolonging the light exposure time to six months led to a reduction of amplitudes in multifocal ERG (mfERG) (LI et al., 2009).

As PRs have a high glycolytic metabolism, they are very susceptible for inhibition of glyceraldehyde-3-phosphate dehydrogenase by iodoacetic acid (IAA) (NOELL, 1953; WINKLER et al., 2003). SCOTT et al. (2011) showed that a single injection of 7.5 mg/kg IAA administered intravenously (i.v.) led to a decrease of PR nuclei and to disturbed rod and cone OS and rod IS in the porcine retina. Scotopic full-field ERG (ffERG) displayed drastically reduced rod signals whereas photopic ffERG was only temporarily diminished in cones (WANG et al., 2011).

Surprisingly, i.v. injection of sodium iodate ($NaIO_3$) did not result in retinal degeneration in pigs, although it is regularly used to induce PR damage in rodents (NOEL et al., 2012). Subretinal injections of $NaIO_3$, however, led to atrophy of outer retinal layers in a circumscribed area (MONÉS et al., 2016).

2.3. Genetically generated pig models

Some pig models for retinal degeneration were also generated by genetic modifications. The first transgenic pigs for RP were produced by mutations in the rhodopsin gene (*RHO*). About a quarter of all dominant RP cases in humans are linked to mutations in *RHO*, where mutant forms seem to be toxic for rods (reviewed in HARTONG et al., 2006). PETTERS et al. (1997) generated a pig model expressing a Pro347Leu mutant *RHO* transgene via pronuclear

microinjection. Founder animals showed a reduction of nuclei in cells of the ONL. Scotopic ERG revealed a drastically reduced b-wave amplitude at one month of age which further diminished to no measurable response at an age of 1.5 years. Photopic ERG showed no changes in four-week-old piglets, but 1.5-year-old pigs had a reduced amplitude. Histology revealed abnormally localized rhodopsin in rods (LI et al., 1998). Inter alia, the P347L model has been used in studies testing the therapeutical benefit of lensectomy, vitrectomy, and neuroretinal transplants (MAHMOUD et al., 2003; GHOSH et al., 2007).

A second rhodopsin model based on the Pro23His mutation was produced by ROSS et al. (2012) by somatic cell nuclear transfer (SCNT) of porcine fibroblasts expressing the human RHO^{P23H} as transgene. In founder animals, changes in ffERG became obvious at an age of three to nine months, correlating with differently pronounced reduction of ONL. Offspring of a more severely affected founder animal never showed rod driven ERG responses and cone responses began to diminish at an age of 30 days (FERNANDEZ DE CASTRO et al., 2014).

Stargardt disease is a form of macular degeneration inherited in autosomal dominant manner. SOMMER et al. (2011) generated two pig models for Stargardt-like macular dystrophy type 3 (STGD3), comprising distinct mutations in *ELOVL4*, a gene responsible for elongation of very long chain fatty acids-4, via pronuclear DNA microinjection or SCNT. The pigs showed a reduction of b-wave amplitude in both scotopic and photopic ERG, and a diminished ONL thickness. Another pig model for Stargardt-like macular dystrophy type 1 (STGD1) is being developed at the moment via gene editing of the causative *ABCA4* gene, but data about the retinal phenotype have not been published yet (TRAPANI et al., 2019).

Furthermore, a pig model for autosomal dominant cone-rod dystrophy 6 (CORD6) in humans has been generated by lentiviral transfer of a mutated *GUCY2D*, a gene coding for the enzyme guanylate cyclase, which is implicated in calcium metabolism of PRs. The phenotype observed in resulting founder animals was heterogenous. Transgenic pigs displayed a reduced b-wave amplitude in ERG, but OCT analysis did not reveal major alterations in retinal morphology. Histology showed displacement of cone nuclei. In behavioral tests, it was noticeable that the mutated $GUCY2D^{E837D/R838S}$ pigs also used other senses than vision to complete an obstacle course (KOSTIC et al., 2013; reviewed in KOSTIC & ARSENIJEVIC, 2016).

3. Evaluation of vision in pigs

The pig has a visual field of 260° to 275°, the binocular field is considered to be between 30° and 50° (MIDDLETON, 2010). Their visual acuity with 0.001 to 0.03 is quite poor compared to standard visual acuity in humans of 1.00 and also compared to 0.04 to 0.08 in other livestock animals such as cattle. Visual acuity is calculated as the reciprocal of the visual angle in minutes of arc; visual acuity of 0.1 for example means that an item of 10 mm can be distinguished in a distance of 3.5 m (ZONDERLAND et al., 2008). As the porcine retina comprises short- and medium-wavelength sensitive cones, the pig is a dichromate (HENDRICKSON & HICKS, 2002).

3.1. Clinical evaluation via ERG and OCT

3.1.1. ERG

Electroretinography is a diagnostic method to assess retinal functionality by measuring the electrical activity of cells in the retina in reaction to a light flash. The ffERG measures the response of the entire retina. Dark- and light-adapted settings test rod- and cone-dominated responses, respectively. In contrast, the mfERG measures local retinal responses from different regions of the retina (MARMOR et al., 2003; TSANG & SHARMA, 2018b).

Diagrams of ERGs have distinct waveforms. Generally, the peak sizes and the times, at which peaks arise, are considered as evaluation parameters. According to the standards published by the International Society for Clinical Electrophysiology of Vision (ISCEV), six protocols differing in flash strength and eye adaptation state are recommended for ffERG. For example, in dark adapted 3.0 ERG, which is the combined rod-cone standard flash ERG, a-waves reflect PR function and b-waves arise from bipolar cell response (Figure 3a). The a-wave amplitude is measured from the baseline to the peak of the a-wave and b-wave amplitude is measured from peak of the a-wave to peak of the b-wave. Peak times or implicit times are measured from onset of the stimulus to the peak of the respective wave (MCCULLOCH et al., 2015). The ISCEV has also published a guideline for mfERG recordings. In mfERG a first negative deflection (N1) is pursued by a positive peak (P1) and a second negative deflection (N2) (Figure

3b). It is supposed that the same cells that lead to the a-wave in photopic ffERG lead to N1 and that P1 and N2 are caused by the same cells that cause the b-wave in photopic ffERG (HOOD et al., 2012).

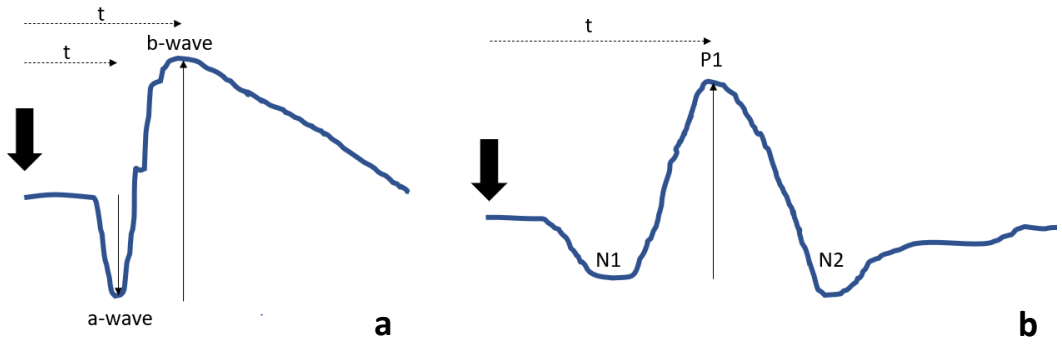

Figure 3: ERG waveforms. Diagram of dark-adapted 3.0 ffERG (a) and of mfERG (b). Bold arrows show the light stimulus, solid-line arrows indicate wave amplitudes and dotted-line arrows illustrate peak times (adapted by HOOD et al., 2012; MCCULLOCH et al., 2015).

Meanwhile, ERGs are recorded routinely in pigs for research purposes. A protocol for ffERG measurement published by AUGSBURGER et al. (2012) documented the sensitivity of this method in pigs. In this study, 162 minipigs were examined and results of female and male pigs were compared. They concluded that except for light-adapted b-wave amplitude, which was higher in female minipigs, there were no differences between genders. This observation correlates to findings in humans (BRULÉ et al., 2007). A protocol for mfERG recordings by VOSS KYHN et al. (2007) proves that porcine mfERGs show the same waveforms as human mfERGs. Importantly, in the visual streak, amplitudes of peaks are also higher and implicit time is faster than in other regions of the retina.

It is essential to avoid movement of pigs and particularly of their eyeballs during ERG recording. Therefore, examinations are usually performed under general anesthesia. However, anesthetics influence ERGs and thus the choice of anesthesia is of great importance. Earlier studies described propofol suitable for electrophysiological recordings (TANSKANEN et al., 1996), yet VOSS KYHN et al. (2007) emphasize that extended time under propofol anesthesia leads to decreased peaks, suggesting that recordings should be completed within one hour. ROSOLEN et al. (1999) delivered reproducible results in an alternative approach by recording light-adapted ERGs in conscious minipigs fixated in a hammock.

3.1.2. OCT

Optical coherence tomography is a noninvasive imaging technique that delivers cross sections of biological structures on the micron scale *in vivo*. It is comparable to ultrasonic imaging, but it uses low-coherence light instead of sound (HUANG et al., 1991; FUJIMOTO et al., 2000). In the eye, OCT visualizes the different retinal layers. PR cell death is shown by a reduction of the ONL thickness (TSANG & SHARMA, 2018a).

Nowadays, OCT imaging is also used for examination of retinal morphology in pigs (KOSTIC et al., 2013; HUCKENPAHLER et al., 2019). CHENG et al. (2018) showed that thickness of retinal layers measured with OCT mostly correlates with findings in histology in wildtype (WT) pigs as well as in P23H pigs, but inner and outer nuclear layer may appear thicker in OCT than in histology, while retinal pigment epithelium can seem thinner.

3.2. Behavioral tests

A lot of work is also being invested to gain more knowledge about the perceptual-cognitive capacity of pigs and the role of sight in recognizing conspecifics. WONDRAK et al. (2018) trained pigs to differentiate between pictures showing the front or back of human heads only dependent on visual information. After intensive training, the majority of pigs were able to fulfill this task. This contradicts the findings of GIELING et al. (2012), who reported that pigs were only able to discriminate between two geometric signs, but not between pictures of other pigs. Animals might have learned this task after a longer training period, but nevertheless, pigs seem to have more problems with visual discrimination than other species. For instance, sheep learned this task in a short time (FERREIRA et al., 2004). By blinding pigs with hoods or contact lenses, EWBANK et al. (1974) found that pig groups do not rely on the visual system to form or maintain social hierarchies, other senses like smell seem to play a more important role. MCLEMAN et al. (2008) describe that some pigs are able to recognize other pigs when deprived of either auditory, olfactory or visual signals, but very few pigs achieve this using only one of those senses. In another study, CRONEY et al. (2003) showed that pigs can discriminate between differently colored pots to receive a food reward, but pigs fared better when olfactory stimuli were used

instead of visual ones. CRONEY and BOYSEN (2021) even reported that pigs can be trained to operate a joystick which leads to cursor movement on a computer screen. Pigs learned to move the cursor to get in contact with targets on the monitor, requiring sufficient visual capacity.

In an experiment on visual acuity by ZONDERLAND et al. (2008), a Landolt-C and a solid circle were printed on two feed lids, but only the feed lid with the Landolt-C would open so that the pig could gain access to the food behind. Once the pig had learned this association, the gap in the C was decreased and the test conducted under different light intensities. Pigs were not able to differentiate between the Landolt-C and the circle when the gap in the C was smaller than 2 cm. With decreasing illuminant levels, pigs made less correct choices. Visual acuity calculated form individual pigs' results differed a lot, visual acuity ranged between 0.001 and 0.03. Similar findings were reported by GRAF (1976), who described a visual acuity of 0.001 at 200 lx. The gap in the C needed to be at least 1.8 cm to enable pigs to discriminate it from the circle and pigs needed a minimum illuminant level of 12 lx. TANAKA et al. (1998) reported a higher visual acuity in pigs ranging from 0.017 to 0.07, but they used a less demanding learning criterion and fewer animals were examined compared to ZONDERLAND et al. (2008).

Regarding color perception, ERG recordings found two different types of cones in the porcine retina with maximum sensitivity at 556 nm (yellow-green) and 439 nm (blue), implying dichromatic vision (NEITZ & JACOBS, 1989). Experiments by TANIDA et al. (1991) indicated that weaned pigs can distinguish blue and gray. Piglets were not able to discriminate green and gray and red and gray, but for these two color combinations, less training sessions had been performed. EGUCHI et al. (1997) reported that wild boars are able to differentiate blue and gray, to a lesser extent also green and gray but not red and gray. Furthermore, pigs show preferences for differently colored food dispensers, they favored blue over red and yellow feeders (KLOCEK et al., 2016). Female piglets seemed to prefer blue water dispensers, whereas male piglets favored red drinkers, green dispensers were less attractive (DELIGEORGIS et al., 2006). To conclude, pigs are able to distinguish colors, but it is unkown to which extent. It is therefore obvious that examining porcine vision in behavior tests must consider these specificities of vision in pigs.

BARONE et al. (2018) described the implementation of an obstacle course to reduce ERG examinations, thereby diminishing the stressful procedure of anesthesia and contributing to animal welfare. After a training period of two weeks, the pigs had learned to complete a course with ten boards as hurdles without stopping. To avoid memory effects, the boards were rearranged after each run. In this setting, pigs treated with IAA after the training period to induce PR degeneration took more time to complete the course than untreated pigs under dim as well as light conditions. Furthermore, IAA-treated pigs regularly hit obstacles, whereas control pigs did not collide with the boards.

To examine the useful vision of their GUCY2D pigs, KOSTIC et al. (2013) also conducted behavioral tests, for comparisons with ERG recordings. Animals were tested in an obstacle course with construction cones, frisbees, and buckets with a luminance level of 800 lx or higher to primarily test cone function at an age of 24 and 52 weeks. GUCY2D pigs took more time to complete the obstacle course than WT pigs, but only a quarter of transgenic pigs accidently hit obstacles. Strikingly, most GUCY2D pigs showed so-called alternative prospection: they examined obstacles by licking or smelling, thereby compensating their visual impairment. Importantly, correlation between behavior and ERG was poor, some pigs with low ERG performed well in the obstacle course, whereas some pigs with almost normal ERG had more problems to complete the course. This could be due to coping strategies and inhomogeneous retinal degeneration.

III. ANIMALS, MATERIALS AND METHODS

1. Animals

All animal experiments were carried out in compliance with the German Animal Protection Law, approved by the Regierung von Oberbayern, the responsible animal welfare authority (AZ 55.2-1-54-2532-70-12 and AZ 02-17-136).

Homozygous female USH1C piglets were produced by SCNT followed by embryo transfer (ET). After reaching fertility, F0 sows were inseminated with WT sperm to found a heterozygous breeding herd. Heterozygous F1 boars were mated to their sisters and mothers for production of homozygous piglets and also to unrelated WT sows for a broadening of the genetic background by outbreeding.

Right after birth, homozygous USH1C piglets showed severe vestibular dysfunction, manifesting in circling and head shaking. This behavior required the separation from their mothers and raising in a rescue deck system (EGERER et al., 2018). They were fed colostrum manually with a syringe or gastric tube for the first 24 h of life. After that the diet was changed to milk substitute (Bonimal SB PowerMilk). Piglets were fed per hand until their balance improved and they were able to drink independently out of the nurturing unit, which was usually possible after 48 to 72 h after birth.

2. Materials

2.1. Devices

Analytik Jena US UVP GelStudio Plus	Thermo Fisher Scientific, USA
Benchtop 96 Tube working rack	Stratagene, USA
Body and Mind Stepboard	Good & Gadgets GmbH, Fürth
Chyo Petit Balance MK-2000B	YMC CO, Japan
Cavaletti-Block klein	Nedlandic Quality Horse Supplies, Netherlands
Cavalettistange-Kunststoff	Hofmeister Handel GmbH & Co. KG, Gevelsberg
Daewoo KOC-154K microwave	Daewoo, South Korea

Eppendorf Centrifuge 5417 R	Eppendorf, Hamburg
Eppendorf Centrifuge 5424	Eppendorf, Hamburg
Eppendorf Centrifuge 5910 R	Eppendorf, Hamburg
EverioR GZ-RX605BE Camcorder	JVC, Japan
Gel documentation system	Bio-Rad Laboratories, USA
Grant JB Nova 5 water bath	Grant Instruments Ltd, UK
HLC Cooling-ThermoMixer MKR 13	Ditabis, Pforzheim
Labcycler thermocycler	SensoQuest GmbH, Göttingen
Luxmeter BL-10 L	Voltcraft, Hirschau
Mastercycler® gradient	Eppendorf, Hamburg
Owl™ EasyCast™ B1A and B2 mini gel electrophoresis systems	Thermo Fisher Scientific, USA
Pipettes (1000 µL, 200 µL, 20 µL, 10 µL, 2 µL)	Gilson Inc, USA
Polytron® homogenizer PT 2500 E	Kinematica, Switzerland
Porky's Fun Strohbox	Meier-Brakenberg, Extertal
Power Pac 300 gel electrophoresis unit	Bio-Rad Laboratories, Munich
Power Station 300 gel electrophoresis unit	Labnet International, USA
Rescue Deck	Provimi, Netherlands
Rotilabo® mini centrifuge	Carl Roth, Karlsruhe
Select vortexer	Select BioProducts, USA
SimpliNano™ spectrophotometer	Biochrom GmbH, Berlin
Spannring Deckelfass	Wittmann Sonderabfall-Entsorgung GmbH, Unterschleißheim
Spectrafuge 24D Microcentrifuge	Labnet International, USA
Stangen-Stopp	Hofmeister Handel GmbH & Co. KG, Gevelsberg
Stop watch CG-501	Genutek Electronics Co., China
Thermo-Shaker TS-100	bioSan, Lativa
Treibbrett Mittel	Schulze Bremer GmbH, Coesfeld

2.2. Consumables

Cellstar® tubes (15 and 50 mL)	Greiner BioOne, Austria
Disposable scalpel #21	Henry Schein, USA
Gastric tube 80 cm x 4 mm	Henry Schein, USA
NitriSense nitrile gloves	Süd-Laborbedarf, Gauting
PCR reaction tubes (0.2 mL)	Brand, Wertheim
Petri dish 94 x 16	Greiner BioOne, Austria
Pipet tips with filter	Greiner BioOne, Austria
Pipet tips	Eppendorf, Hamburg
SaveGrip® latex gloves	SLG, Munich
Safe-Lock reaction tubes (1.5 and 2 mL)	Eppendorf, Hamburg
Top Marker, animal marking crayon	MST Stall und Hoftechnik, Eichendorf

2.3. Chemicals

Acetic acid (glacial)	Carl Roth, Karlsruhe
Bromphenolblue	Carl Roth, Karlsruhe
Chloroform (Trichloromethane)	Sigma-Aldrich, USA
EDTA (Ethylenediaminetetraacetic acid)	Carl Roth, Karlsruhe
Ethanol Rotipuran® 99.8%	Carl Roth, Karlsruhe
Formaldehyde	Carl Roth, Karlsruhe
Formamide	Carl Roth, Karlsruhe
Glycerol	Carl Roth, Karlsruhe
GelRed® Nucleic Acid Gel Stain	Biotium, USA
HCL (Hydrochloric acid)	Bernd Kraft GmbH, Duisburg
Isopropanol	Carl Roth, Karlsruhe
NaOH (Sodium hydroxide 2N)	Carl Roth, Karlsruhe
$MgCl_2$ (Magnesium chloride)	Thermo Fisher Scientific, USA
Tris (Tris-(hydroxymethyl)aminomethane)	Carl Roth, Karlsruhe
TRIzol® Reagent	Thermo Fisher Scientific, USA
Universal Agarose	Bio&SELL, Nuremberg

2.4. Enzymes

BigDye® Terminator v3.1	Applied Biosystems, USA
DNase I, RNase-free (1 U/µL)	Thermo Fisher Scientific, USA
Herculase II Fusion DNA Polymerase	Agilent Technologies, USA
HotStarTaq Plus DNA Polymerase (5 U/µL)	Qiagen, Hilden
Proteinase K, ready to use	Agilent Technologies, USA
SuperScript® III Reverse Transcriptase (200 U/µL)	Thermo Fisher Scientific, USA
Taq DNA Polymerase (5 U/µL)	Qiagen, Hilden

2.5. Oligonucleotides

Oligonucleotides were designed with the primer designing tools Primer-BLAST by NCBI and PrimerQuest by IDT. They were then purchased from Biomers.net GmbH, Ulm.

GAPqf1	**5′**- CAG AAC ATC ATC CCT GCT TC -**3′**
GAPqr1	**5′**- GCT TCA CCA CCT TCT TGA TG -**3′**
hUSHREV	**5′**- CCT TGG TTC CTG CGT CT -**3′**
huUSHEV	**5′** CAC TGT CTT ACC TGA TGG -**3′**
huUSHFOR	**5′**- TGT GGT GGG ACG GAC AGA C -**3′**
hUSHFOR2	**5′**- GAG GAA ATT GCA TCG CAT TG -**3′**
hUSHREV3	**5′**- CTG AAG CCA GAC AGG AAA CCT -**3′**
iRPF2for	**5′**- AGC CTG ACC TCT TGA CCT GCG -**3′**
iRFP4rev	**5′**- TGC AGG CCT AGT TTT GAC TCG AC -**3′**
neoFOR3	**5′**- GCA AGC AAG GGC AGG AT -**3′**
neoREV3	**5′**- GTA TCC CAA GGG TTC TGG AAG -**3′**
urt3r	**5′**- CCT TTG ATG AGG TGG GAG ATG AAG -**3′**
urt4r	**5′**- ACA GGG ATC AGG CCA ATG TG -**3′**
urt5f	**5′**- CCA TGG ACC GGA AGG TGG -**3′**
urt6f	**5′**- CCT GAA GGA GCG AGC TGT A -**3′**
ush3arm1r	**5′**- CAC CTC AGA AGA ATC TGT TCC C -**3′**
ush3arm2r	**5′**- GAC CTTT CTC ACT CCC ACA TC -**3′**
ush5arm1f	**5′**- TGG GCA TGG GTT CTG TTT AG -**3′**
ush5arm2f	**5′**- GGG TTC TGT TTA GGT AGG TGA G -**3′**

ush5arm2r	**5′**- CTA GCT TGG CTG GAC GTA AA -**3′**
ushrt1s	**5′**- GGT GTC AGC TGG TCG TAC TCC -**3′**
ushrt2f	**5′**- CGG AGC CTG AAG GAG CGA G -**3′**
ushrt2r	**5′**- TTG TTT TCC CGA CTG CCA GA -**3′**
ushwt1f	**5′**- TTC CCT CCT CTT CTC ACA ACC AT -**3′**
ushwt1r	**5′**- AGA GCC ACG CAC AGC ACC TCT -**3′**
ushwt2f	**5′**- CAT GGT CGG CGC AGT CTC ATG T -**3′**
ushwt2r	**5′**- TTG AAC CTC TCG GAC TAT CTG -**3′**
ushwt3f	**5′**- GGG AAT CAA ATG GAC ACG CC -**3′**
ushwt3r	**5′**- ATC TCC CCT CAC TAG GCC AC -**3′**
ushwt4f	**5′**- GGC ATT TCC GGT CCT ATC CC -**3′**
ushwt4r	**5′**- GGC ATT TCC GGT CCT ATC CC -**3′**
ushwt5f	**5′**- CCA GTA AGT GTG CTG GGT CC -**3′**
ushwt5r	**5′**- CAG CCA GTG GTA GGA GCT TAT -**3′**

2.6. Buffers and solutions

Aqua bidest., deionized in Barnstead™ EASYpure™ II ultrapure water system (Wilhelm Werner GmbH, Leverkusen) was used as solvent.

DNA loading buffer (10x)

10 % glycerol in aq. bidest.

1 spatula tip of bromphenolblue

0.5 M NaOH until color turns blue

stored in aliquots at 4°C

2 mM dNTP-mix

2 mM dATP, dCTP, dGTP, dTTP

mixed in aq. bidest.

stored in aliquots at -20°C

10 mM dNTP-mix

10 mM dATP, dCTP, dGTP, dTTP

mixed in aq. bidest.

stored in aliquots at -20°C

GeneRuler™ 1kb DNA molecular weight standard

100 µL GeneRulerTM 1kb DNA

100 µL 6x loading dye

400 µL aq. bidest.

stored in aliquots at -20°C

Sequencing buffer (5x)

17.5 mL 1 M Tris/HCL (pH 9.0)

125 µL 1 M $MgCl_2$

50 mL aq. bidest.

stored in aliquots at -20°C

TAE buffer (50x)

242 g 2 M Tris

100 mL 0.5 M EDTA (pH 8.0)

57 mL acetic acid (glacial)

1000 mL aq. bidest.

For storage at room temperature, the buffer solution was filtrated and autoclaved. Buffer solution was diluted to single concentration with aq. bidest. before usage.

2.7. Other reagents

0.1 M DTT	Thermo Fisher Scientific, USA
5× Herculase II Reaction Buffer	Agilent Technologies, USA
5× Reaction Buffer for RT	Thermo Fisher Scientific, USA
5x Q-Solution	Qiagen, Hilden
6× DNA loading dye	Thermo Fisher Scientific, USA
10× CoralLoad PCR buffer	Qiagen, Hilden
10× DNase reaction buffer with $MgCl_2$	Thermo Fisher Scientific, USA
25 mM $MgCl_2$	Qiagen, Hilden
100 mM dNTP mix	Agilent Technologies, USA
DMSO	Agilent Technologies, USA
dNTPs (dATP, dCTP, dGTP, dTTP)	Thermo Fisher Scientific, USA
Gene Ruler™ (1 kb DNA ladder)	Thermo Fisher Scientific, USA
Oligo$(dT)_{18}$ primer (0.5 µg/µL)	Thermo Fisher Scientific, USA

2.8. Kits

DNeasy® Blood & Tissue Kit (250)	Qiagen, Hilden
Nexttec™ Isolation of Genomic DNA from Tissue & Cells Kit	Nexttec Biotechnologie GmbH, Leverkusen
NucleoSpin® Gel and PCR Clean-up kit	Macherey-Nagel, Düren

2.9. Drugs and feed

Altrenogest (Regumate®)	MSD Animal Health, Unterschleißheim
Atracurium (Atracurium-hameln 10 mg/mL)	Hameln pharma plus GmbH, Hameln
Atropine sulfate (Atropinsufat 0.5 mg/mL)	B. Braun Melsungen AG, Meisungen
Azaperone (Stresnil®)	Elanco Animal Health, Bad Homburg
Bananen-Nektar	Rio d'oro, Rinteln
Bonimal SB PowerMilk with blood plasma	Bonimal, Munich
Choco Bistro Vollkorn-Butterkeks	Coverna Süßwaren Vertriebs-GmbH, Polch
Choriongonadotropine (hCG) (Ovogest®)	MSD Animal Health, USA
Cloprostenol (Estrumate®)	MSD Animal Health, USA
Embutramide, mebezonium, tetracaine (T61®)	MSD Animal Health, USA
Fentanyl (Fentadon ®)	Dechra Veterinary Products Deutschland GmbH, Aulendorf
Isoflurane (Isothesia ®)	Henry-Schein Vet GmbH, Hamburg
Ketamine hydrochloride (Ursotamin® 10%)	Serumwerk Bernburg AG, Bernburg
Lactated Ringer's solution (Ringer-Lactat-Lösung ad us. vet.)	WDT, Garbsen
Midazolam (Midazolam 5 mg/mL)	Rotexmedica GmbH, Trittau
Oxytocin (Oxytocin 10 IE/mL)	cp-pharma, Burgdorf
Peforelin (Maprelin®)	Veyx-Pharma GmbH, Schwarzenborn

Propofol (Narcofol ®)	CP-Pharma Handelsgesellschaft GmbH, Burgdorf
Xylazine (Xylazin 2%)	Serumwerk Bernburg AG, Bernburg

2.10. Software

BioEdit Sequence Alignment Editor v.7.0.5	Informer Technologies, Inc., USA
EndNote X9	Clarivate Analytics, UK
FinchTV Version 1.4.0	Geospiza Inc., USA
Graphpad Prism v.5.04	GraphPad Software, USA
Macromedia Freehand MX v11.0.2	Adobe Inc., USA
Microsoft Office 2016 ProPlus	Microsoft Corporation, USA
VLC media player 3.0.11	VideoLAN, France

3. Methods

3.1. Molecular analyses

3.1.1. Genotyping of piglets

3.1.1.1. Genomic DNA isolation

Tail biopsies of newborn piglets were taken for the isolation of genomic DNA. DNA was isolated with the DNeasy Blood & Tissue Kit (Qiagen) following the manufacturer's instructions. Part of the tail was cut into very small pieces and up to 25 mg were transferred to a 1.5 mL tube, mixed with 180 µL buffer ATL and 20 µL proteinase K and incubated in a thermomixer at 56°C at 1200 rpm overnight to ensure complete lysis of tissue. After adding 200 µL buffer AL and 200 µL 100% ethanol, the mixture was transferred to a DNeasy Mini spin column placed into a collection tube and centrifuged for 60 s at 6000 g. For washing, the spin column with the DNA bound to the DNeasy membrane was then put into a new collection tube, 500 µL buffer AW1 were added and centrifuged for 60 s at 6000 g. The spin column was placed into a new collection tube thereafter and washed for a second time with 500 µL buffer AW2. To dry the membrane, it was

centrifuged for 3 min at 20.000 g, the collection tube emptied afterwards and centrifuged another time for 60 s at 20.000 g. To elute the DNA, the spin column was transferred in a 1.5 mL tube, 200 µL buffer AE were placed on the membrane, incubated for 1 min at room temperature and centrifuged for 60 s at 6000 g. Then DNA concentration was measured with a spectrophotometer (SimpliNano™, Biochrom GmbH), DNA diluted to 20 ng/µL and used for genotyping PCRs. Genomic DNA was then stored at 4° C.

Alternatively, DNA was isolated according to the protocol for Isolation of Genomic DNA from Tissue & Cells by nexttec™. For lysis, up to 30 mg of tissue were mixed with 265 µL buffer G1, 10 µL buffer G2, 25 µL buffer G3, and 3 µL DTT and incubated in a thermomixer at 60° C at 1200 rpm for 2h. 120 µL of the lysate were then transferred to a nexttec™ cleanColumn, which had been equilibrated by adding PrepBuffer beforehand. After 3 min incubation time at room temperature, it was centrifuged at 700 g for 60 s. In contrast to the Qiagen kit, the eluate was containing the purified DNA.

3.1.1.2. Genotyping PCRs

Several PCRs were applied to characterize the genotype of each piglet. The humanized exon 2 with the R31X mutation was detected with two different primer pairs. The neomycin selection cassette, if still present, could be detected with the primer pair ush5arm-2f and ush5arm-2r. The primer pair neoFOR3 and neoREV3 showed a deletion of the neo cassette. The wildtype *USH* allele could be discovered with ushwt-2f and ushwt-2r or ushwt-3f and ush-wt3r. A heterozygous CAG-iRFP boar was used for outbreeding, the presence of this protein was detected with iRFP2for and iRFP3rev. Table 4, Table 5, Table 6, and Table 7 show the master mix compositions and the cycler protocols. PCR components were mixed to a volume of 20.1 µL in 0.2 mL reaction tubes on ice. Previously isolated DNA of 5613 (δ-neo), 5614 (neo), 6812 (WT), and 10346 (CAG-iRFP) were used as positive controls. Master mix without DNA was used as non-template control.

Table 4: Master mix composition for genotyping PCRs (neo, δ-neo, wt).

10× CoralLoad PCR buffer	2.0 µL
dNTPs (2 mM)	2.0 µL
Forward primer (10 µM)	0.4 µL
Reverse primer (10 µM)	0.4 µL
HotStarTaq (5 U/µL)	0.2 µL
aq. dest.	14 µL
DNA template	1.1 µL

Table 5: Cycler protocol for genotyping PCRs (neo, δ-neo, wt).

Denaturation	95 °C	5 min	
Denaturation	94 °C	30 s	35×
Annealing	58 °C	30 s	
Elongation	72 °C	40 s *	
Final elongation	72 °C	10 min	
Termination	4 °C	5 min	

* 60 s for ushwt-3f/ushwt-3r

Table 6: Master mix composition for genotyping PCRs (CAG-iRFP).

10× CoralLoad PCR buffer	2.0 µL
Q-Solution	4.0 µL
$MgCl_2$	1.25 µL
dNTPs (2 mM)	1.0 µL
iRFP2for (2 µM)	1 µL
iRFP4rev (2 µM)	1 µL
Taq polymerase (5 U/µL)	0.2 µL
aq. dest.	8.65 µL
DNA template	1.1 µL

Table 7: Cycler protocol for genotyping PCRs (CAG-iRFP)

Denaturation	95 °C	5 min	
Denaturation	94 °C	30 s	30×
Annealing	65 °C	30 s	
Elongation	72 °C	80 s	
Final elongation	72 °C	10 min	
Termination	4 °C	5 min	

3.1.1.3. Agarose gel electrophoresis

A 1% agarose gel was produced by heating 1 g Universal Agarose per 100 mL 1 x TAE buffer in a microwave until the agarose was completely dissolved. The gel was then poured into a gel electrophoresis chamber and the chamber was filled with 1 x TAE buffer as running buffer once the gel had solidified. PCR samples and 6 µL GeneRuler^{TM} 1 kb DNA molecular weight standard were pipetted into individual gel slots after adding 2.5 µL of a 1:250 mixture of GelRed® and DNA loading buffer (10x). By applying an electric current to the gel electrophoresis chamber, DNA fragments were separated according to their size. DNA fragments were then visualized under UV light and analyzed in relation to the DNA molecular weight standard.

3.1.2. RT-PCR

RNA was isolated from tissue samples and reversely transcribed into cDNA for expression analysis at transcript level.

3.1.2.1. RNA isolation

RNA was isolated using the guanidine isothiocynate-phenol extraction with TRIzol^{TM} (Thermo Fisher Scientific) according to the manufacturer's instructions. Samples of the retina, olfactory epithelium, cerebrum, cerebellum, hippocampus, lung, heart, duodenum, jejunum, ileum, caecum, colon, liver, gall bladder, spleen, pancreas, kidney, and adrenal gland were cut into small parts. Subsequently, they were deep-frozen on dry ice as quickly as possible to prevent degradation. Until isolation of RNA, the samples were stored in 2 mL Eppendorf tubes at -80°C.

Tissue samples were powdered with a hammer first and a pestle and mortar afterwards. Instruments and samples were cooled in liquid nitrogen to avoid thawing of the samples. To avoid possible pollution with DNA, the grinding took place in a separate room were no DNA isolation is performed. 50-100 mg of the ground tissue was then transferred with a microspoon to a 2 mL Eppendorf tube filled with 1ml TRIzol^{TM}. Immediately after that, it was homogenized for 10 s at 30.000 rpm with the homogenizer POLYTRON® PT 2500 E (Kinematica GmbH). The rotor was cleaned with aq. dest. after each sample to avoid contamination between samples. After five minutes incubation time at room temperature, 0.2 mL chloroform (Sigma-Aldrich) were added, the tube was

shaken and again incubated at room temperature for 3 minutes. Next, the sample was centrifuged for 15 min at 12.000 g at 4°C, separating it into an upper aqueous phase, an interphase, and a lower phenol-chloroform phase. The upper phase containing the RNA was then transferred to a new 1.5 mL tube. To precipitate the RNA, the aqueous phase was mixed with 0.5 mL isopropanol, incubated 10 min at room temperature and centrifuged for 10 min at 12.000 g at 4°C. Afterwards the supernatant could be discarded as the RNA was forming a pellet at the tube's bottom. To wash the pellet, it was resuspended in 1 mL of 75% ethanol, vortexed and centrifuged for 5 min at 7500 g at 4°C. The supernatant was removed to let the pellet air-dry for 6 min. Subsequently, the pellet was resuspended in 20 µL RNase-free water and incubated for 15 min at 55°C. RNA concentration was measured with a spectrophotometer (SimpliNano™, Biochrom GmbH) by determining the absorbance at 260 nm and 280 nm. RNA samples were stored at -80°C.

3.1.2.2. DNase digestion

Samples were treated with DNase, an endonuclease that digests single- and double stranded DNA, in order to remove a possible pollution with gDNA. RNA was diluted to 100 ng/µL. 5 µL RNA (100 ng/µL) were mixed with 2 µL 10x reaction buffer with $MgCl_2$, 2 µL DNase I (Thermo Fisher Scientific), RNase-free, 11 µL aq. dest. and incubated at room temperature for 60 min. By adding 2 µL of 50mM EDTA and incubating the mixture for 10 min at 65°C, DNase was inactivated. The samples were put on ice for 1 min afterwards. To prove complete DNA digestion, the DNase digest was later loaded on the gel in addition to the cDNA samples.

3.1.2.3. cDNA synthesis

For first strand cDNA synthesis with SuperScript™ III Reverse Transcriptase (Thermo Fisher Scientific) 10 µL of the DNase digest were mixed with 1 µL 10 mM dNTP and 1 µL of the primer Oligo $(dT)_{18}$. Samples were then incubated for 5 min at 65°C and put on ice for 1 min afterwards. Next, 5 µL 5xRT-Buffer, 2 µL 0.1M DTT, 1 µL Superscript™ III, and 5 µL aq. dest. were added, the samples were vortexed and incubated at 50°C for 60 min and for 5 min at 85°C thereafter. cDNA was stored at -20°C or directly used in RT-PCR.

3.1.2.4. RT-PCR

By amplification of the ubiquitously expressed housekeeping gene *GAPDH* the cDNA was checked for integrity. Table 8 and Table 9 show the master mix composition and the cycler protocol.

Table 8: Master mix composition for cDNA verification PCRs.

10× CoralLoad PCR buffer	2 µL
dNTPs (2 mM)	2 µL
GAPqf1 (10 µM)	0.4 µL
GAPqr1 (10 µM)	0.4 µL
Taq polymerase (5 U/µL)	0.1 µL
aq. dest.	14.1 µL
DNA template	1.1 µL

Table 9: Cycler protocol for cDNA verification PCRs.

Denaturation	95 °C	5 min	
Denaturation	94 °C	30 s	35×
Annealing	58 °C	30 s	
Elongation	72 °C	45 s	
Final elongation	72 °C	5 min	
Termination	4 °C	5 min	

Then cDNA was used in RT-PCRs with primers spanning exons upstream and downstream of exon 2. Table 10 and Table 11 show the master mix composition and the cycler protocol. RT-PCR was run with the primer pairs ushrt-2f and ushrt-2r or ushrt-2f and urt-4r.

Table 10: Master mix composition for USH RT-PCR.

10× CoralLoad PCR buffer	2 µL
dNTPs (2 mM)	2 µL
Forward primer (10 µM)	0.4 µL
Reverse primer (10 µM)	0.4 µL
HotStarTaq (5 U/µL)	0.2 µL
aq. dest.	14 µL
DNA template	1.1 µL

Table 11: Cycler protocol for USH RT-PCR.

Denaturation	95 °C	5 min	
Denaturation	94 °C	30 s	35×
Annealing	58 °C	30 s	
Elongation	72 °C	45 s	
Final elongation	72 °C	5 min	
Termination	4 °C	5 min	

3.1.2.5. PCR purification

The PCR was cleaned up using the NucleoSpin® Gel and PCR Clean-up kit (Macherey-Nagel) according to the manufacturer's protocol. 20 µL of the PCR product were mixed with 80 µL aq. dest. and 200 µL buffer NTI and then transferred into a NucleoSpin® Gel and PCR Clean-up Column placed into a collection tube. Afterwards, it was centrifuged for 30 s at 11.000 g, the flow-through was loaded into the column again and the centrifugation step was repeated to increase the amount of DNA binding to the silica membrane. The membrane was then washed twice by adding 650 µL buffer NT3 and centrifuging for 30 s at 11.000 g. Samples were centrifuged for 60 s at 11.000 g and incubated for 4 min at 70°C thereafter to dry the silica membrane. To elute the DNA, the NucloSpin® Gel and PCR Clean-up Column was placed into a 1.5 ml tube, 40 µL buffer NE heated to 70°C were added, incubated for 5 min at room temperature and then centrifuged for 60 s at 11.000 g. 15 µL of the cleaned-up DNA were loaded on gel.

3.1.2.6. Sequencing PCR

The residual cleaned-up DNA was used for sequencing reactions. Each sample was sequenced with the primers ushrt-2f, ushrt-2r, and ushrt-1s in 0.2 mL reaction tubes in a final volume of 10 µL. Table 12 and Table 13 show the master mix composition and cycler protocol for the sequencing PCR.

Table 12: Master mix composition for sequencing PCRs.

5× Sequencing buffer	4 µL
BigDye®	1 µL
Primer (10 µM)	0.5 µL
Aq. dest.	0.5 µL
DNA template	4 µL

Table 13: Cycler protocol for sequencing PCRs.

Denaturation	95 °C	1 min	
Denaturation	95 °C	5 s	40×
Annealing	54 °C	10 s	
Elongation	60 °C	4 min	
Termination	4 °C	5 min	

3.1.2.7. Ethanol precipitation

For precipitation of DNA, 1.5 µL 125 mM EDTA were added to the sequencing product and then transferred to a 1.5 mL tube filled with 30 µL 100 % EtOH. After 15 min incubating on ice, the samples were centrifuged at 13.300 rpm for 30 min at 4°C and the supernatant discarded afterwards. The pellet was washed in 50 µL 70 % EtOH, centrifuged at 13.300 rpm for 2.5 min and the supernatant was removed again. The pellet was then air dried for 6 min, resuspended in 30 µL aq. dest. and transferred to 96- well plates.

Finally, capillary electrophoretic separation was performed at the Genome Analysis center at the Helmholtz Centre in Munich and at the Genomics Service Unit at LMU Biocenter. The resulting nucleotide sequences were then analyzed with FinchTV Version 1.3.1 and the BioEdit Sequence Alignment Editor.

3.2. Behavioral analyses

3.2.1. Obstacle course

The obstacle course took place in an empty part of the pigsty. The dimensions of the course were 6.15 m in length and 1.58 m in width in the beginning and 2.48 m in the end. Eleven different obstacles were used, whereof most were built from obstacle bars used in equestrian sport (Cavalettistange-Kunststoff and Stangen-Stopp, Hofmeister Handel GmbH & Co. KG; Cavaletti-Block klein, Nedlandic Quality Horse Supplies). Other obstacles were a stepboard (Body & Mind Steppbrett, Good & Gadgets GmbH) and barrels (Porky's Fun Strohbox, Meier-Brakenberg GmbH & Co. Kg; Spannring Deckelfass, Wittmann Sonderabfall Entsorgung GmbH).

Following a training period, pigs were examined weekly in the course. After entering the course individually in a random order, pigs had to pass the obstacles to reach their reward at the end of the course, a cookie (Choco Bistro Vollkorn-Butterkeks, Coverna Süßwaren Vertriebs-GmbH) in a feed trough. Obstacles were rearranged after almost every test day. The experiment was performed under two different light conditions, referred to as light and dark.

For evaluation, every run was filmed (camcorder EverioR GZ-RX605BE, JVC). To facilitate identification, pigs were marked with numbers on their backs (animal marking crayon Top Marker, MST Stall und Hoftechnik). Times the pigs took to pass the course were measured (stop watch CG-501, Genutek Electronics Co.) and obstacle and wall contacts were counted. Additionally, animals' trajectories were analyzed with the R package TrajR by Gianluca Santamaria (Clinic for Cardiology, Klinikum rechts der Isar, TU Munich). Exclusion criteria for one test day were lameness or turning around before getting to the end of the course.

Wolfgang Hitzl (Biostatistics and Data Science, Paracelsus Medical University, Salzburg, Austria) supported data analysis. Data were first checked for consistency and normality. To analyze cross tabulations, Fisher's Exact test or Pearson's test were used. Continuously distributed variables were tested applying generalized linear models with Poisson distribution, Median tests, bootstrap-t tests based on 5000 Monte Carlo simulations, t-tests with and without the assumption of homogeneity, and Mann-Whitney U tests. Reported tests were two-sided and differences between WT and USH1C pigs were considered significant when $p < 0.05$ ($p < 0.05$: *, $p < 0.01$: **, $p < 0.001$: ***, $p < 0.0001$: ****). Analysis of data were performed using STATISTICA 13 (StatSoft, USA), NCSS 10 (NCSS LLC, USA), Mathematica 12 (Wolfram Research, UK), Champaign, IL (2018), GraphPad Prism v.5.04 (GraphPad Software, USA), and PASW 24 (SPSS by IBM Corp, USA).

3.2.2. Barrier course

Another course was adapted from Barone et al. (2018). Ten obstacles (boards of Schulze Bremer GmbH, used to herd pigs, with attached angle connectors, measurement of boards 94 cm x 76 cm x 2.5 cm) were placed in a distance of one meter in the pigsty's aisle (12 m x 2.2 m) alternating in the right, left, and middle in different setups.

Pigs were assessed in the course once a week after a training period. The animals went into the course individually in random order and were rewarded with banana juice (rio d'oro) after passing the barriers. After first runs under light condition, the course was performed alternately in the dark and in the light. Illumination level was measured in pigs' head height at three different locations in the course, in the beginning, middle, and end, with the Luxmeter BL-10L (Voltcraft).

Every run was filmed (camcorder EverioR GZ-RX605BE, JVC) and to facilitate identification, pigs were again marked with numbers on their backs (animal marking crayon Top Marker, MST Stall und Hoftechnik). Times animals needed to go through the course were measured in seconds (stop watch CG-501, Genutek Electronics Co.). Every barrier contact, circling, and turning around before reaching the end of the course was counted.

When pigs showed more interest in playing with barriers than walking straight to their reward at the end of the course or when animals did not walk through the course reliably after a training period of six weeks, they were excluded from the study due to motivational problems. An exclusion criterion for a single experimental day was lameness or when a pig was outside of its pen for another reason on the test day. Furthermore, pigs were also excluded from a single experiment when they were circling or turning around so often that they needed more time than two minutes to get to the endpoint of the course. Nevertheless, circles and turns within those two minutes were still documented.

3.3. Complementary analyses

The examination of the USH1C pig model involved the methods described in this thesis as well as OCT, ERG, and auditory brainstem response (ABR). OCT and ERG examinations in one-year old pigs were performed by Dominik Fischer (Centre for Ophthalmology, University of Tübingen and Oxford Eye Hospital, University of Oxford). ERG analysis in three-week old piglets was conducted by Anna Döring (Small Animal Clinics, LMU Munich). ABR was performed by Andrea Fischer (Small Animal Clinics, LMU Munich). Andrea Bähr (Clinic for Cardiology, Klinikum rechts der Isar, TU Munich) conducted anesthesia for OCT and ERG examinations. Pigs were sedated via i.m. administration of 10 mg/kg azaperone (Stresnil®), 20 mg/kg ketamine (Ursotamin® 10%), 1 mg/kg

midazolam (Midazolam 5 mg/mL) and 0.02 mg/kg atropine sulfate (Atropinsulfat 0.5 mg/mL). Deepening of anesthesia was achieved via i.v. administration of 0.001 mg/kg fentanyl (Fentadon ®). Anesthesia was prolonged via i.v. administration of 2 mg/kg propofol (Narcofol ®) as required. To prevent eye movements, 0.5 mg/kg of the muscle relaxant atracurium (Atracurium-hameln 10 mg/mL) were administered intravenously. Pigs were intubated and ventilated, and lactated Ringer's solution (Ringer-Lactat-Lösung) was administered as liquid substitution. For ABR examinations, anesthesia did not need to be as deep. Pigs were sedated via i.m. administration of ketamine and azaperone and anesthesia was prolonged with isoflurane (Isothesia ®). After termination of clinical examinations, pigs were euthanized via i.v. injection of embutramide, mebezonium, and tetracaine (T61®, 1 mL/10 kg). Samples were taken for molecular and histological analysis with support of Andreas Parzefall (Institute of Experimental Genetics, Helmholtz Center Munich). Histological analyses were conducted by the working group of Uwe Wolfrum (Institute of Molecular Physiology, Molecular Cell Biology, JGU Mainz).

IV. RESULTS

1. Molecular analyses

1.1. Generation of the USH1C pig model

The pig model is based on the human-relevant R31X mutation in *USH1C*, which leads to a premature translational stop in the N-terminal end of harmonin and the consequent lack of this protein. The porcine *USH1C* gene was modified by replacing the porcine exon 2 and surrounding intronic regions with the orthologous human fragment carrying the R31X mutation via CRISPR/Cas induced homologous recombination as described in VOCHOZKOVA et al. (2019). A BAC vector containing the porcine *USH1C* gene was modified to contain the humanized fragment by bacterial recombineering (Figure 4b), and then co-transfected with plasmids expressing gRNA and Cas9 into pig primary cells. Single cell clones were produced as demonstrated by RICHTER et al. (2012), screened for carrying the desired modification and then lipofected with Cre-mRNA for excision of the neo selection cassette (Figure 4c). Cell clones were used as donors in SCNT (Figure 4a) by injection into enucleated oocytes and embryos were transferred to synchronized sows (KUROME et al., 2015). SCNT experiments were performed by Mayuko Kurome, Valeri Zakharchenko, Barbara Keßler, and Tuna Güngör at the Chair of Molecular Animal Breeding and Biotechnology. ET was carried out by Barbara Keßler and Arne Hinrichs.

Twelve ETs with homozygous female cell clones led to 5 pregnancies resulting in 4 litters and 18 USH1C$^{-/-}$ piglets (Table 14). In 5 out of 15 founder pigs, excision of the neo selection cassette was accomplished, a single lox site was left as remnant (Figure 5). One ET with a heterozygous cell line was performed, leading to six USH1C$^{+/-}$ piglets, but none of those heterozygous piglets reached breeding age. Therefore, establishment of breeding herds was founded on USH1C$^{-/-}$ F0 sows. Parallel attempts were carried out at the Center for Innovative Medical Models (CiMM) at the Chair of Molecular Animal Breeding and Biotechnology and the Institute of Animal Physiology and Genetics (IAPG, Czech Academy of Science, Libechov, Czech Republic). After reaching fertility, USH1C sows were inseminated to produce an intermediate generation of heterozygous animals. For generating USH1C piglets, heterozygous F1 boars were mated either to

homozygous F0 or heterozygous F1 sows. For broadening of the genetic background, F1 boars were also mated with WT sows (Table 15).

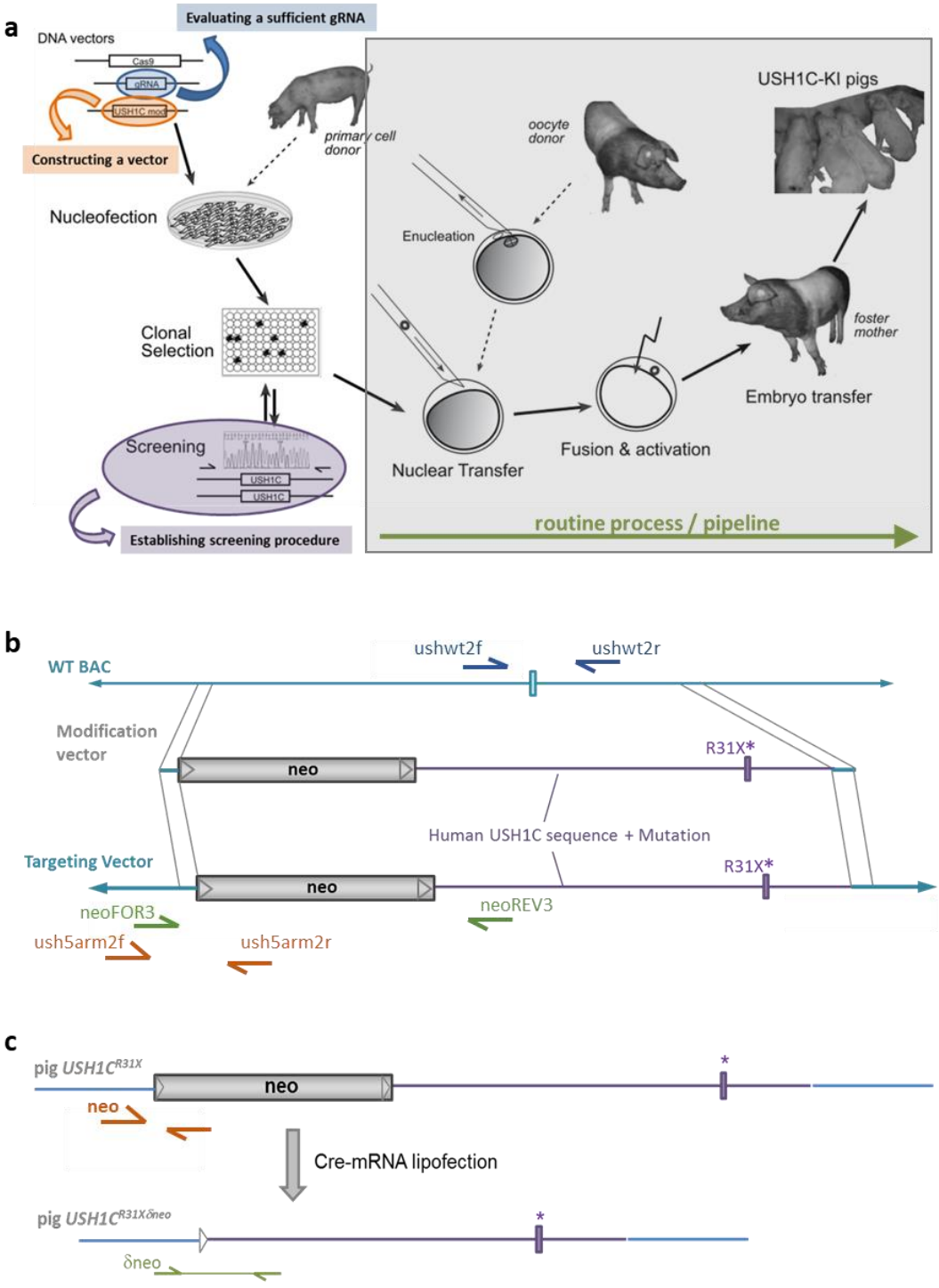

Figure 4: Generation of the USH1C pig model. Founder pigs were generated by SCNT of genetically modified pig primary cells (a). A BAC vector containing the porcine *USH1C* gene was modified to carry a humanized fragment with the R31X mutation by bacterial recombineering (b). Positions of primers used for genotyping are indicated by arrows. The neo cassette in successfully modified single cell clones was removed by lipofection of a Cre-encoding mRNA (c). Positions of primers discriminating the two different constellations are indicated.

Table 14: Generation of founder pigs.

ET	donor cell[1]	pregnancy	offspring
March 2017	1519 (USH1C$^{-/-}$)	-	-
June 2017	1519 (USH1C$^{-/-}$)	-	-
June 2017	1519 (USH1C$^{-/-}$)	+	5 (5613-5617)
July 2017	1535 & 1494 (USH1C$^{-/-}$)	-	-
August 2017	1535 & 1494 (USH1C$^{-/-}$)	+	9 (10050-10058)
November 2017	1348 & 1385 & 1547 (USH1C$^{+/-}$)	+	6 (10153-10158)
July 2018	5613& 1535 & 1494 (USH1C$^{-/-}$)	-	-
October 2018	1535 & 1494 (USH1C$^{-/-}$)	-	-
October 2018	1535 & 1494 (USH1C$^{-/-}$)	-	-
February 2019	5613	+	3 (10439-10441)
February 2019	5613	-	-
May 2019	1535 & 1494 (USH1C$^{-/-}$)	+	1 (10618)
May 2019	1535 & 1494 (USH1C$^{-/-}$)	+	-

[1] Either single cell clones (1348, 1385, 1494, 1519, 1535, and 1547) or primary cells from cloned founder animal 5613 were used.

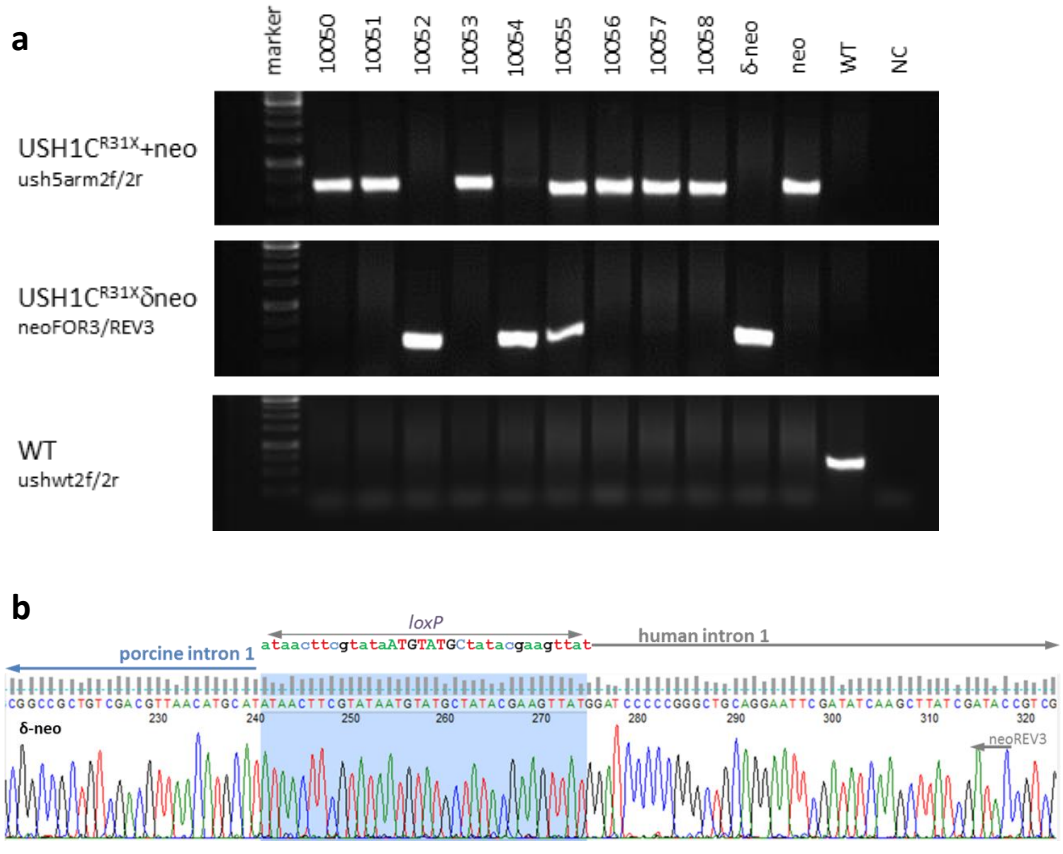

Figure 5: Representative genotyping of a founder litter. Primer pairs ush5arm2f/2r detect the modification plus the selection cassette, neoFOR3/REV3 show a deletion of neo cassette and ushwt2f/2r amplify the porcine USH1C gene (a). Animals with deleted neo cassette show a single lox site as a remnant (b).

Table 15: Breeding of USH1C pigs

sow	boar	birth	offspring	USH1C$^{-/-}$	USH1C$^{+/-}$	WT	
10051 (USH1C$^{-/-}$)	K91 (WT)	December 2019	AM1 - AM 12	-	12	-	*
10054 (USH1C$^{-/-}$)	K91 (WT)	March 2020	AM13 - AM23	-	11	-	*
10439 (USH1C$^{-/-}$)	10345 (CAG-iRFP/WT)	June 2020	11222 - 11234	-	13	-	
FK 32 (WT)	AM8 (USH1C$^{+/-}$)	October 2020	AM24 - AM27	-	1	3	*
AM11 (USH1C$^{+/-}$)	AM3 (USH1C$^{+/-}$)	December 2020	AM28 - AM35	1	3	4	*
AM12 (USH1C$^{+/-}$)	AM5 (USH1C$^{+/-}$)	January 2021	AM36 – AM42	0	n.d.	n.d.	*
10051 (USH1C$^{-/-}$)	AM1 (USH1C$^{+/-}$)	January 2021	AM43 – AM52	5	5	-	*
10439 (USH1C$^{-/-}$)	128 (WT)	January 2021	11657 - 11670	-	14	-	
10618 (USH1C$^{-/-}$)	10771 (WT)	February 2021	11703 - 11714	-	12	-	

* Litters produced at IAPG Libechov, Czech Republic; n.d.: not determined.

1.2. Genetic variation in USH1C breeding herds

Expansion of USH1C pigs was based on the available USH1C founder animals. Due to the vestibular dysfunction of these animals, mating was only possible by artificial insemination. The first mating at IAPG Libechov was performed with founder sow 10051, which contained the neo selection cassette in the modified locus and an unrelated WT boar of the Libechov minipig population. Although any offspring from this mating was expected to be heterozygous, the WT-allele was detected in only 8 out of 12 piglets with the primer pair ushwt2f/2r and the humanized allele was detected in only 7 out of 12 piglets with ush5arm2f/2r (Figure 6). As anticipated, PCR with neoFOR3/REV3 did not give evidence for a mutated fragment lacking the neo cassette. Similar results were found in genotyping of a second litter from a mating of a WT boar with sow 10054 at IAPG, which showed a deletion of the neo cassette. Not in all piglets a WT-allele could be detected with the primer pair ushwt2f/2r and only in some piglets the humanized allele was detected with the primer pair neoFOR3/REV3. PCR with ush5arm2f/2r did not show evidence for a mutated fragment containing the neo cassette, as expected (Figure 10e). The breeding, thus, revealed two independent genetic puzzles.

The failure to amplify the porcine WT allele was very likely caused by naturally occurring genetic variations in the pig population. Therefore, alternative PCRs were tested. Using a distinct forward primer (ush5arm1f) led to the same result, but using a different reverse primer (ush3arm1r) detected WT bands in all piglets of the litter of sow 10051 (Figure 7a). For evaluating the causative mutation, the

region around the binding site of primer ushwt2r was explored by Sanger sequencing and indeed revealed a single nucleotide polymorphism (SNP) (Figure 7b).

Furthermore, an insertion of a GGAT-quadruplet was detected 107 bp 3' of ushwt2f in all piglets that did not show a WT band in the genotyping PCR (Figure 8a). An influence of this 4nt-insertion on the formation of secondary structure in PCR fragments might have caused a decreased PCR efficacy for the alternative allele. Therefore, the thermodynamic stability of the different PCR products was calculated with Mfold (Figure 8b and c), a software used to predict secondary structures of DNA and RNA (ZUKER, 2003). Folding was simulated at 60°C, 50mM Na^+, and 2mM Mg^{2+}. Secondary structures of amplicons containing the GGAT insert appeared more stable and thus might impair PCR efficacy.

To improve genotyping of the WT allele, new primers were designed with the binding site of the forward primer being downstream of the GGAT-insertion and neither of the primer binding sites being affected by any of the known SNPs in the porcine *USH1C* locus. Different primer constellations were tested and eventually, the pair ushwt3f/3r was chosen for future genotyping (Figure 9).

The failure to amplify the mutated allele in all animals was more intricating. As the founder sow 10051 revealed a mutated band with ush5arm2f/2r but not with neoFOR3/REV3, the abundance of an allele with an excised neo selection cassette was not expected (Figure 5a). This was confirmed in the F1 animals as none of them produced a PCR product with neoFOR3/REV3 (Figure 6). Next, a long-ranging PCR detecting both the unaffected WT and the mutated allele, including the humanized fragment as well as the neo cassette, was performed. This PCR revealed that all animals contained a WT copy, but only the same seven animals as before showed the slightly larger mutated allele (Figure 10a). Sanger sequencing proved existence of the humanized exon 2 and surrounding intronic regions for piglets which showed a band in genotyping PCRs. Several other PCRs using primers in this region were performed, all of them delivering the same result, the abundance of the mutated allele in seven piglets and an unknown modification of the *USH1C* gene on the other allele (Figure 10d and e). A precise determination of the mutation at genomic level was not performed, but analysis was conducted at transcriptional level instead.

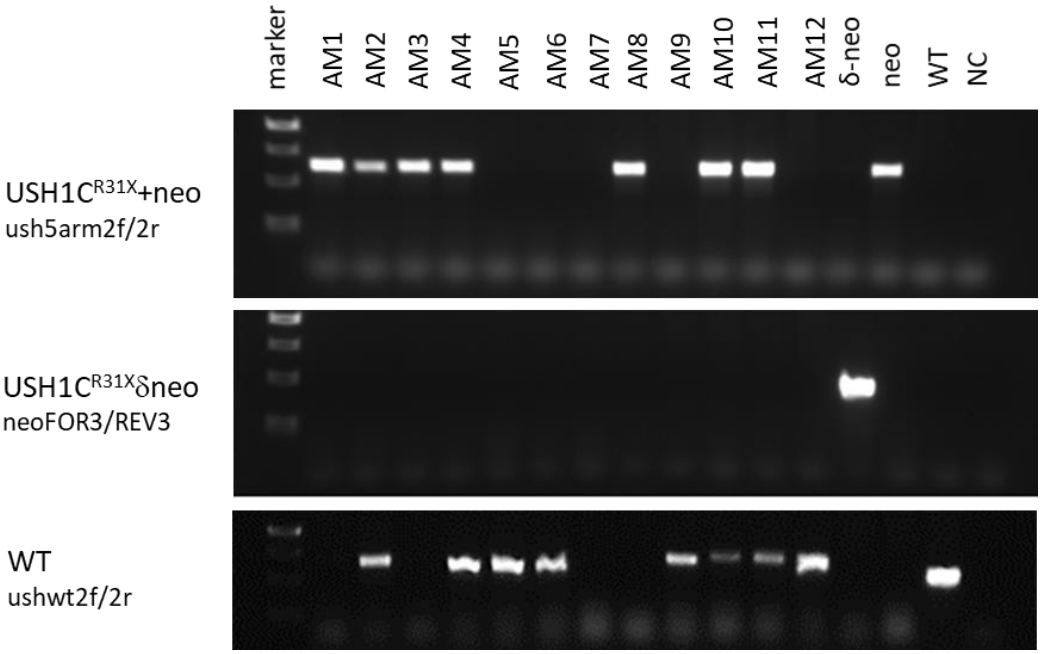

Figure 6: Genotyping of the first naturally bred litter of founder sow 10051. Surprisingly, the humanized allele containing the neo cassette was not detected in all piglets with primer pair ush5arm2f/2r. As expected, in no piglet a humanized allele with deleted neo cassette was detected with neoFOR3/REV3. Unexpectedly, PCR with ushwt2f/2r did not show evidence for the WT allele in all piglets.

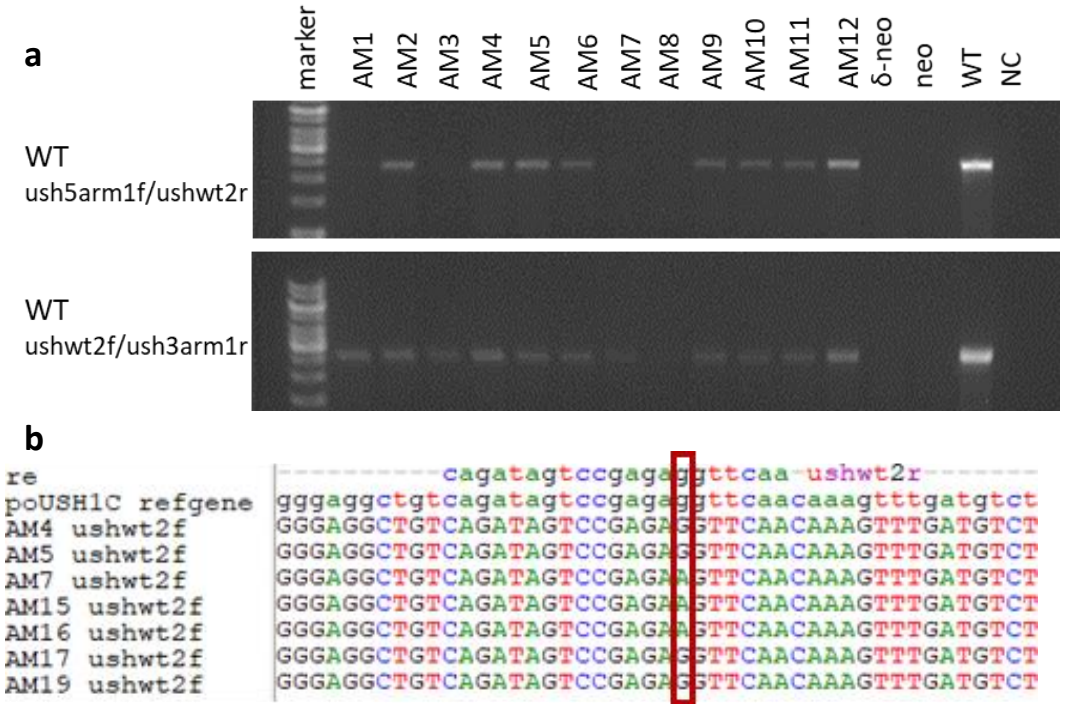

Figure 7: Single nucleotide polymorphism in breeding herds. As the WT PCR with ushwt2f/2r did not reveal signals for all piglets of a litter from a mating of a USH1C founder sow with a WT boar, other PCRs were tested. Using the forward primer ush5arm1f instead of ushwt2f led to the same result, whereas using ush3arm1r instead of ushwt2r as reverse primer detected bands in all piglets (a). Sanger sequencing showed a SNP at the binding site of ushwt2r (b).

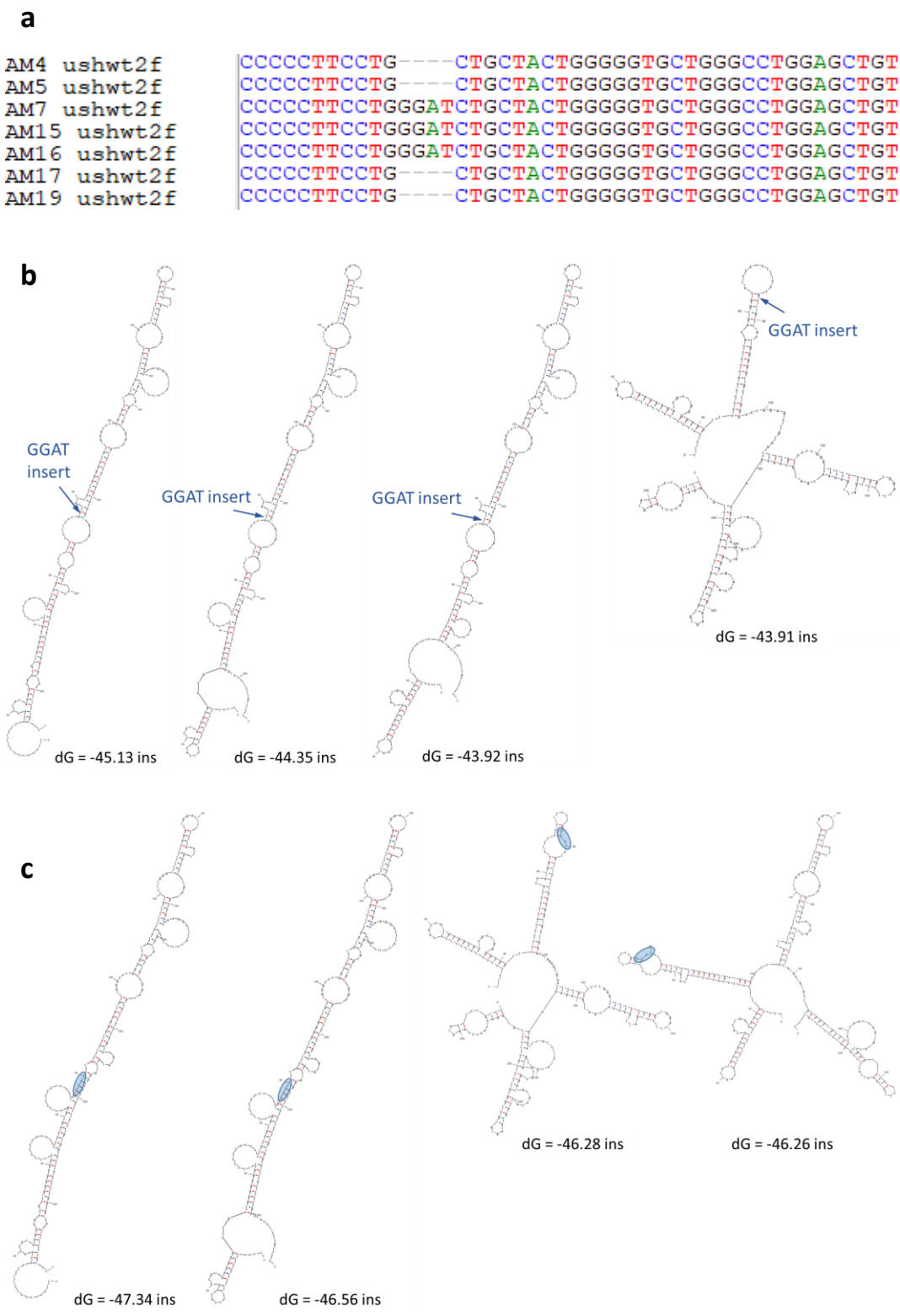

Figure 8: Insertion of additional nucleotides in breeding herds. Sanger sequencing revealed an insertion of GGAT in animals that had not shown a WT band in genotyping PCRs (a). Proposed secondary structure of genotyping PCR product without (b) or with GGAT insert (c), shown by blue circles, calculated by Mfold.

a

ushwt3f	**5′**- GGG AAT CAA ATG GAC ACG CC -**3′**
ushwt3r	**5′**- ATC TCC CCT CAC TAG GCC AC -**3′**
ushwt4f	**5′**- ATT CTG CCC TTG GGT TTT CCA -**3′**
ushwt4r	**5′**- GGC ATT TCC GGT CCT ATC CC -**3′**
ushwt5f	**5′**- CCA GTA AGT GTG CTG GGT CC -**3′**
ushwt5r	**5′**- CAG CCA GTG GTA GGA GCT TAT -**3′**

b

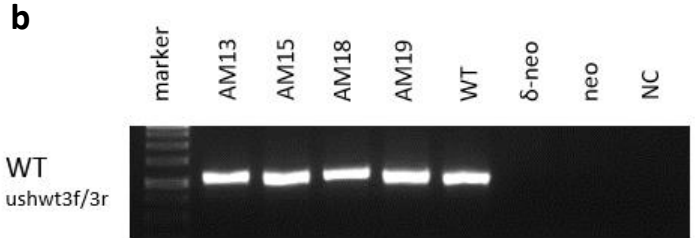

Figure 9: Optimizing WT-PCR for background variability. New primers tested for genotyping PCR (a), ushwt3f/3r were chosen for future genotyping (b).

a

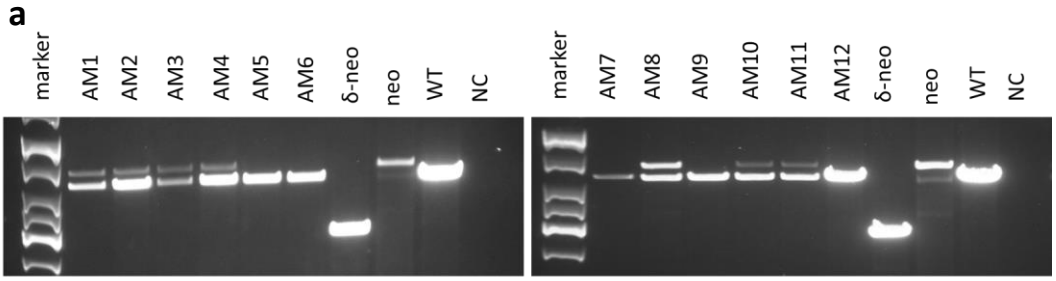

b

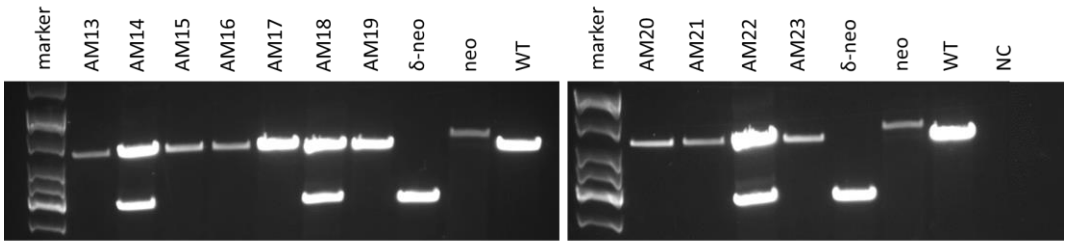

c

Denaturation	95 °C	2 min	
Denaturation	95 °C	20 s	30×
Annealing	58 °C	30 s	
Elongation	72 °C	3 min	
Final elongation	72 °C	3 min	
Termination	4 °C	5 min	

5x Herculase II reaction buffer	5 µL
5x Q-solution	5 µL
dNTPs (100 mM)	0.25 µL
ush5arm1f (10 µM)	0.4 µL
ush3arm2r (10 µM)	0.4 µL
Herculase II	0.5 µL
aq. dest.	12.45 µL
DNA template	1.1 µL

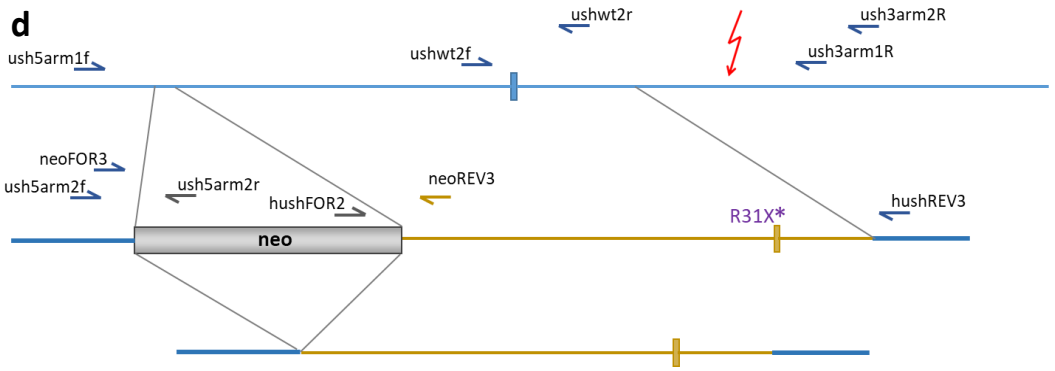

e

primer	ush5arm2f-ush5arm2r	hushFOR2-hushREV3	neoFOR3-neoREV3	ushwt2f-ushwt2r	ushwt2f-ush3arm1r	ush5arm1f-ushwt2r	ush5arm1f-ush3arm2r	ush5arm1f-ush3arm2r
bp	550	2000	450	550	2500	2000	2700 (δ-neo) 4600 (neo)	4200 (WT)
AM1	+	+	-	-	+	-	+	+
AM2	+	+	-	+	+	+	+	+
AM3	+	+	-	-	+	-	+	+
AM4	+	+	-	+	+	+	+	+
AM5	-	-	-	+	+	+	-	+
AM6	-	-	-	+	+	+	-	+
AM7	-	-	-	-	+	-	-	+
AM8	+	+	-	-	+	-	+	+
AM9	-	-	-	+	+	+	-	+
AM10	+	+	-	+	+	+	+	+
AM11	+	+	-	+	+	+	+	+
AM12	-	-	-	+	+	+	-	+
AM13	-	n.a.	-	-	+	n.a.	-	+
AM14	-	n.a.	+	+	+	n.a.	+	+
AM15	-	n.a.	-	-	+	n.a.	-	+
AM16	-	n.a.	-	-	+	n.a.	-	+
AM17	-	n.a.	-	+	+	n.a.	-	+
AM18	-	n.a.	+	+	+	n.a.	+	+
AM19	-	n.a.	-	+	+	n.a.	-	+
AM20	-	n.a.	-	-	+	n.a.	-	+
AM21	-	n.a.	-	-	+	n.a.	-	+
AM22	-	n.a.	+	+	+	n.a.	+	+
AM23	-	n.a.	-	-	+	n.a.	-	+
δ-neo	-	-	+	-	-	-	+	-
neo	+	+	-	-	-	-	-	-
WT	-	-	-	+	+	+	-	+

Figure 10: Unexpected genotypes in bred USH1C pigs. A long ranging PCR that amplified both the porcine and the humanized allele revealed WT bands for all piglets of the litters of founder sow 10051 (a) and of founder sow 10054 (b),

but also did not show the humanized fragment for all piglets. Cycler protocol and master mix composition for this long ranging PCR (c). Diagram showing binding site of primers used for further genotyping PCRs (d) and table displaying results of those PCRs (e); n.a.: not analyzed.

1.3. USH1C transcript splicing

For expression analysis at transcript level, RNA was isolated from tissue samples (Table 16) and reversely transcribed into cDNA. To detect correct splicing of exon 2 in RT-PCRs, the forward primer was required to be within exon 1 whereas the reverse primer was located downstream of exon 2. For this limitation, Primer-Blast and PrimerQuest did propose only a limited number of primer pairs. One of them, ushrt2f/2r, worked to a certain extent, but did not prove to be working consistently. Therefore, new primer constellations were tested, combining either ushrt2f with alternative reverse primers or ushrt2r with alternative forward primers (Table 17). Eventually, the new pair ushrt2f/urt4r performed robustly and was selected for future RT-PCRs.

Transcription of *USH1C* was detected in bowel segments, kidney, liver, olfactory epithelium, and retina of both WT and USH1C pigs. Lung, heart, spleen, pancreas, and brain revealed RT-PCR signals as well, but with weaker band intensities. Sanger sequencing confirmed that USH1C pigs express *USH1C* transcripts including the humanized exon 2 with the R31X mutation, but interestingly, also alternatively spliced RNA lacking exon 2 could be detected (Figure 11).

The reason for the latter became more obvious when heterozygous offspring from USH1C founder animals were euthanized and analyzed for *USH1C* transcripts: the heterozygous piglet 11224, comprising the humanized exon 2 without the neo cassette in genotyping (Figure 12a), showed transcripts from the porcine wildtype *USH1C* allele as well as transcripts comprising the humanized exon 2 with the R31X mutation (Figure 12b). The situation was different for heterozygous piglets 11225 and 11226, which both did not show a band for the humanized allele in genotyping PCR. In those piglets, RT-PCR of different organs revealed mainly transcripts comprising the porcine exon 2 and, at lower levels, transcripts lacking exon 2 (Figure 12c and d). The WT control piglet 11140 exclusively showed transcripts with the porcine exon 2 (Figure 12e).

Those findings led to the conclusion that by generating USH1C$^{-/-}$ founder pigs, only one *USH1C* allele in the pig primary cells had been correctly humanized, whereas the second allele had been affected by a larger deletion as a result of non-homologous end-joining after CRISPR/Cas mediated double strand break. This was not detected at the level of single cell clones for the limited amount of DNA available, but became obvious in F1 generation as a matter of Mendelian segregation. Effectively, this unexpected constellation of *USH1C* mutations did still result in the proposed consequences, namely the disruption of *USH1C* function. Thus, this molecular analysis proved the suitability of the model for *USH1C* dysfunction.

Table 16: Organs examined with RT-PCR.

	lung	heart	duodenum	jejunum	ileum	caecum
USH1C$^{-/-}$	1	4	11	11	7	7
USH1C$^{+/-}$	0	0	3	3	0	0
WT	1	2	8	8	5	5

	colon	liver	gall bladder	spleen	pancreas	c. renalis
USH1C$^{-/-}$	11	3	3	3	2	6
USH1C$^{+/-}$	3	0	0	0	0	3
WT	8	3	1	2	1	6

	m. renalis	adrenal gland	c. cerebri	c. cerebelli	retina	olfactory eptihelium
USH1C$^{-/-}$	6	2	2	5	12	2
USH1C$^{+/-}$	3	0	0	0	0	0
WT	6	2	2	2	6	2

Table 17: Primers tested for RT-PCR.

urt3r	**5′**- CCT TTG ATG AGG TGG GAG ATG AAG -**3′**
urt4r	**5′**- ACA GGG ATC AGG CCA ATG TG -**3′**
urt5f	**5′**- CCA TGG ACC GGA AGG TGG -**3′**
urt6f	**5′**- CCT GAA GGA GCG AGC TGT A -**3′**

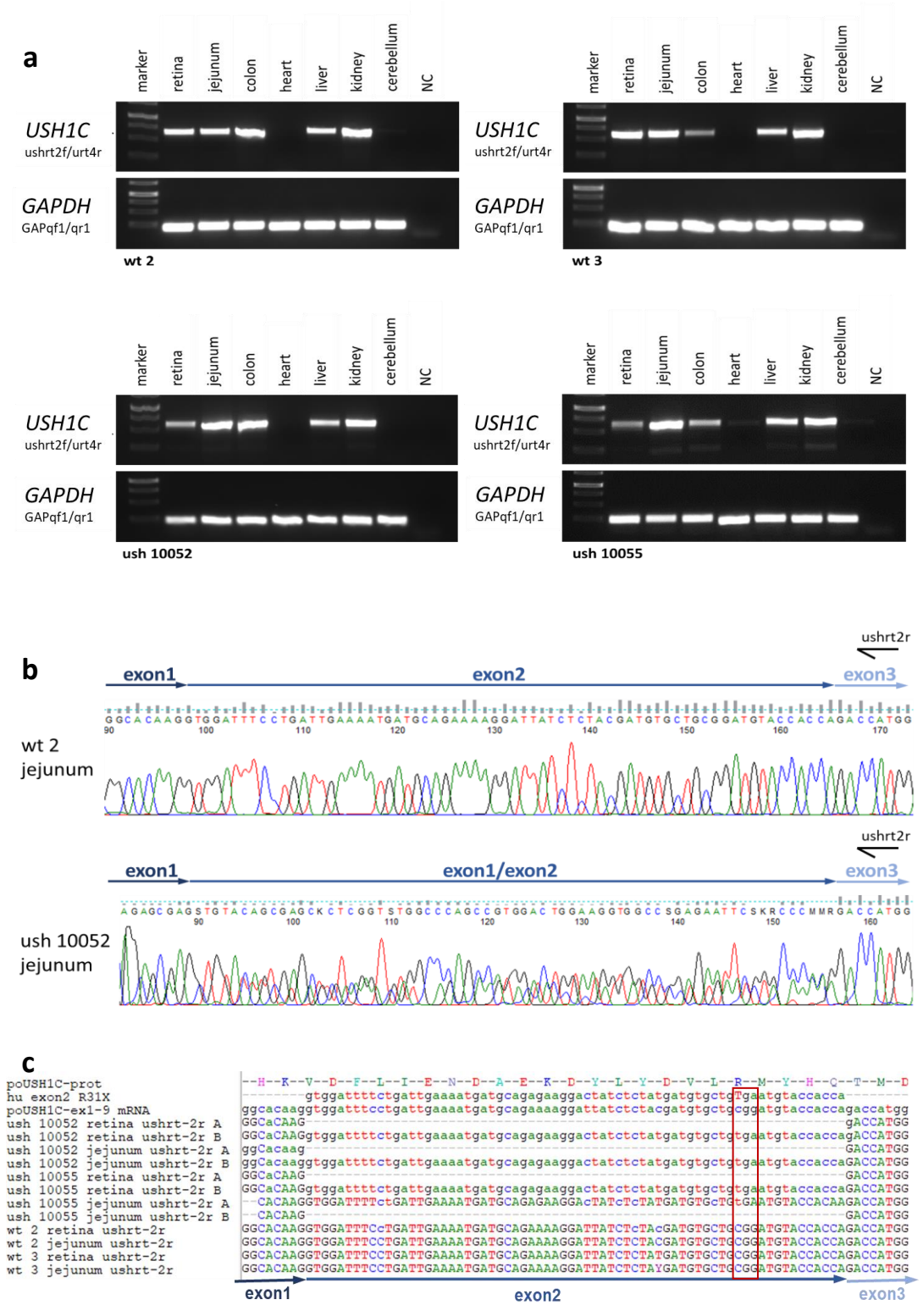

Figure 11: *USH1C* transcript splicing. RT-PCR confirmed transcription of *USH1C* in different organs of WT and USH1C pigs and cDNA was checked for integrity by amplification of the housekeeping gene *GAPDH* (a). Sanger sequencing showed overlaying sequences of the mutated exon 2 on exon 1 when sequenced with the reverse primer ushrt2r, indicating alternative splicing of exon 2 in USH1C pigs (b). Humanization of exon 2 in USH1C pigs with the TGA stop codon was deducted from the overlaying electropherograms (c).

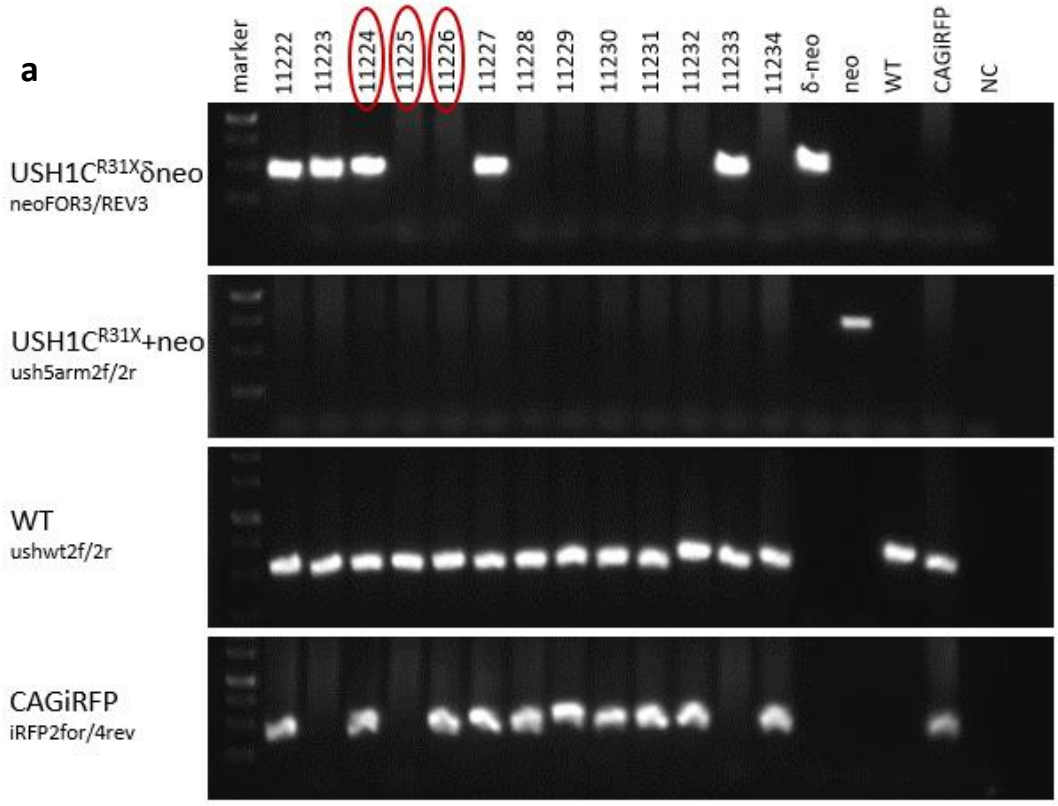
a
marker
11222
11223
11224
11225
11226
11227
11228
11229
11230
11231
11232
11233
11234
δ-neo
neo
WT
CAGiRFP
NC
USH1C^R31Xδneo
neoFOR3/REV3
USH1C^R31X+neo
ush5arm2f/2r
WT
ushwt2f/2r
CAGiRFP
iRFP2for/4rev

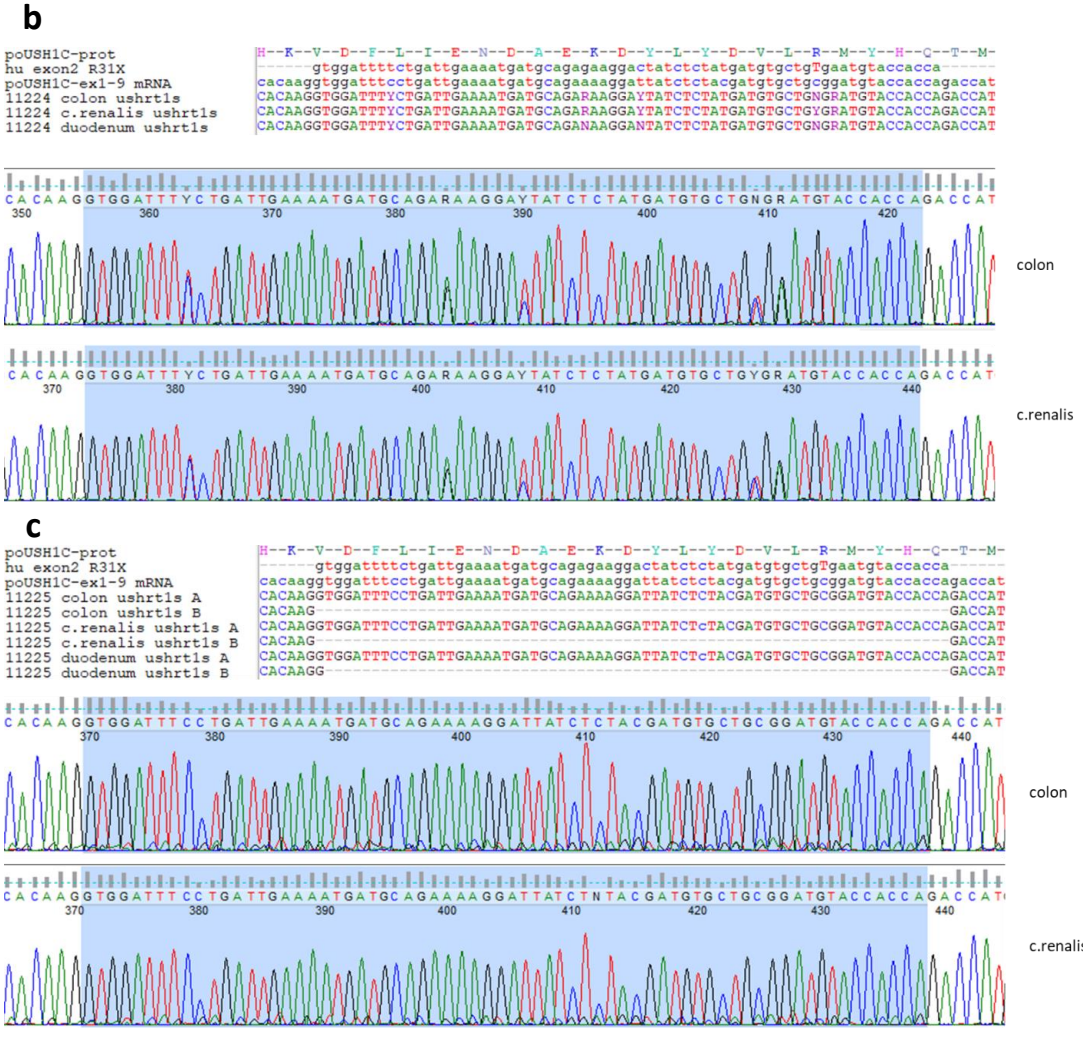
b
poUSH1C-prot
hu exon2 R31X
poUSH1C-ex1-9 mRNA
11224 colon ushrt1s
11224 c.renalis ushrt1s
11224 duodenum ushrt1s
colon
c.renalis
c
poUSH1C-prot
hu exon2 R31X
poUSH1C-ex1-9 mRNA
11225 colon ushrt1s A
11225 colon ushrt1s B
11225 c.renalis ushrt1s A
11225 c.renalis ushrt1s B
11225 duodenum ushrt1s A
11225 duodenum ushrt1s B
colon
c.renalis

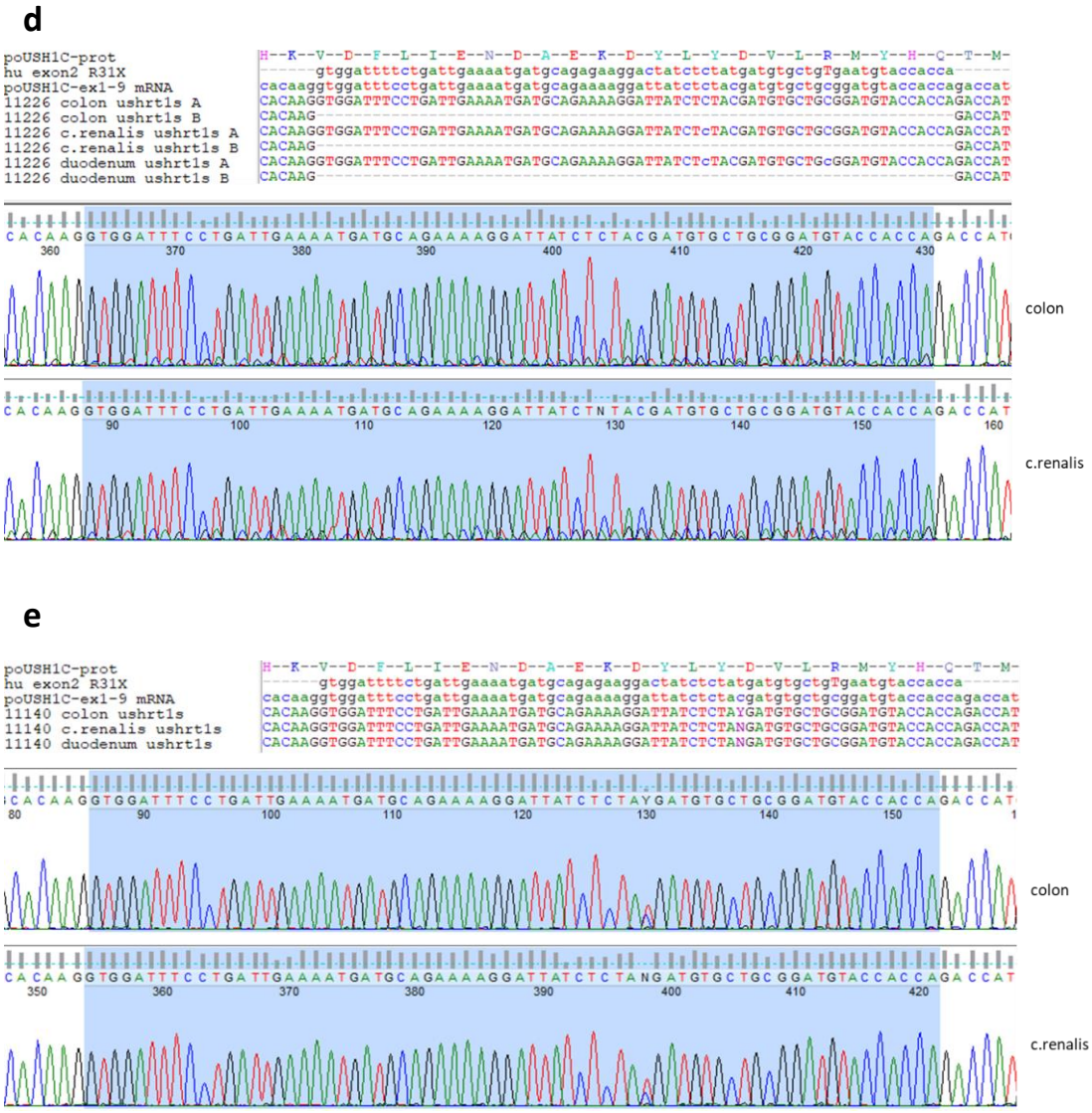

Figure 12: Transcriptional consequences of an unknown *USH1C* modification. Genotyping of the first naturally bred heterozygous USH1C litter in CiMM from a mating of sow 10439, which showed a deleted neo cassette and a CAG-iRFP boar (a). Sequencing of a piglet 11224 with confirmed humanized exon 2 showed transcripts comprising the humanized exon 2 and transcripts from the porcine *USH1C* gene (b). Sequencing of the piglets 11225 and 11226 without humanized exon 2 revealed transcripts from the porcine exon 2 and also transcripts lacking exon 2 (c and d). Sequencing of a WT piglet 11440 exclusively showed transcripts from the porcine *USH1C* (e).

1.4. Minor splicing artefacts

At a closer look, in most founder animals tested, additional bands with much lower intensity could be detected with RT-PCRs (Figure 13a). Bands were cut from the gel separately, cleaned up and sequencing revealed that the smaller bands represented transcripts with spliced out exon 2 – 4 (Figure 13b). This cryptic

splicing is likely a consequence of the unexpected deletion of a region around exon 2 on one allele in founder pigs. That finding is in line with other reports, which describe the occurrence of additional transcripts at low frequency once the original splice structure has been destroyed (PLOG et al., 2015).

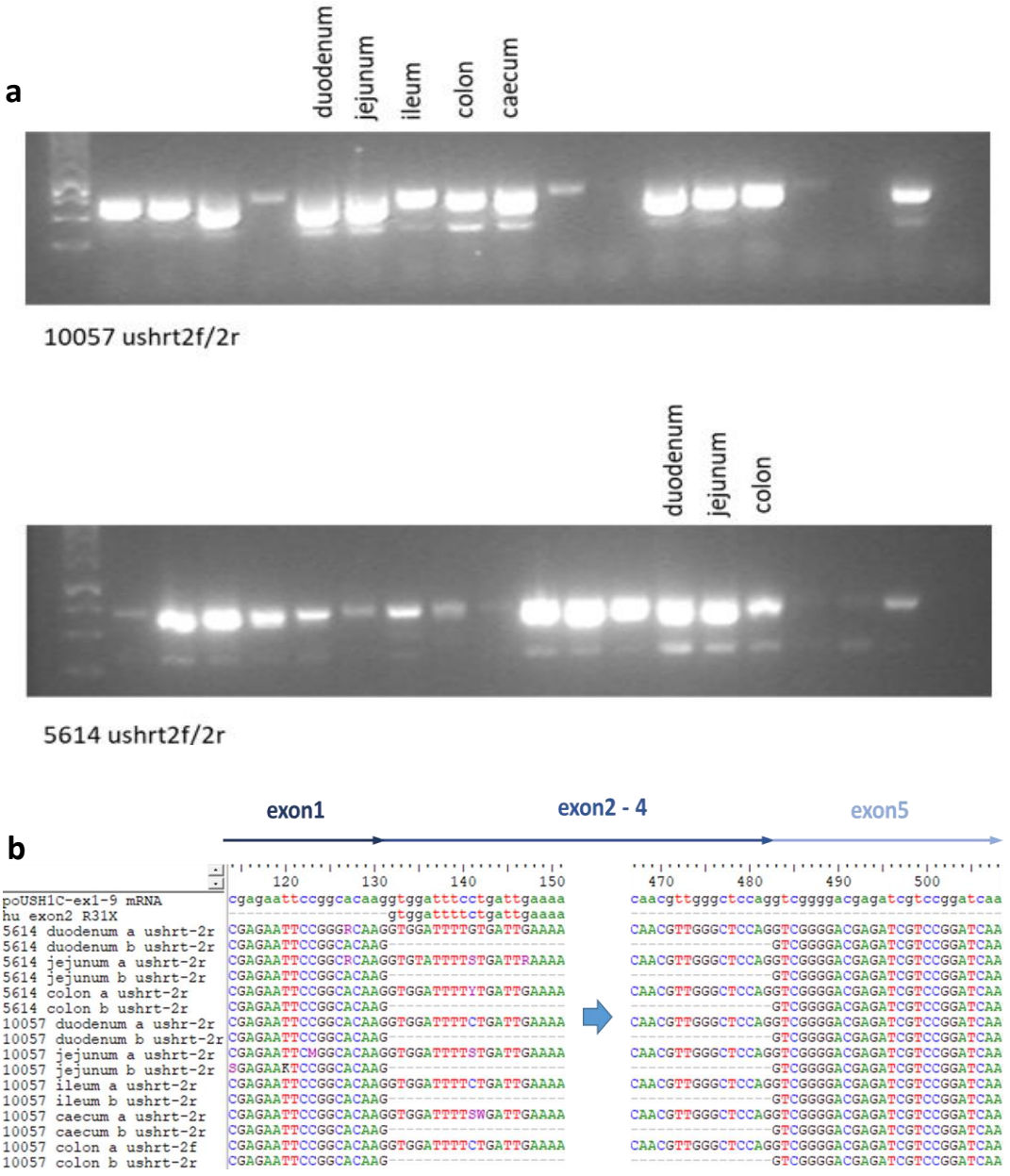

Figure 13: Minor splicing artefacts. In RT-PCR, additional bands with lower intensity were detected (a). For those weak bands, Sanger sequencing showed transcripts from which exon 2 – 4 had been spliced out (b).

2. Behavioral analyses

2.1. Obstacle course

2.1.1. Training of animals for the obstacle course

Five WT and five USH1C pigs were trained for the obstacle course. Training started when pigs were six months old and was performed three times a week. At the beginning, all pigs of one group were brought together to the part of the pigsty where the obstacle course was supposed to take place so they could get used to this new environment. Pigs of both groups were curious and explored their new surroundings. One USH1C pig was afraid to leave its pen initially, but it also got accustomed to walking out into the aisle. After a few visits to the training site, some obstacles were placed in the course. Then, the pigs were brought to the course in smaller groups of 2 - 3 animals. They all were interested in the obstacles, examining and playing with them. Thereafter, every pig was taken to the course individually and cookies were placed on the floor between the obstacles to lure them to cross the obstacles and walk to the end of the course. USH1C pigs took more time to reach the end and they also touched obstacles more often than WT pigs. However, every pig was looking forward to getting out of its pen and they seemed to enjoy training. Continuously, the number of cookies was reduced until only one cookie was left in the feed trough at the end of the course. After three weeks, when all pigs had learned to walk through the course to get their reward at the end, training was considered to be completed.

2.1.2. Obstacle course setup

After the training, five USH1C and five WT pigs were performing the course weekly over a period of four months. After a break of four months, the experiment continued for another month with the five WT and three USH1C pigs. The pigs were brought to the course individually in random order, they had to pass the obstacles and were rewarded with a cookie at the end. The course was performed 22 times under light condition (50 – 150 lx) and six times under dark condition (0.1 – 12 lx). Sometimes a pig had to be excluded from one test day because it was lame or turned around before getting to the end of the course. Only one pig finished all 28 runs (Table 18). Eleven different obstacles were used in the course (Figure 14). Pigs had to bypass obstacles that are more challenging for the vestibular system, such as the cavaletti or obstacles that are more demanding for

three-dimensional vision, like the blue barrel hanging from the ceiling. To prevent pigs from remembering the obstacles positions, obstacles were rearranged after most of the test days (Figure 15). In the last week, the course was conducted daily with the same obstacle setup, alternatingly in the light and in the dark, to see if there was a learning effect.

a

Number	Description	Symbol
1	Step board	
2	Cavaletti	
3	"F" formed out of poles	
4	Barrel hanging from the ceiling	
5	One pole diagonally through the couse	
6	Two poles diagonally through the course, forming "X"	
7	Barrel placed on the floor	
8	Two bars lenghwise behind each other	
9	Two bars forming "T"	
10	One elevated pole	
11	Short cavaletti	

b

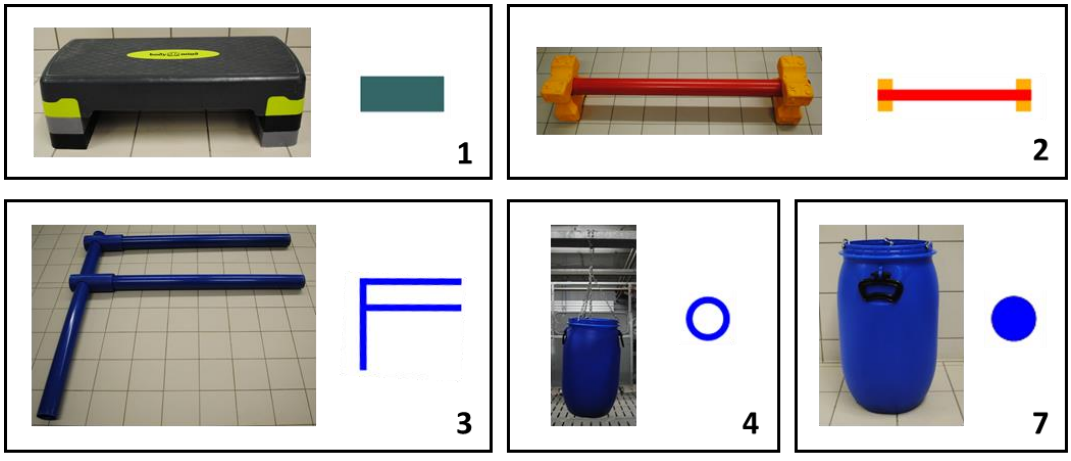

c

obstacle	1	2	3	4	5	6	7	8	9	10	11
light	20	20	12	17	1	1	11	3	1	1	1
dark	6	6	5	2	0	0	8	0	0	0	0

Figure 14: Obstacles. Table describing all obstacles used in the course (a), photographs and symbols of most frequently used obstacles (b) and table showing how often each obstacle has been used in the course (c).

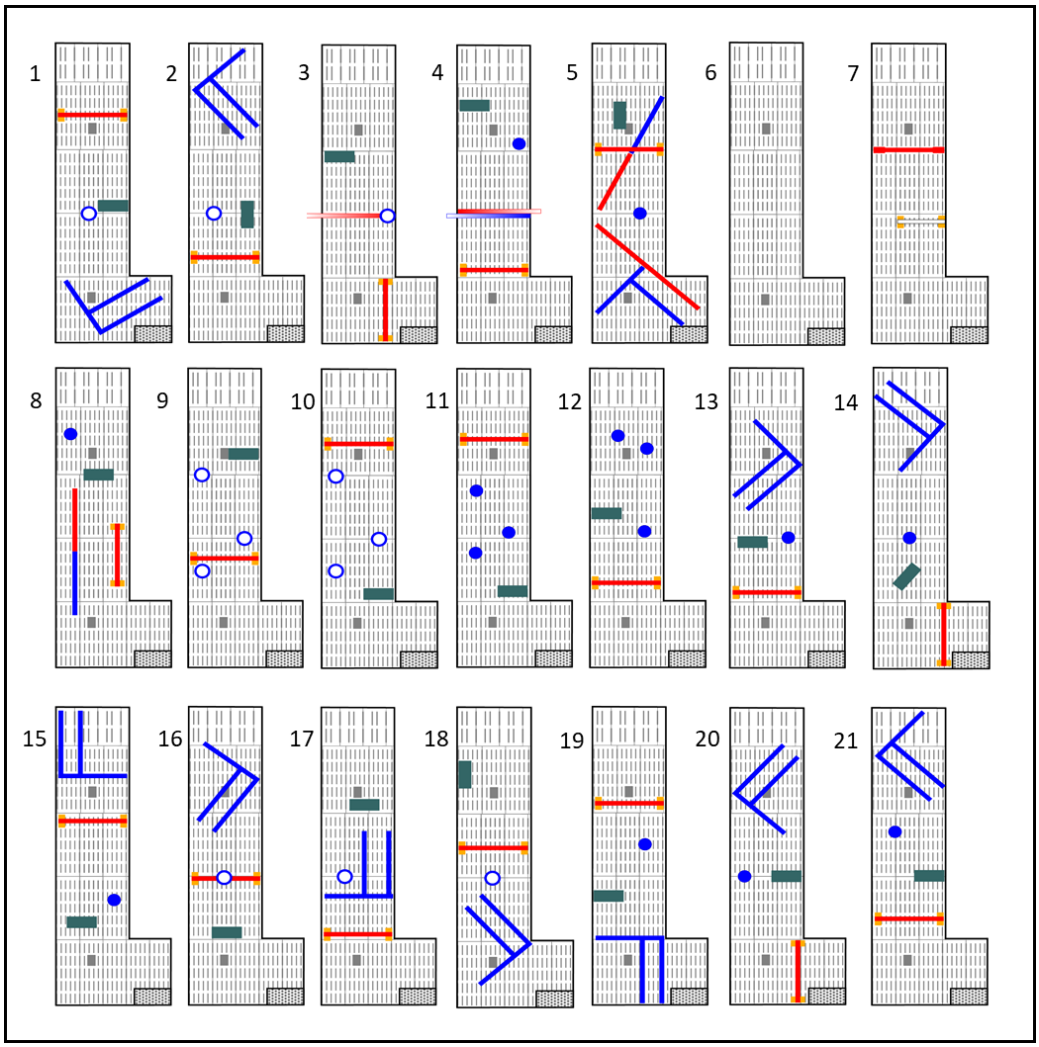

Figure 15: Obstacle course setups. 21 different obstacle setups were used.

Table 18: Number of runs per animal.

	WT					USH1C				
pig	1	2	3	4	5	6	7	8	9	10
light	21	21	19	21	21	20	15	22	17	16
dark	6	6	5	6	6	6	4	6	6	3

2.1.3. Obstacle course's data evaluation

2.1.3.1. Time

The time span from passing the start line with the snout to crossing the stop line with the snout was measured for each pig (Figure 19b). Time was measured in seconds, rounded to one decimal place (lower than five: rounded down, five or higher: rounded up, Supplementary Table 1). USH1C pigs needed significantly longer than WT pigs to complete the course in light conditions, but not in dark conditions. WT pigs needed more time to pass the course in the dark than in the light, whereas USH1C pigs were faster in the dark than in the light, but the differences were insignificant (Figure 16a – d).

In the last week, the course was performed daily with the same obstacle setup, but with alternating light and dark conditions, to exclude potential influences by different obstacle settings. It was expected that USH1C pigs should be equally fast in both light conditions, WT pigs should be faster in the light than in the dark. The time the pigs needed to pass the course could possibly diminish over the course of the week due to familiarization with the obstacle setup. However, it appeared that animals lost motivation under this regimen and data were even less informative than in the more complicated constellation used before (Figure 16e).

2.1.3.2. Obstacle contacts

As pigs use alternative sensing in addition to vision, snout contacts with obstacles or the walls enclosing the course could be interpreted as alternative orientation. However, classifying the contact events was difficult, and hence, following definitions were used: (i) the number of total contacts included both touching of obstacles and touching of walls; (ii) when the pig was playfully nudging one obstacle more than once in the same spot, it was still considered as one touch; (iii) when a pig had contact with one obstacle at distinct positions, each touch was counted separately; (iv) in the case a pig was stroking along one barrier with its snout, it was considered as two touches (Supplementary Table 2 and Supplementary Table 3). By using these considerations, USH1C pigs touched obstacles significantly more often than WT pigs in light conditions and to a lesser extent also in dark conditions (Figure 17). Contacts were also evaluated for each of the most frequently used obstacles. The step board, the cavaletti, the blue "F", and barrels hanging from the ceiling or placed on the floor were all touched

significantly more often by USH1C pigs than by WT pigs in the light (Figure 18).

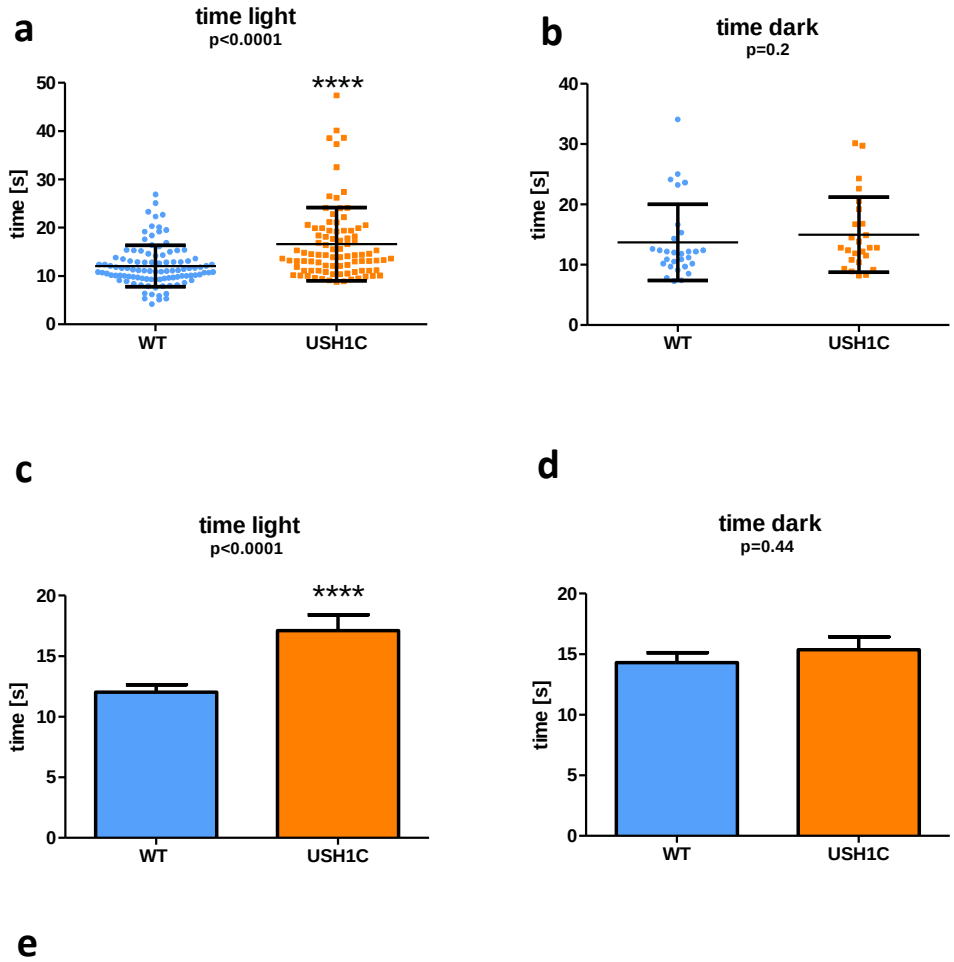

e

	WT					USH1C		
Pig	1	2	2	4	5	6	8	9
Day 1 light	9.4	11	11.6	11.3	9.5	10.2	13.9	11.9
Day 2 dark	11.8	10.5	25	10.9	10.9	8.9	9.2	12.2
Day 3 light	12.4	11.7	23.3	9.5	10	10	9.4	-
Day 4 dark	9.7	10.2	-	12.6	7.3	9.3	8.2	19.2
Day 5 light	7.6	10.1	-	10.8	10.2	11.1	8.8	-

Figure 16: Times. WT pigs (mv: 12.08, sd: 4.28) are significantly faster than USH1C pigs (mv: 16.61, sd: 7.6) in light condition (a), but there is no significant difference between WT pigs (mv: 13.70, sd: 6.33) and USH1C pigs (mv: 14.98, sd: 6.22) in dark condition (b) tested by Mann-Whitney-U test. Similar results were obtained using generalized linear models not taking all data into account: WT pigs (mv: 12.02, se: 0.62) are significantly faster than USH1C pigs (mv: 17.1, se: 1.32) in light condition (c), but there is no significant difference between WT pigs (mv: 14.3, se: 0.82) and USH1C pigs (mv: 15.36, se: 1.08) in dark conditions (d). Table showing times pigs needed to complete the course in the last week with same obstacle setup (e).

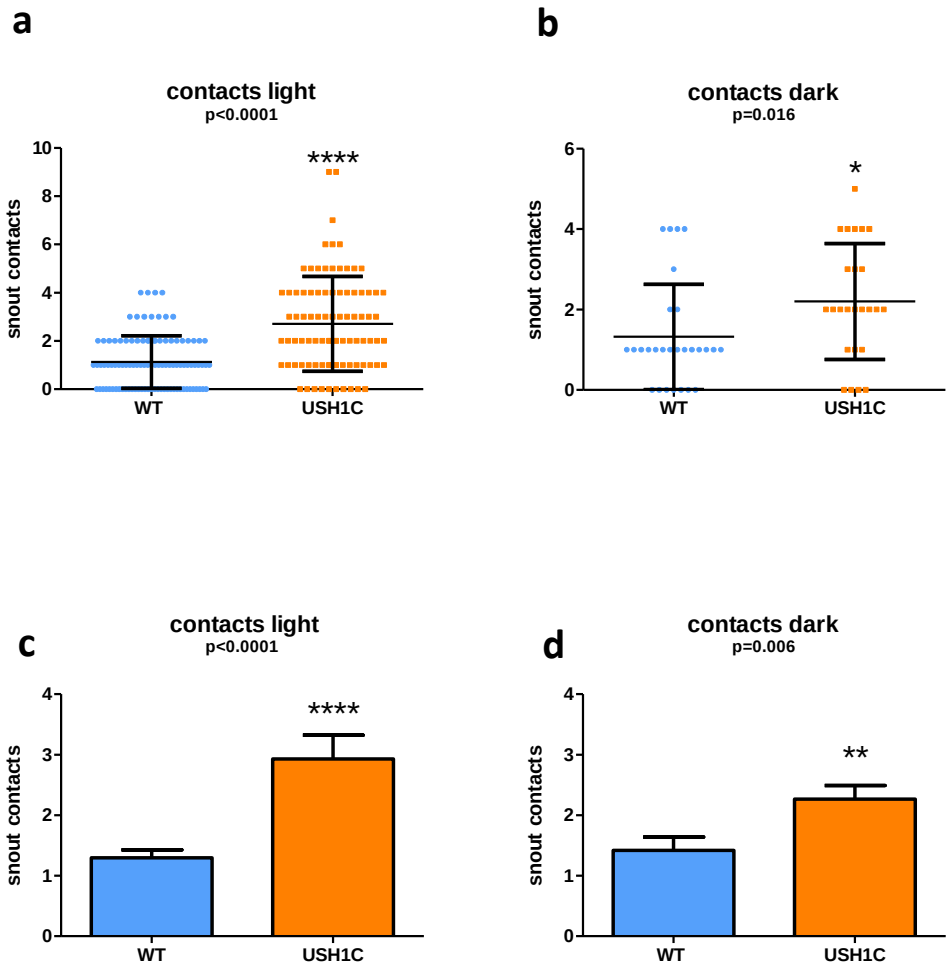

Figure 17: Obstacle contacts. USH1C pigs (mv: 2.71, sd: 1.96) touched obstacles significantly more often than WT pigs (mv: 1.31, sd: 1.09) in light condition (a), and USH1C pigs (mv: 2.2, sd: 1.44) also touched obstacles significantly more often than WT pigs (mv: 1.32, sd: 1.31) in dark conditions (b), tested by Mann-Whitney-U test. Similar results were obtained using generalized linear models not taking all data into account: USH1C pigs (mv: 2.93, se: 0.39) touched obstacles significantly more often than WT pigs (mv: 1.3, se: 0.13) in light condition (c), and USH1C pigs (mv: 2.27, se: 0.22) also touched obstacles significantly more often than WT pigs (mv: 1.42, se: 0.22) in dark conditions (d).

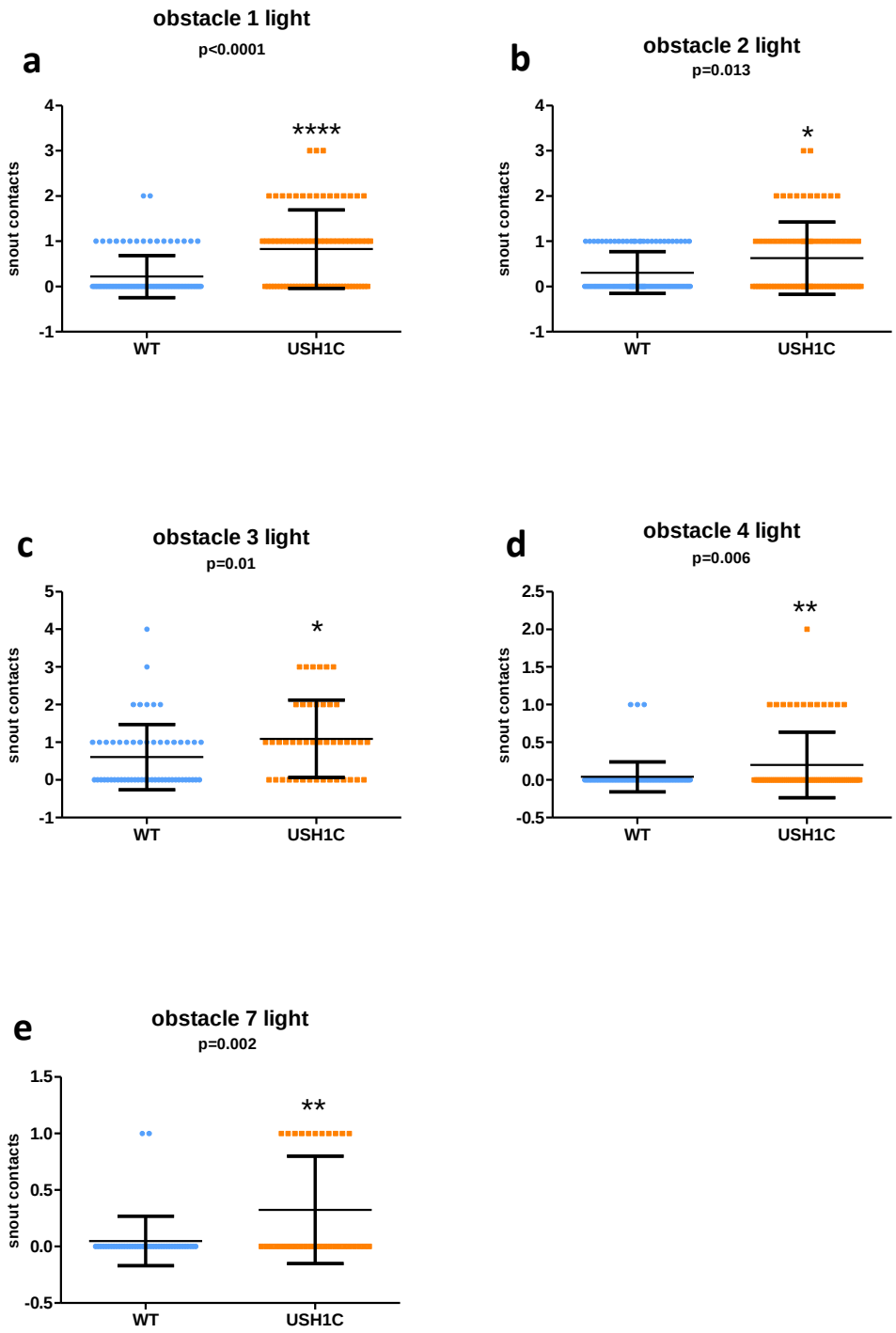

Figure 18: Contacts of most frequently used obstacles in the light. The step board was touched significantly more often by USH1C pigs (mv: 0.83, sd: 0.87) than by WT pigs (mv: 0.22, sd: 0.47) (a), the cavaletti was touched significantly more often by USH1C pigs (mv: 0.63, sd: 0.81) than by WT pigs (mv: 0.31, sd: 0.46) (b), the blue "F" was touched significantly more often by USH1C pigs (mv: 1.09, sd: 1.03) than by WT pigs (mv: 0.61, sd: 0.87) (c), the barrel hanging from ceiling was touched significantly more often by USH1C pigs (mv: 0.2, sd: 0.44) than by WT pigs (mv: 0.04, sd: 0.2) (d), the barrel placed on floor was touched significantly more often by USH1C pigs (mv: 0.32, sd: 0.47) than by WT pigs (mv: 0.05, sd: 0.22) (e), tested by Mann-Whitney-U test.

2.1.3.3. Trajectories

Aiming at analyzing the movement of a pig in the obstacle course in a more holistic manner, the courses of each run were compared in trajectory analysis. To see which route the animals took through the obstacle course, a plan of the course was plotted by measuring the positions of gaps in the slatted floor and the dimensions of the course. A map at a scale of 1:10 was drawn (Macromedia FreeHand MX). Position and time of each step of the right and left forelimb was noted in the plan after watching the videos (VLC media player) of each pig and each test day (Figure 19b). Then the X and Y coordinate of every footstep was transferred to an Excel file with the corresponding time (Figure 19c). Gianluca Santamaria, Clinic for Cardiology, TU Munich, analyzed the data set with the R package TrajR. First, the data were imported and then smoothed by applying a Savitzky-Golay smoothing filter to avoid any source of noise (SAVITZKY & GOLAY, 1964; LUO et al., 2005). To characterize the trajectories, all functions of the TrajR packages were then called (MCLEAN & SKOWRON VOLPONI, 2018). Motion parameters like tortuosity, straightness, speed, distance, length, and duration were evaluated.

Several of those parameters describe the 2-dimensional structure of a run. TrajLength shows the total length of the trajectory, while TrajDistance describes the straight-line distance from beginning to end of the trajectory. Emax (maximum expected displacement) is an index of straightness, indicating how abruptly direction is changed. Higher Emax values imply straighter paths. Sinuosity, in contrast, measures how much animals sway around the most direct line from the start to the end. Greater numbers indicate more bending in the path.

Both TrajLength and TrajDistance were significantly longer for USH1C pigs than for WT pigs while Emax was significantly smaller for USH1C pigs and sinuosity did not show significant differences (Figure 20a - d). This indicates that WT pigs could see the obstacles from a distance, as they tried to avoid them and walked around them. In contrast, USH1C pigs could not recognize the obstacles in advance, they walked on a relatively straight line through the course towards the estimated goal, the feed trough. In case they were suddenly confronted with an obstacle, they abruptly changed direction. Furthermore, TrajDuration showed that USH1C pigs spend significantly more time in the course than WT pigs, confirming the data from 2.1.3.1, as their mean speed is significantly slower. In

addition, USH1C pigs' step length is also significantly shorter than WT pigs' step length (Figure 20e – g).

To conclude, WT pigs move faster, more bending, and smoother, as they have a good overlook, they pass the obstacles more effectively and skillfully. USH1C pigs are slower and less foreseeing, they aim more directly for the cookies at the end of the course and walk around obstacles when they are appearing.

a

b

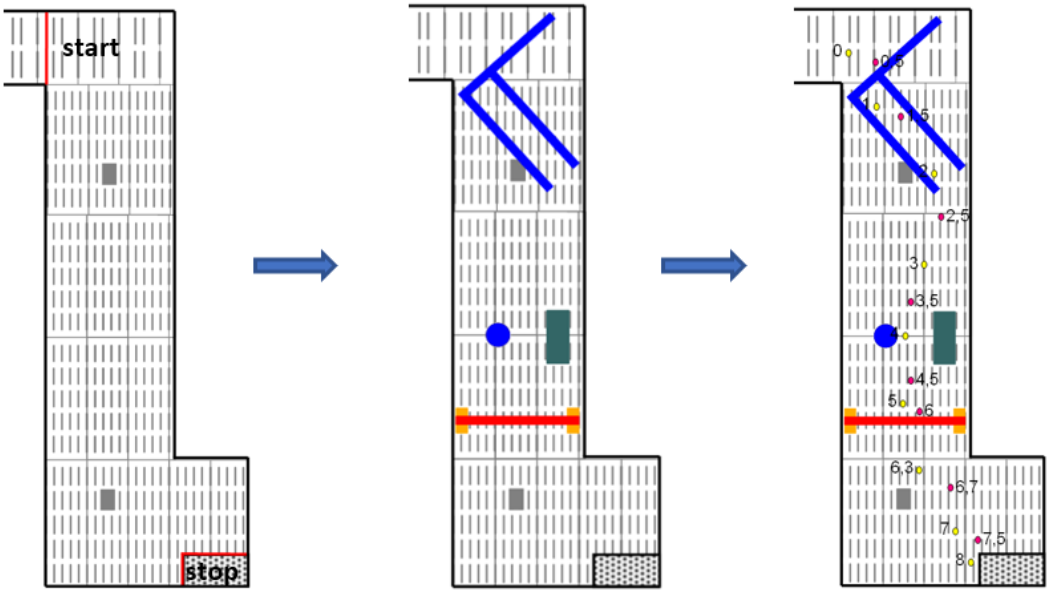

c

ID (PIG)	group	experiment No	course number	light condition	time	left foot x coord	left foot y coord	right foot x coord	right foot y coord	obstacle 1 contacts	obstacle 2 contacts	obstacle 3 contacts	obstacle 4a contacts
3	control	25.07.2018	2	light	0			-7.0	4.3	0	0	0	0
3	control	25.07.2018	2	light	0.5	-3.7	3.3			0	0	0	0
3	control	25.07.2018	2	light	1			-3.8	-2.1	0	0	0	0
3	control	25.07.2018	2	light	1.5	-0.9	-8.3			0	0	0	0
3	control	25.07.2018	2	light	2			3.4	-10.3	0	1	0	0
3	control	25.07.2018	2	light	2.5	4.4	-15.5			0	0	0	0
3	control	25.07.2018	2	light	3			2.1	-21.2	0	0	0	0
3	control	25.07.2018	2	light	3.5			0.6	-26.0	0	0	0	0
3	control	25.07.2018	2	light	4			-0.2	-30.0	0	0	0	0
3	control	25.07.2018	2	light	4.5	0.5	-35.6			0	0	0	0
3	control	25.07.2018	2	light	5			-0.6	-38.6	0	0	0	0
3	control	25.07.2018	2	light	6	1.5	-39.4			0	0	0	0
3	control	25.07.2018	2	light	6.3			1.5	-46.5	0	0	0	0
3	control	25.07.2018	2	light	6.7	5.3	-48.5			0	0	0	0
3	control	25.07.2018	2	light	7			6.0	-54.1	0	0	0	0
3	control	25.07.2018	2	light	7.5	8.7	-55.2			0	0	0	0
3	control	25.07.2018	2	light	8			8.0	-58.0	0	0	0	0

Figure 19: Path analysis. USH1C pig in the obstacle course (a). Map of the slatted floor with red lines indicating start and stop of time measurement, map showing obstacle setup and route a pig took through the course, yellow dots indicate the positions of the right forelimb, red dots the positions of the left forelimb with the time (in seconds) when the pig touched the floor (b). Data in excel file for this animal (c).

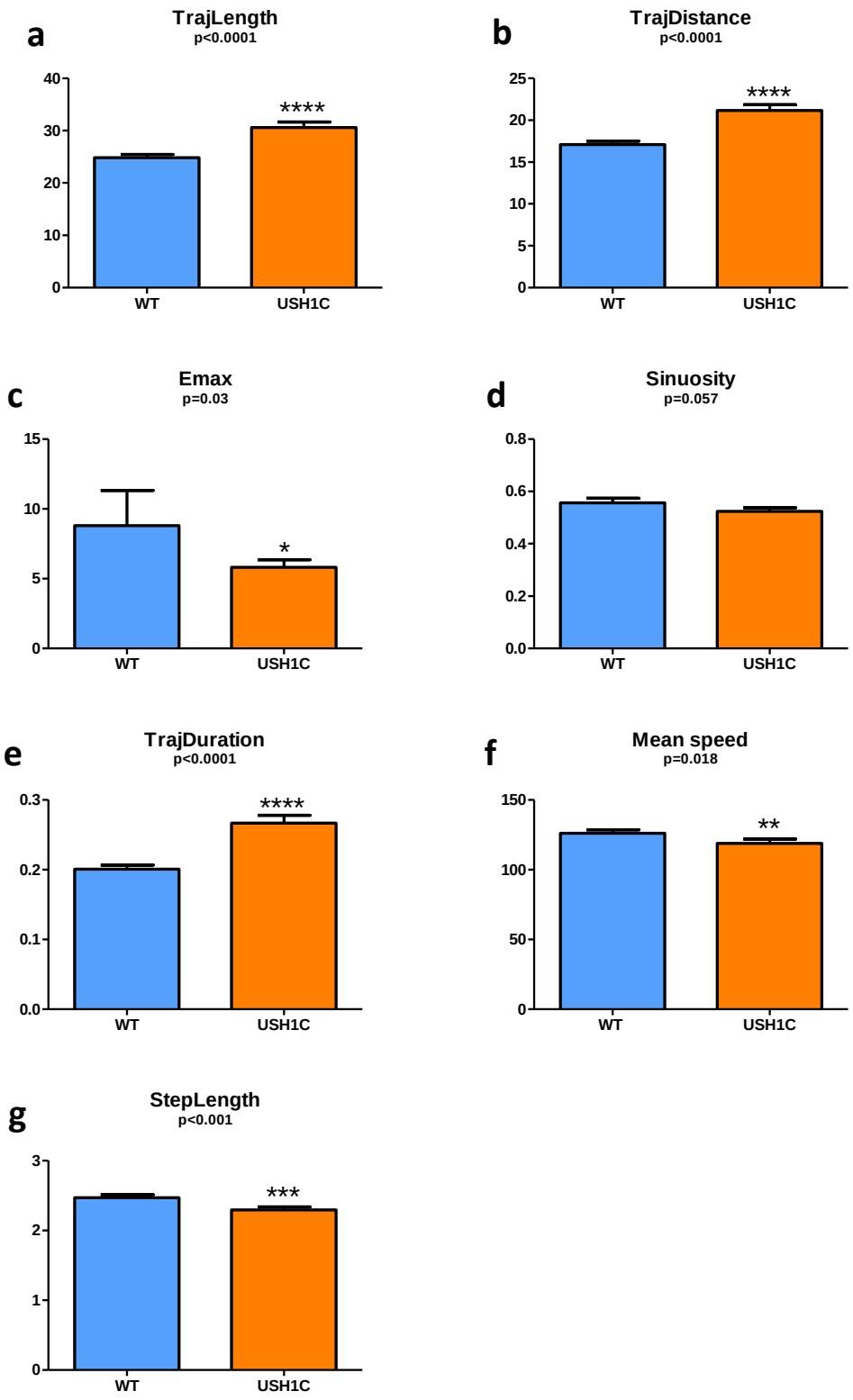

Figure 20: Trajectory analysis in the light. TrajLength is significantly longer for USH1C pigs (mv: 30.61, se: 1.05) than for WT pigs (mv: 24.81, se: 0.63) (a), TrajDistance is significantly longer for USH1C pigs (mv: 21.16, se: 0.68) than for WT pigs (mv: 17.1, se: 0.42) (b), Emax is significantly lower for USH1C pigs (mv: 5.82, se: 0.53) than for WT pigs (mv: 8.8, se: 2.54) (c), sinuosity is lower for USH1C pigs (mv: 0.52, se: 0.01) than for WT pigs (mv: 0.56, se: 0.02) (d), TrajDuration is significantly longer for USH1C pigs (mv: 0.27, se: 0.01) than for

WT pigs (mv: 0.2, se: 0.006) (e), mean speed is significantly slower for USH1C pigs (mv: 119.0, se: 3.0) than for WT pigs (mv: 126.1, se: 2.41) (f), StepLength is significantly shorter for USH1C pigs (mv: 2.3, se: 0.04) than for WT pigs (mv: 2.47, se: 0.04) (g). Y-axis of the parameters are given according the TrajR output, data were tested with Mann-Whitney-U test. TrajR analyses were performed by Gianluca Santamaria.

2.2. Barrier course

2.2.1. Training of animals for the barrier course

Two groups of animals were trained for this type of course. Group 1 consisted of one USH1C and two WT pigs, the training started when pigs were three months old. Group 2 was composed of one USH1C and six WT pigs, training for those animals started at an age of two months. For both groups, training took place three times a week. To begin with, pigs of one group were brought together to the aisle of the pigsty where the course was planned to take place to get used to the new surroundings. Initially, pigs were hesitant to leave their pen, but then they seemed to enjoy training. In contrast to training for the obstacle course, these pigs were trained in the empty aisle until they realized that their reward was only placed at the end of the course before obstacles were positioned in the course. Additionally, the pigs did not like cookies, so banana juice, applesauce, dried bananas, popcorn, and chips were tested as alternative rewards. Banana juice was identified as the preferred treat. To further motivate the animals, the experiments were conducted in the morning before feeding.

After the pigs had learned to walk straight to the end of the course, initially in groups, then on their own, first barriers were put on the aisle. Some pigs were ignoring them, walking directly to the end of the course, whereas other pigs were examining them. Then number of barriers was increased until all ten boards were included in the course. All pigs were able to learn to go around the barriers to the end. However, USH1C pigs had more problems learning this task, they were turning around, walking back more often before reaching the end and walked in circles. At first, the USH1C pig of group 1 was not even able to find its way around the barriers to the end, it was nervous and walked in circles when confronted with the boards. But after following a WT pig through the course several times, it became adapted to the challenge and managed to go through the course on its own. Training was considered to be completed when animals walked

straight through the barrier course without hesitating or stopping for at least two times in a row. The training lasted seven weeks for group 1 and four weeks for group 2.

2.2.2. Barrier course setup

Following the training period, the course was conducted weekly. Group 1 was tested over a period of 13 months with a break of two months in between. The test was conducted 25 times under light condition (average of 135 lx) and 16 times under dark condition (average of 2 lx). One WT pig of group 1 had to be excluded due to motivation problems. Group 2 was tested over a period of ten months with a break of one month in between and performed the course 16 times under light and 11 times under dark condition.

The animals went into the course individually in random order. Pigs had to bypass ten boards that were placed in the middle, left, and right side of the aisle. Four different setups of barriers were used alternatingly (Figure 21). Dark adaptation of pigs was difficult to achieve as the infrastructure in the pigsty allowed the switching off of the light in the waiting zone and the course itself, but not in the transition zone in between (>15m).

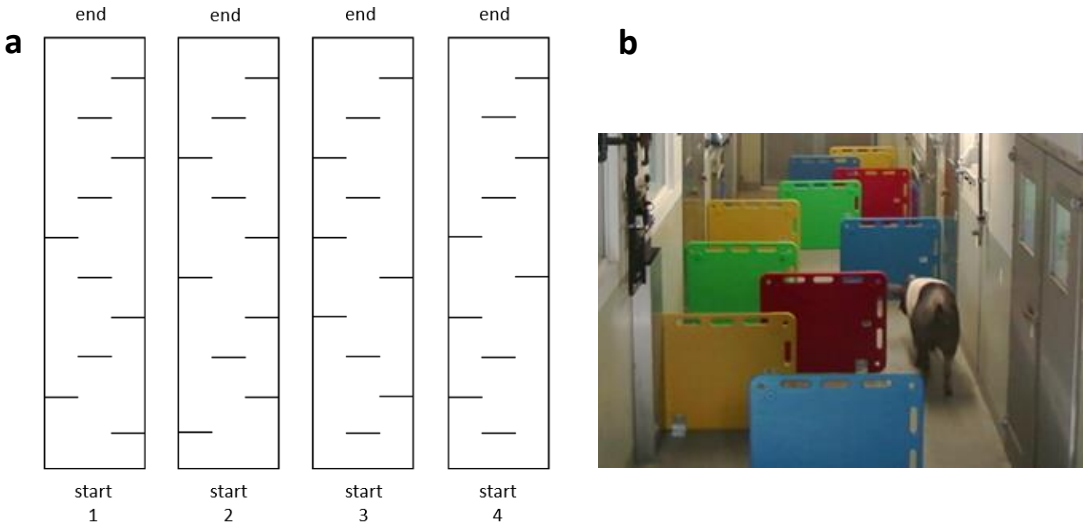

Figure 21: Barrier course. Different barrier setups (a) and USH1C pig in the course (b), adapted from BARONE et al. (2018).

2.2.3. Barrier course's data evaluation

For limited availability of USH1C animals, evaluation of pigs' behavior in the barrier course was impaired. Thus, the data of two USH1C pigs of group 1 and 2 were compared to the data of seven WT pigs of group 1 and 2 and statistical analysis was not performed.

2.2.3.1. Time

Times animals needed to go through the course were measured in seconds to one decimal place, from pig moving across the start line until reaching the food bowl at the end of the course. Both USH1C and WT pigs needed more time to complete the course in dark condition than in light condition. Under both conditions, USH1C animals seemed slower, but deviation was also more pronounced (Figure 22a - b).

2.2.3.2. Barrier contacts

Every barrier contact was documented. Lateral contacts meant a touching of the boards with shoulders or hips. When an animal was touching the barrier with its head or snout, the contact was identified as a frontal contact. Lateral contacts happened mostly because the pigs were too eager to reach their reward at the end of the course and ran too fast through the course to pass around the barriers. It is striking that WT pigs touched the boards almost equally often in the light and in the dark, but USH1C pigs touched them more often in the dark than in the light (Figure 22c - d). Frontal contacts occurred almost exclusively when USH1C pigs were passing the barrier course in the dark (Figure 22e – f). It is also noteworthy that USH1C pigs in general walked up closer to barriers before they walked around them, whereas WT pigs moved more foreseeing.

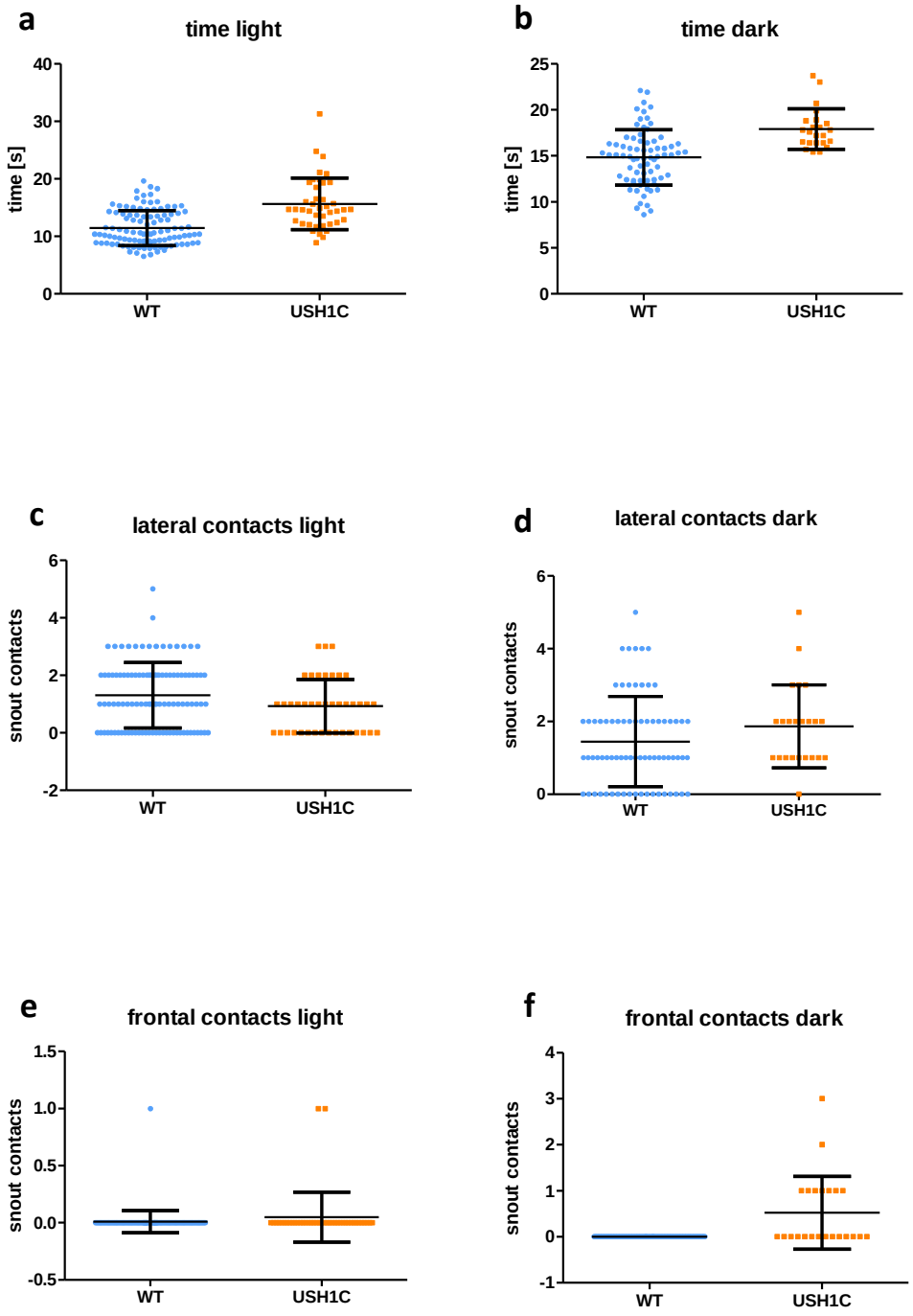

Figure 22: Times and contacts. USH1C pigs (mv: 15.63, sd: 4.5) were slower than WT pigs (mv: 11.44, sd: 3.06) in light condition (a) and USH1C pigs (mv: 17.91, sd: 2.2) were slower than WT pigs (mv: 14.83, sd: 3.02) in dark condition (b). USH1C pigs (mv: 0.93, sd: 0.93) touched barriers laterally less often than WT pigs (mv: 1.31, sd: 1.14) in light condition (c), but USH1C pigs (mv: 1.87, sd: 1.14) touched barriers laterally more often than WT pigs (mv: 1.45, sd: 1.24) in dark condition (d). Neither USH1C pigs (mv: 0.05, sd: 0.21) nor WT pigs (mv: 0.009, sd: 0.1) frequently touched barriers frontally in light condition (e), in dark condition, WT pigs never touched barriers frontally, in contrast to USH1C pigs (mv: 0.52, sd: 0.8) (f).

2.2.3.3. Turns and circles

It was also documented when an animal was turning around and going back before reaching the end of the course. Here, turns in the course and turns in front of the course were differentiated. Those runs were excluded and the pigs were sent back into the course after turning around. The new run was then recorded with contacts and times when the pig walked through the course to the end. Furthermore, it was documented when a pig was circling. Runs were not excluded as long as pigs were just walking in circles and not going back, time measurement was continuing during the circling behavior. In addition, it was recorded when an animal was walking in circles in front of the start line before entering the course, however, time measurement only began when the pig was walking across the start line. WT pigs never walked in circles and very rarely turned around before reaching the end of the course; in USH1C pigs, this behavior occurred almost exclusively in the dark (Figure 23).

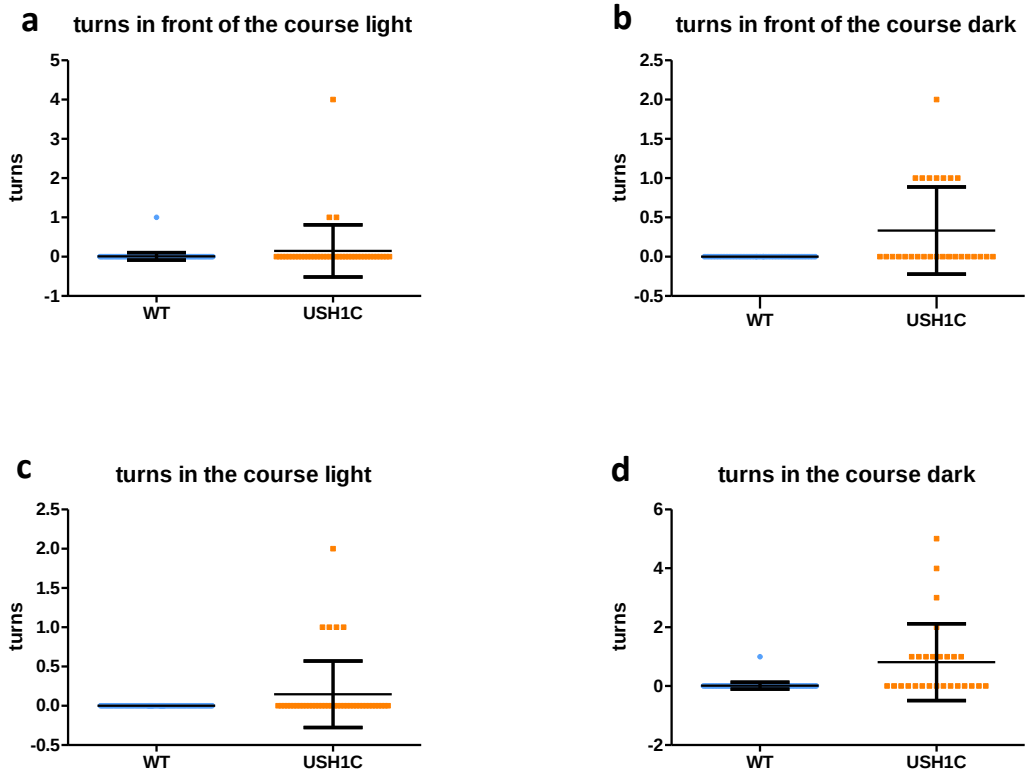

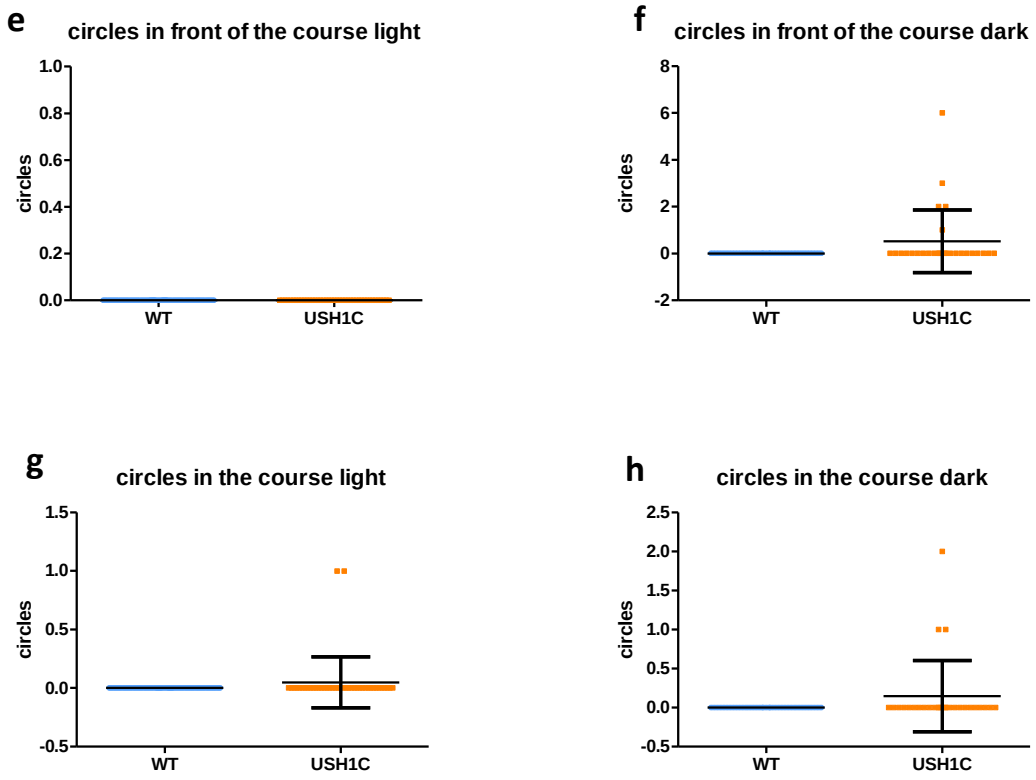

Figure 23: Turns and circles. Neither USH1C pigs (mv: 0.15, sd: 0.66) nor WT pigs (mv: 0.009, sd: 0.1) frequently turned around in front of the course in light condition (a), in dark condition, WT pigs never turned around in front of the course, in contrast to USH1C pigs (mv: 0.33, sd: 0.55) (b). WT pigs also never turned around in the course in light condition, unlike USH1C pigs (mv: 0.15, sd: 0.42) (c), turning around in the course occurred more often in dark condition in USH1C pigs (mv: 0.81, sd: 1.3) than in WT pigs (mv: 0.01, sd: 0.11) (d). Both WT and USH1C pigs never walked in circles in front of the course in the light (e), and in the dark, WT pigs also never walked in circles in front of the course, in contrast to USH1C pigs (mv: 0.52, sd: 1.34). WT pigs never walked in circles in the course and USH1C pigs walked in circles within the course more often in the dark (mv: 0.15, sd: 0.46) than in the light (mv: 0.05, sd: 0.22) (g and h).

3. Complementary analyses

3.1. Retinal phenotype

3.1.1. ERG

Three USH1C and four WT piglets were examined with photopic ffERG at an age of three weeks. USH1C piglets showed a decreased a- and b-wave amplitude (Figure 24a). Furthermore, two one-year old USH1C and WT pigs each were evaluated more closely. Photopic and scotopic ffERG revealed both reduced cone and rod responses (Figure 24b - c). Examination with mfERG demonstrated a reduced cone function in the area of the visual streak (Figure 24f). ERG recordings were conducted by Dominik Fischer (Centre for Ophthalmology, University of Tübingen and Oxford Eye Hospital, University of Oxford) and Anna Döring (Small Animal Clinics, LMU Munich). Andrea Bähr (Clinic for Cardiology, Klinikum rechts der Isar, TU Munich) performed anesthesia.

3.1.2. OCT

SD-OCT measurements of two one-year-old USH1C pigs and WT pigs each showed a reduced retinal thickness in the visual streak area, caused primarily by reduction of ONL thickness (Figure 26). OCT examinations were performed by Dominik Fischer.

3.1.3. Photoreceptor morphology

Already in three-week-old piglets, the rod morphology was altered. Vertically orientated photosensitive membrane disks were discovered in the outer segment of USH1C pigs (Figure 25b). Those changes were even more pronounced in one-year-old USH1C pigs (Figure 25c). In WT pigs, these disks were arranged in a strictly parallel horizontal manner (Figure 25a). Further, interstitial gaps and vesicle like structures at the base of the OS occurred in one-year-old USH1C pigs (Figure 25d – e). Cone OS structure appeared normal in USH1C pigs in the first twelve months of life. Histological analyses were performed by the working group of Uwe Wolfrum (Institute of Molecular Physiology, Molecular Cell Biology, JGU Mainz).

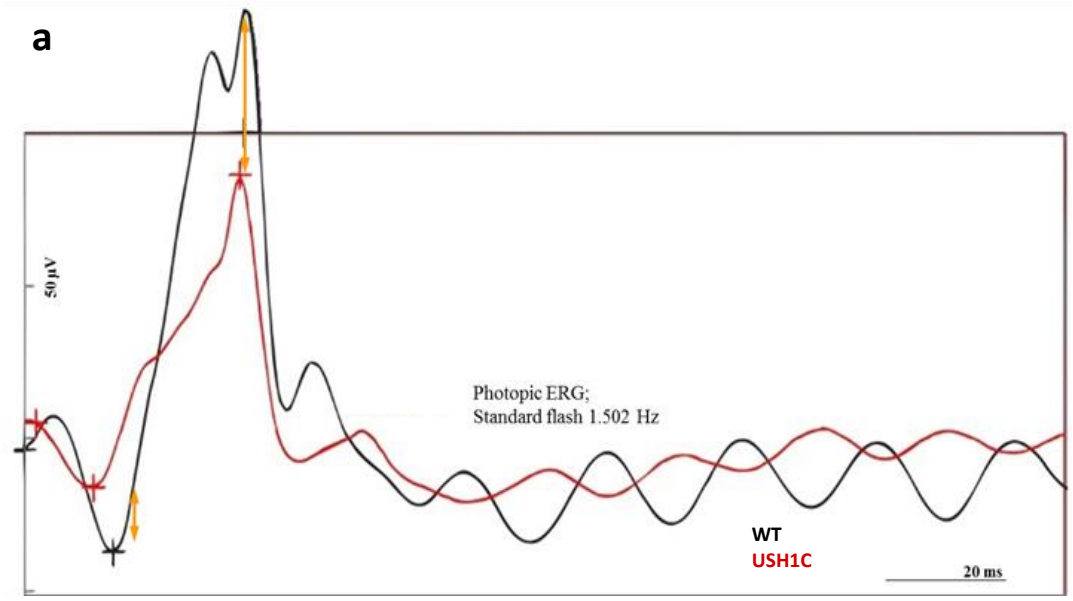
a
50 µV
Photopic ERG;
Standard flash 1.502 Hz
WT
USH1C
20 ms

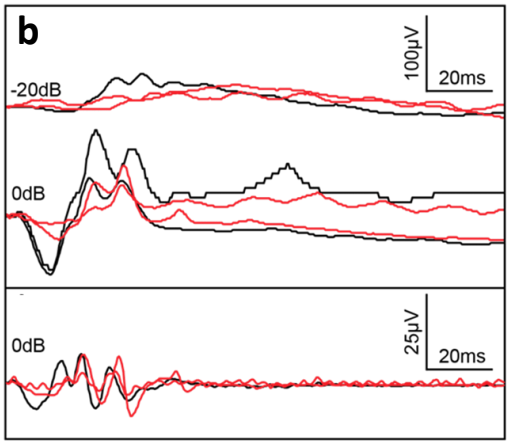
b
-20dB
100µV
20ms
0dB
0dB
25µV
20ms

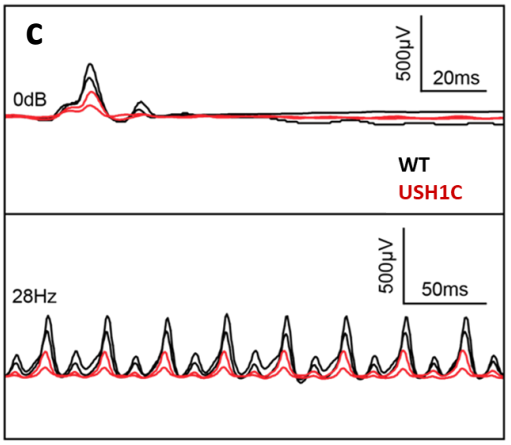
c
0dB
500µV
20ms
WT
USH1C
28Hz
500µV
50ms

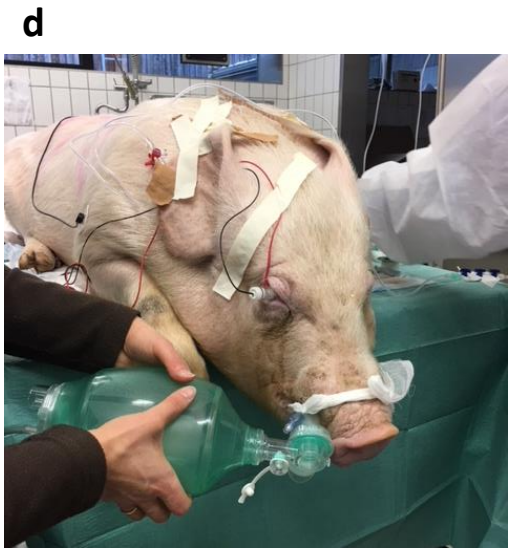
d

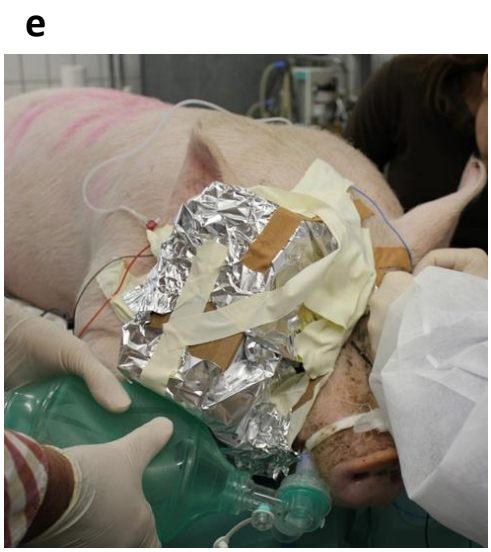
e

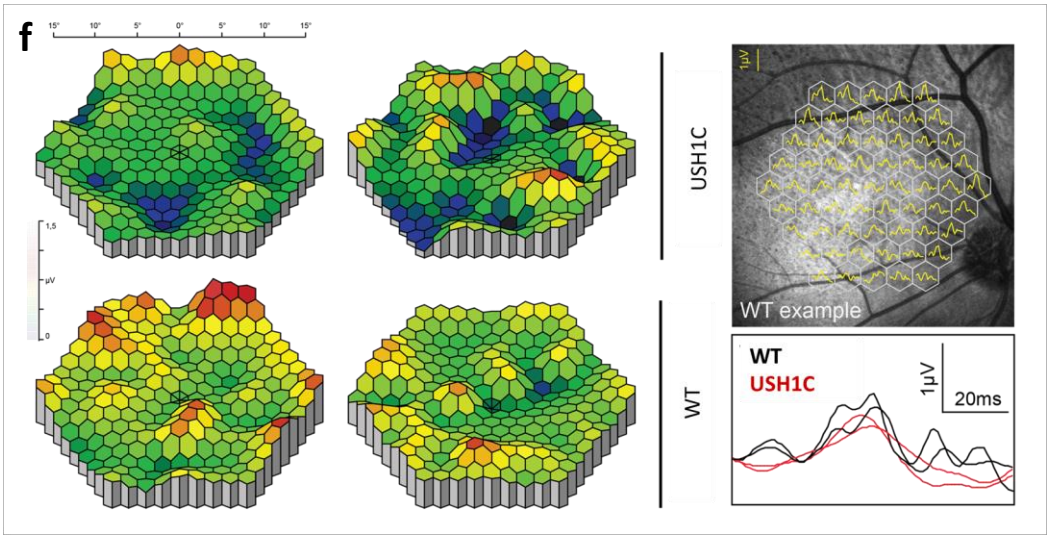

Figure 24: ERG. Photopic ffERG of three-week-old piglets showed reduced a- and b-wave amplitudes (a). Scotopic ffERG of one-year old pigs showed a 70% reduced a-wave amplitude (USH1C: 21±18 µV, WT: 79±2 µV) and a 50% reduced b-wave amplitude (USH1C: 75±32 µV, WT: 154±39 µV) (b), photopic ffERG revealed a 50% reduced a-wave amplitude (USH1C: 10±0 µV, WT: 20±5 µV) and a 60% reduced b-wave amplitude (USH1C: 86±49 µV, WT: 215±50 µV) (c). ERG measurement of a WT pig under general anaesthesia (d), same pig being prepared for scotopic ERG measurements (e). mfERG showed reduced cone function in the visual streak area (f). Numbers are presented as [mv±sd]. Data provided by Anna Döring and Dominik Fischer.

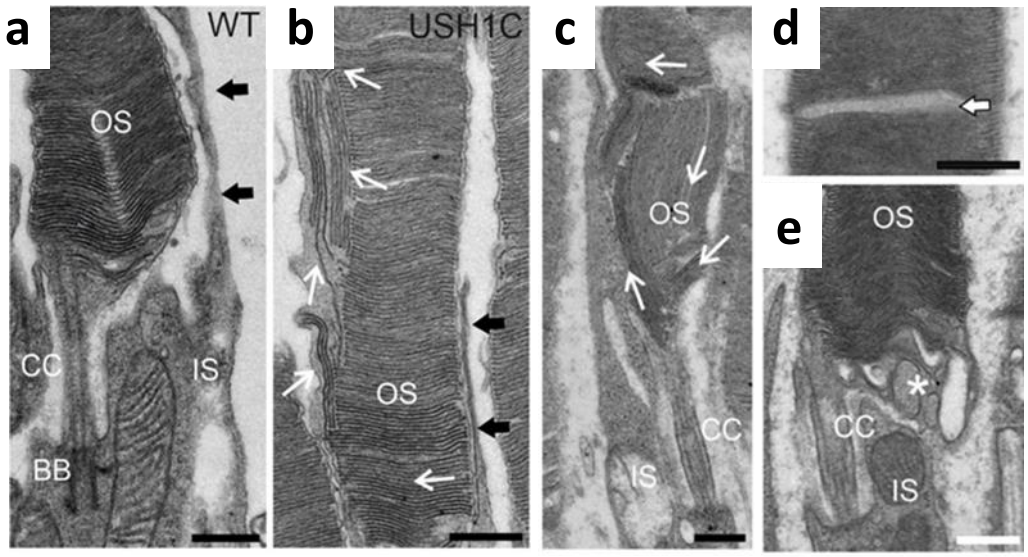

Figure 25: Rod morphology. In three-week-old WT piglets, OS structure appeared normal, including calyceal processes (black arrows) (a), whereas vertically orientated discs (white arrows) were detected in USH1C piglets (b). This disarrangement of disks became more prominent in one-year-old USH1C pigs (c), in addition, interstitial gaps (d) and vesicle like structures (asterisk) were found at the base of the OS (e). Scale bars indicate 0.6 µm (a), 0.75 µm (b), 0.55 µm (c), 0.5 µm (d) and 0.85 µm (e). TEM images provided by Uwe Wolfrum.

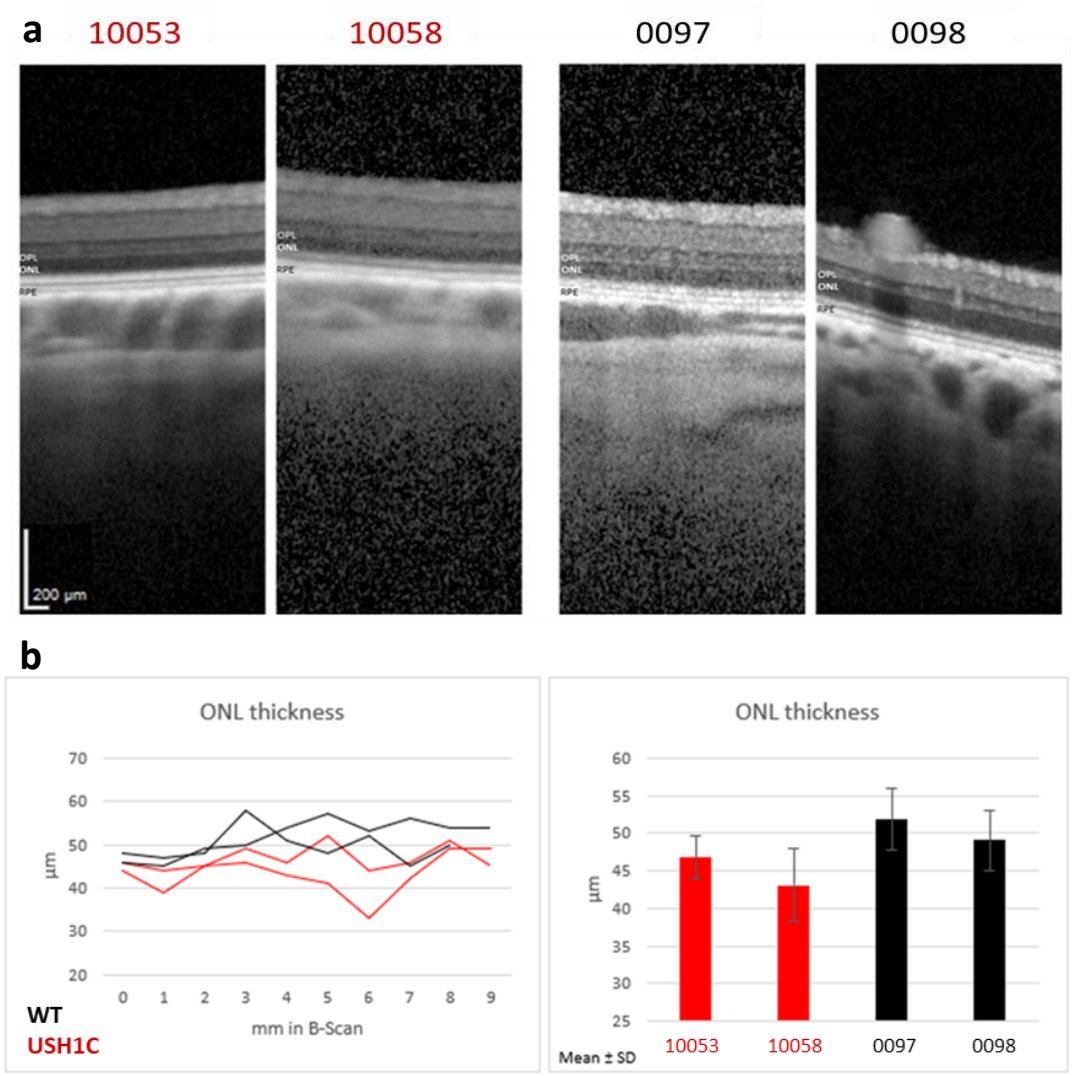

Figure 26: SD-OCT measurements. OCT measurement revealed a reduced retinal thickness caused by a reduction of the ONL (a and b; data provided by Dominik Fischer). OCT measurement of a USH1C pig under general anesthesia (c).

3.2. Audiovestibular phenotype

3.2.1. ABR

Hearing ability of three USH1C and three WT piglets was examined with auditory brainstem response tests at an age of three weeks. Almost complete hearing loss was revealed by this test in USH1C piglets, as they showed no reaction to a click stimulus of 100 dB (Figure 27a). One out of the three USH1C piglets showed a response to a sound pressure level of 120 dB, whereas WT piglets were already reacting to 40 dB. ABR measurements were performed by Andrea Fischer (Small Animal Clinics, LMU Munich).

3.2.2. Vestibular dysfunction

Right after birth, USH1C piglets showed a circling phenotype (Figure 27b), requiring motherless raising. This behavior ceased around weaning. Later on, circling occurred in stress related situations, when pigs were faced with new situations. For example, some USH1C pigs were walking in circles when they were first confronted with obstacles in the training for behavioral tests. Occasionally, a nystagmus was observed at an age of three to six months.

3.2.3. Hair cell morphology

Scanning electron microscopy showed altered hair cell morphology in USH1C piglets at an age of three weeks. Rows of stereocilia were absent (Figure 27c). JOHNSON et al. (2003) reported similar findings in an USH1C mouse model. Samples were taken by Andreas Parzefall (Institute for Experimental Genetics, Helmholtz Center Munich) and histological analyses were performed by the working group of Uwe Wolfrum.

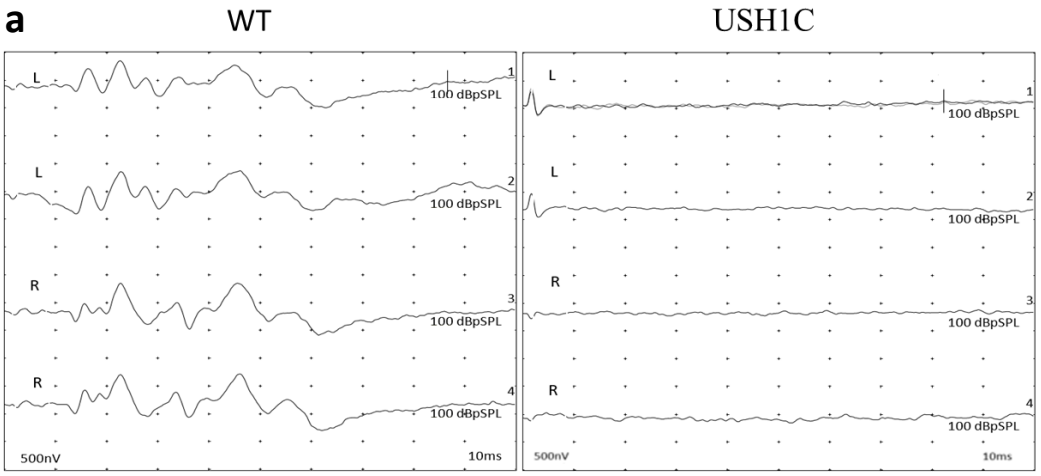

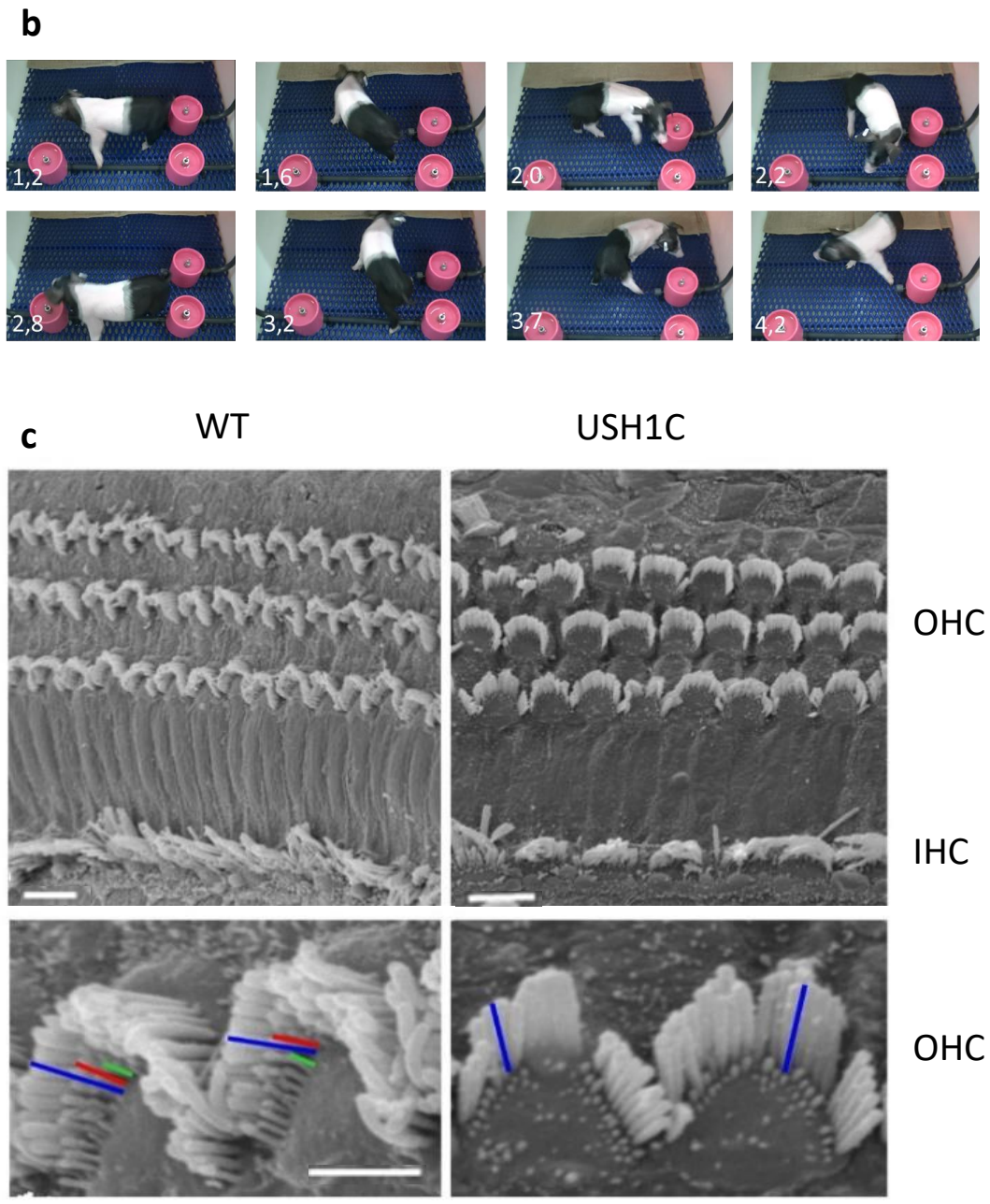

Figure 27: Audiovestibular alterations in USH1C pigs. ABR tests showed that USH1C piglets are almost completely deaf at an age of three weeks, they showed no response to a click stimulus at a sound pressure level of 100 dB, data provided by Andrea Fischer (a). USH1C piglets were circling in the first weeks of life, they were walking in circles clockwise and counterclockwise. Pictures show an 18-days-old piglet, numbers indicate seconds after recording started (b). SEM imaging revealed altered hair cell morphology in USH1C pigs. Scale bars indicate 10 µm (upper panels) and 5 µm (lower panels), provided by Uwe Wolfrum (c).

V. DISCUSSION

USH1 is characterized by a combination of blindness, deafness, and vestibular dysfunction. Up to date, no animal model has been generated that truly reflects all those symptoms. Mouse models show, if any, only a mild retinal phenotype. This has also hindered the understanding of the pathophysiology and finding of treatment for the ocular component of USH (reviewed in TOMS et al., 2015). Transgenic pigs are well suited for translational research and pig models already exist for different diseases (reviewed in AIGNER et al., 2010; reviewed in PERLEBERG et al., 2018). As the human and porcine eye share a similar morphology, pigs are also often used in eye research (reviewed in SANCHEZ et al., 2011). Therefore, a pig model for USH1C has been generated at the Chair of Molecular Animal Breeding and Biotechnology.

This pig model was generated by humanizing exon 2 and introducing the R31X mutation in *USH1C*. A transition of CGA to TGA results in a stop codon instead of arginine, leading to a premature translational stop. Molecular biological analysis showed that USH1C F0 pigs are expressing the humanized exon 2 including the nonsense mutation in different tissues. Surprisingly, genotyping of heterozygous offspring of homozygous founder sows generated via SCNT and ET revealed that F0 animals do not carry the R31X mutation on both alleles, but just on one. The other allele presumably shows a deletion of exon 2 and of surrounding intronic regions. Although this was not the initially intended outcome, it does evidently not affect the phenotype of the model. Both the R31X mutation and the deletion of exon 2 cause a lack of harmonin on protein level and thus result in a harmonin null function. Therefore, pigs can be fully used for phenotype characterization and also for therapeutical studies. For certain approaches such as read-through therapies or gene repair attempts that aim at changing the stop codon back to an arginine codon, it is necessary to have a least one *USH1C*^{R31X} allele in USH1C pigs. For this reason, maintaining the humanized R31X in the future breeding herd of USH1C animals is mandatory and for the ease of breeding, the exclusive maintenance of USH1C^{R31X} animals is the preferred strategy. On the other hand, it would be more desirable to maintain both alleles in the model, as it better reflects the situation found in patients. Many different mutations in *USH1C* are causative for Usher syndrome and patients are

mostly heterozygous, carrying distinct mutations on each allele (ZWAENEPOEL et al., 2001; AHMED et al., 2003; OUYANG et al., 2005). In particular, no patient with an R31X mutation on both alleles has been described (Jennifer Lentz, Neurosciences Center, Louisiana State University, personal communication).

The major question after generating a new animal model is to which extent it mirrors the phenotype of the human disease. This appeared challenging for the USH1C pig model, because first, it combines three phenotypic hallmarks of hearing loss, vestibular dysfunction, and vision loss. Second, the characterization of vision in pigs is not well established. Therefore, pigs were examined comprehensively for all aspects of the disease.

Like USH1 patients, USH1C pigs exhibit vestibular dysfunction. Piglets showed a pronounced circling phenotype right after birth, which ceased around weaning. Afterwards, USH1C pigs only walked in circles in response to stressful situations. Occasionally, a nystagmus was observed at an age of 3-6 months, a symptom that has been associated with vestibular dysfunction (DOUGHERTY et al., 2020). The gait of USH1C pigs also proved to be more unsteady than the one of WT pigs. In the obstacle course, USH1C pigs had more difficulties crossing obstacles like the cavaletti, which requires a vertical movement for transition and is thus challenging the vestibular system. Hence, these findings closely resemble the vestibular phenotype in USH1 patients, who sometimes manifest a nystagmus, are late to walk and show an unstable gait (MOLLER et al., 1989).

ABR tests revealed that USH1C pigs show a severe hearing loss, they did not show a reaction to click stimuli of 100 dB SPL. Similar data have been gained at our partner institute IAPG Libechov. This was also confirmed by daily behavior in the stable, as USH1C pigs do not react to sounds like WT pigs do. EDWARDS et al. (1998) reported that USH1 patients have a pure-tone average of 100 dB or greater. For these reasons, also the hearing phenotype in the USH1C pig model correlates with the auditory phenotype found in USH1 patients.

The examination of the retinal phenotype appeared most challenging, because it is difficult to estimate actual visual function from electrophysiological function recorded by ERG or from morphological assessment by OCT. For example, patients with barely detectable electroretinographic amplitudes are reported to be still able to read the newspaper (reviewed in HARTONG et al., 2006; KOSTIC et

al., 2013). In RP patients, visual acuity better correlates with their ability to deal with difficulties in daily life than ERG measurements (SZLYK et al., 1997). Still, clinical examinations by ERG and OCT represent an essential component in monitoring RP patients. Therefore, it is essential to measure those parameters in USH1C pigs as well and compare them to behavioral tests that sufficiently assess useful vision.

ERG recordings demonstrated reduced sensitivity for visual stimulation in USH1C pigs. Scotopic ffERG recordings revealed 70% reduced rod-derived responses and photopic ffERG showed 50% reduced cone-derived responses in one-year-old pigs, indicating a rod-cone dystrophy. Mesopic ERG recordings in USH1 children under six years of age also revealed reduced amplitudes or even absent ERG responses (FLORES-GUEVARA et al., 2009). ffERG responses in adult USH1 and USH2 patients are described as low to not detectable (SEELIGER et al., 1999). STINGL et al. (2019) reported that in only 4 out of 62 adult USH1 patients scotopic ffERG responses and in only 6 out of those 62 patients photopic ffERG responses were still detectable. The measurable ERG responses in these few patients proved to be abnormal. Furthermore, assessment with mfERG revealed reduced cone function in the area of the visual streak in one-year-old USH1C pigs. In USH patients, mfERG also showed reduced cone function (SEELIGER et al., 2009).

In OCT imaging, only mild changes could be observed. USH1C pigs exhibited a reduced retinal thickness, primarily caused by ONL thickness reduction. In USH patients, a phenotypical variability ranging from a intact central retinal area to advanced retinal damage has been described (LENASSI et al., 2014).

For comparing these essential clinical examination tools, I conducted two different behavioral tests for estimating the visual capacity of WT and USH1C pigs. In an obstacle course, USH1C pigs had more difficulties to pass the course in light condition. They were significantly slower than WT pigs and they also touched obstacles more often. On the contrary, WT and USH1C pigs behaved more similar in dark condition. USH1C pigs still touched obstacles significantly more often and were slower than WT pigs in the dark, but the difference was less pronounced. Strikingly, USH1C pigs were examining obstacles more closely. For example, they often stroked along the red bar of the cavaletti with their snout before passing it, a behavior that was hardly observed in WT pigs. USH1C pigs

were also smelling and licking the obstacles more often. Similar findings were reported by KOSTIC et al. (2013), who tested GUCY2D pigs in an obstacle course and defined this behavior as so-called alternative prospection. This suggests that vision alone is not sufficient for those pigs to assess their environment.

A more detailed trajectory analysis with TrajR revealed that USH1C pigs do have an impaired overlook compared to WT pigs. The path of USH1C pigs was straighter (lower sinuosity), indicating that they walk straight ahead through the course, aiming at the feed trough at the end and just turn around when an obstacle is appearing in front of them. WT pigs on the other hand showed a higher sinuosity, they moved more forward-looking and tried to avoid obstacles in advance. WT pigs walked straight (higher Emax) on their bending way through the course, whereas USH1C pigs changed direction more abruptly when faced with obstacles and moved more unsteady, even when they were not confronted with obstacles. This presumed vestibular component might have also contributed to the decreased Emax in USH1C pigs. Furthermore, their step length was shorter than WT pigs' one and they had more problems to cross obstacles like the cavaletti that is challenging the balance of pigs. To sum up, the obstacle course revealed that USH1C pigs have an impaired vision and balance. Moreover, the designed course shifted the immediate recognition of an obviously altered behavior towards a quantifiable output. This will not only allow the assessment of disease progression over time, but also the determination of treatment success in preclinical trials of therapies.

A second behavioral test, that had been priorly described useful by BARONE et al. (2018) to detect differences between WT pigs and IAA-treated pigs, was also tested for its ability to reveal different behavior in WT and USH1C pigs. In this barrier course, pigs had to bypass vertical boards, so this course was supposed to be less challenging for vestibular function. Again, USH1C pigs seemed to be slower than WT pigs in light and dark conditions. In the dark, USH1C pigs also hesitated to enter the course, they collided frontally with obstacles, turned around before reaching the end of the course and walked in circles. It was also observed that USH1C pigs walked closer up to barriers before they walked around them, while WT pigs moved more anticipatory. One WT pig had to be excluded from this test due to motivation problems, the pig was more interested in playing with

barriers and never walked reliably to the end of the course. It also turned out to be useful to perform the course before pigs were fed, as pigs were tired and not as motivated to go fast to their reward after feeding. Differences between USH1C pigs and WT pigs were not as clear as differences described in the original publication. It needs to be noted that IAA-treated pigs proved to be completely blind, whereas USH1C pigs have an impaired vision. This does not only indicate that USH1C pigs retain some visual ability, but also confirms that pigs in general use a more complex sensing or alternative prospection in the case of impaired vision.

Behavioral tests are also applied in human medicine. CHUNG et al. (2018) described a multi-luminance mobility test to assess vision in inherited retinal dystrophy patients and to differentiate patients from normal sighted persons. Patients with retinitis pigmentosa, Leber congenital amaurosis, choroideremia, Usher syndrome, and Stargardt disease as well as normal sighted persons were supposed to track arrows. On their way they had to avoid obstacles, overcome steps, and find a door at the end of the course. This test was conducted under different light conditions, ranging from 1 to 400 lx, and twelve different setups were used alternately. Subjects were tested with one eye patched or with both eyes unpatched. It was evaluated how often persons collided with obstacles, how often they deviated from the path and had to be led back on the course and time to complete the course was measured. Control subjects were able to pass the mobility test at all light levels. Results of visually impaired patients differed widely and some declined over the period of one year in which the test was performed. Error frequency correlated with visual acuity and visual field found in patients. This mobility test was also applied in phase 1 and 3 trials to detect improvements in patients with Leber congenital amaurosis, caused by mutations in RPE65, who were treated with voretigene neparvovec (Luxturna, MAGUIRE et al., 2019). Of note, this behavior test setup for human patients has been published during my thesis. In fact, the composition of my obstacle course appears to be similar to the test described by MAGUIRE et al. (2019) although it had been developed independently. This does not only support the relevance of the obstacle test for pigs, but also facilitates future correlations to such tests in human USH patients.

For future behavioral testing, a combination of the obstacle and barrier course is

planned. This was already tried with the two groups of animals that were tested in the barrier course after the testing phase in this course had ended. Therefore, four boards of the barrier course were combined with the stepboard, cavaletti, and barrel hanging from the ceiling of the obstacle course. Testing was conducted in the same area of the pigsty's aisle where the barrier course had taken place. In the beginning, new obstacles were examined in detail by WT and USH1C pigs. Remarkably, after checking the dimensions of the cavaletti that was placed in the middle of the aisle, the two USH1C pigs opted to walk around it, whereas WT pigs jumped over this obstacle. Already in the second or third trial, animals were walking again reliably to the reward at the end of the course and the combination of the two courses proved well feasible. For evaluation, time was measured and obstacle contacts were counted. This proved that components of both behavioral tests can be combined in future attempts, whereas the limited number of runs conducted so far did not allow a statistical examination.

In total, our examination of clinical parameters and of the newly developed behavior tests confirm that the USH1C pig reflects the situation found in patients and therefore presents a relevant large animal model. So far, due to the limited availability of USH1C pigs, clinical data were only obtained of a few animals per time point. Furthermore, not all of those pigs have been evaluated in behavior tests. As a next major step, a natural history study is being planned for a longitudinal characterization of pigs. Eight homozygous USH1C and eight WT pigs will be followed over the course of one year. It is intended to examine those pigs with ERG, OCT, fundus photography, and ABR at an age of six weeks, three months, six months, and one year to further study disease progression. Importantly, conducting behavioral tests will be an essential component to correlate clinical examinations to true visual function. Specifically, it is again intended to evaluate behavioral tests by trajectory analysis in this study.

So far, the trajectory analysis in the obstacle course by watching videos, noting footsteps in relation to the slatted floor in a map of the course and transferring coordinates to an excel file was doable, but time-consuming. No path analysis was conducted for the barrier course, because it would have been difficult to document coordinates of footsteps as there was no slatted floor in the testing area of the barrier course. Positioning one camera at the ceiling in the starting area of the course also did not allow to determine exactly where the pigs placed their feet on

the ground in the videos, as the barriers were often in the way. Nevertheless, trajectory analysis in correlation to barriers would be important, because USH1C pigs obviously walked closer up to barriers whereas WT pigs moved around them more proactively. Trajectory analysis would allow quantification of this observation.

Automatic video tracking offers the advantages of being more reliable and independent as algorithms are not biased and do not suffer from observational fatigue (NOLDUS et al., 2001). Image based tracking is well established and applied in mammals, fish, insects, and birds. Many different tracking systems exist (reviewed in DELL et al., 2014) and LIND et al. (2005) even described a tracking system which records pigs' movement to within two centimeters. It is important to consider how videos should be recorded prior to video analysis. Good contrast between objects to be tracked and the background is essential, it also helps to avoid placing unnecessary items in the observation area and filming at a high frame rate is crucial (SRIDHAR et al., 2019, Supporting Information). Furthermore, filming orthogonal to the ground of the arena is of high importance, as recording with an angle complicates calculations substantially. To correlate pixels and real world measures, it also helps to place a grid with known dimensions in the filming area (MÖNCK et al., 2018, User Guide). For establishing automatic video tracking in future behavior tests, it is planned to use a system of more than one camera that records from above, orthogonal to the ground. Further it will be necessary to mark defined parts of the pig body to improve contrast between animals and floor. Such adaptations can be made in the existing facility, but alternatively, the behavior tests might be conducted in a different environment.

The latter would be also helpful to overcome some restrictions regarding light conditions. In my behavioral tests, experiments with light conditions of 0.1 – 10 lx were described as "dark" whereas light conditions of 50 – 150 lx were referred to as "light". This suggests that testing in the "dark" took place under mesopic conditions and testing in the "light" under mesopic to photopic conditions. Photopic is defined as the light range, where cones are responsible for vision, scotopic in contrast means that vision only results from rods. Mesopic is the light range, where both types of photoreceptors contribute to vision (BARBUR & STOCKMAN, 2010). Therefore, it would make sense to test under scotopic and

photopic conditions to exclusively test rod and cone function. However, testing scotopic behavior would require a specifically designated environment, facilitating complete darkness, which is presently not feasible in our pigsty. Testing photopic behavior might be easier to achieve in the existing facility by installing additional light sources. In mice it is described that rod activity is reduced to 50% at 150 lx and rod saturation level in humans is discussed to be between 10 and 100 lx (KOSTIC et al., 2013). As the pig's retina is very similar to the human one, the authors drew the conclusion that 500 lx, a light intensity that is achievable with additional spotlights, should be enough to reduce contribution of rods to a minimum.

In future studies, it is also planned to perform an additional behavioral test to determine visual acuity of USH1C pigs. Therefore, two previously described experiments should be combined. Pigs will be trained to differentiate a Landolt-C and a circle as reported by ZONDERLAND et al. (2008). By stepwise decreasing the gap in the C, visual acuity can be defined. But it is intended to conduct this experiment in a more automatic way as illustrated by WONDRAK et al. (2018). The signs are supposed to be displayed on screens, touching of the right screen automatically leads to the delivery of a reward. With such a device, not only visual acuity, but also color vision can be tested.

Obstacle courses are not only useful to examine vision, but can be also applied to evaluate the phenotype of pig models of different diseases. SCHRAMKE et al. (2016) developed a number of behavioral tests to characterize a transgenic pig model for Huntington's disease, a neurodegenerative disorder with cognitive and motor deficit symptoms. Among other things, the pigs had to cross two obstacles in a hurdle test and times were measured for evaluation. However, the test did not show significant differences between transgenic and WT pigs in an observation period of three years (SCHULDENZUCKER et al., 2017). More complex obstacle courses might be necessary to reveal differences between the pigs. Furthermore, behavioral tests were conducted to characterize a pig model of Duchenne muscular dystrophy, that has been generated at the Chair of Molecular Animal Breeding and Biotechnology. This model exhibits a muscular weakness due to lack of dystrophin in skeletal musculature. In comparison to WT pigs, nine-week-old transgenic pigs failed to climb a 25 cm step (BURKHARDT, 2012). Experience gained with my obstacle courses can be transferred to assessment of

the muscular phenotype in those pigs. Consequently, adapted obstacle courses might also be a useful method to evaluate other pig models showing a behavioral phenotype.

Overall, the main question arising from this study is why the porcine USH1C model is showing an ocular phenotype while murine USH models show no or only mild retinal symptoms. TOMS et al. (2015) argued that mice models possibly do not have the same phenotype as human patients, because their lifespan is shorter, their PR architecture is different, USH1 proteins are differently distributed in PRs, and light exposure is also dissimilar.

PENG et al. (2011) hypothesized that *shaker1* mice (*Myo7a*$^{sh1–11J}$) do not develop a retinal phenotype because light intensities are too low under normal rearing conditions and increasing light intensities might lead to retinal degeneration. To test their hypothesis, they exposed the mice that are normally kept under 200 lx and do not exhibit a retinal phenotype to 2500 lx over six days. This led to a PR number reduction of 30% in *shaker1* mice, whereas only 10% of PRs degenerated in WT mice. Additionally, *shaker1* mice showed 40% degenerated rods when kept under 1500 lx for 12 h a day over a period of three months. WT mice, in contrast, did not develop significant degeneration. Similar findings were reported for *whirler* mice (TIAN et al., 2014). On the contrary, LOPES et al. (2011) demonstrated that shaker1 mice (*Myo7a*^{4626SB}) show resistance to acute light damage. After exposing WT and shaker1 mice to 15.000 lx for a period of 2 h, retinae of WT mice exhibited a significant PR loss while retinae of shaker1 mice did not show changes. These findings are in line with ERG recordings in the mice. Those contradictory statements let assume that light exposure is possibly not the reason for the different phenotype in mouse models and human USH patients. This is also supported by the fact that USH1C pigs developed a retinal phenotype, although they were not kept under high light intensities, lux in the pigsty ranged between 80 and 150 lx.

USH1C pigs already exhibit an altered ERG at an age of three weeks, therefore, the shorter lifespan of mice can be ruled out as reason for the lacking retinal phenotype. PR architecture in mice is indeed different as they lack CPs, which are present in human retinae. Their function is poorly understood, but it is supposed that they stabilize the OS. USH1 proteins can be detected in the CPs themselves and also in the connection site between CPs and OSs in primates, but in mice,

USH1 proteins are not present in this region of the PR. Thus, it is assumed that retinal degeneration in USH1 patients is a consequence of the missing stabilizing function of CPs due to defective USH proteins (SAHLY et al., 2012; MAY-SIMERA et al., 2017). Pigs do have CPs and harmonin can also be found in those CP, the CCi, and the base of OS in WT pigs, supporting this line of argumentation. In conclusion, differing PR architecture in combination with different distribution of USH proteins most likely explains the different retinal phenotype in mice in contrast to porcine and human USH patients.

Strikingly, an altered rod OS morphology was found in USH1C pigs. Photosensitive disks were not stacked strictly in a parallel horizontal manner as in retinae of WT pigs, but vertically orientated disks were detected in USH1C pigs. Cone structure proved to be normal. Similar changes were described in pcdh15 (USH1F) and cdh23 (USH1D) knock-down claw frog larvae. In PRs of these morphant larvae, OSs were not arranged parallel and were also outgrowing. Moreover, CPs were lacking in cones. As protocadherin connects CPs to the OS membrane, it seems like CPs are necessary for normal shape and growth of the OS (SCHIETROMA et al., 2017). USH1 proteins are present at the base of the OS and surrounding CPs and are hence thought to build a belt that connects the OS and CPs. This is similar to the inner ear, where protocadherin and cadherin connect hair bundles through tip links and myosin, SANS, and harmonin function in anchoring those links to stereocilias' actin filaments (SAHLY et al., 2012). Lacking harmonin in USH1C pigs therefore probably leads to misarranged rod outer segments, because CPs cannot function in their role to stabilize formation of OSs. Those morphological findings can be linked to ERG responses. Rod-derived ERG responses were more reduced than cone-derived responses, which correlates with a more disturbed architecture in rods.

Thus, the novel USH1C pig model offers the possibility to evaluate different therapeutical methods. A pilot study was already conducted at IAPG Libechov to test the applicability of AAV-mediated gene therapy. AAV based vectors (serotype 8, 9, and Anc80), which express eGFP controlled by a CMV promoter, were injected subretinally in WT pigs to assess transduction patterns. PRs were transduced by all tested vectors and Müller glia cells were additionally transduced by serotype 9 and Anc80. Following the subretinal injection, no relevant off-target expression of eGFP could be found. COLELLA et al. (2014) also reported

that AAV vectors can transduce porcine PRs, they conducted experiments with vectors encoding eGFP, *MYO7A* (USH1B), and *ABCA4* (Stargardt disease) genes. At the moment, plans for gene therapy studies with AAV vectors expressing harmonin are developed within the USH1C pig project. Homozygous USH1C piglets will be trained for behavioral tests before AAVs are administered subretinally. Injecting only one eye per pig offers the advantage of the second eye serving as control. For behavioral tests, the untreated eye would then need to be covered. While this has been demonstrated to be feasible (EWBANK et al., 1974), it is questionable how well a covering of eyes is accepted by pigs with already impaired senses. Further, optimal performance in obstacle courses could be hindered, as pigs' binocular field is small and pigs would basically just see one-sided without turning their heads. Additionally, YU-WAI-MAN et al. (2020) reported that vision in patients with Leber hereditary optic neuropathy improved in both eyes after unilateral injection of AAVs. Studies with primates revealed that viral vector DNA is transferred from the injected eye to the contralateral one via the optic nerve. Therefore, injecting both eyes of one animal and using littermates as controls seems to be more justified. The efficacy of AAV treatment will be evaluated by behavioral tests, ERG, and OCT *in vivo* and by transduction efficacy, transcription efficacy, and morphological changes *ex vivo*. For instance, TOMS et al. (2020b) examined the suitability of different clinical outcomes to detect therapeutic efficacy in a longitudinal study with USH2A patients. Here, ellipsoid zone length constriction measured with OCT and reduction of hyperautofluorescent outer retinal ring area proved to be suited best. Visual acuity, in contrast, was not applicable as measurement as it declined too slowly. The measurement of retinal thickness did also not prove to be suitable as macular edema confounded the measurements.

Another therapeutical option is gene repair using CRISPR/Cas technology. As exon 2 and surrounding regions were humanized, human-specific gene repair approaches can be evaluated in this pig model. *Ex vivo* experiments, conducted by Hannah Auch at the Chair of Molecular Animal Breeding and Biotechnology, with primary cells from USH1C founder pigs, showed an efficacy of up to 40% to change the stop codon TGA into CGA coding for arginine by homology directed repair. In the future, it has to be tested if *in vivo* application of Cas9, gRNA, and repair oligonucleotides in eyes of homozygous USH1C$^{R31X/R31X}$ pigs delivers the

same results. Because of its immune-privileged status and its small size, requiring only small vector amounts, the eye is perfectly suited for this method. The components for gene editing are usually delivered to the eye via viral vectors. In rodents, subretinal delivery of CRISPR components already proved to be able to induce gene repair in PRs (reviewed in YU & WU, 2020).

Furthermore, a study evaluating subretinal transplantations of PRs in pigs derived of human retinal organoids generated with induced pluripotent stem cells is conducted in the Center for Regenerative Therapies Dresden under supervision of Marius Ader and Dierk Wittig. Experiments concerning the transplantation of PRs have been previously performed in mice (PEARSON et al., 2012; BARBER et al., 2013), but as retinal morphology is different in humans and mice, results are transferable to a limited extent. Large animal models can therefore help in the translational process. In preliminary studies, WT pigs are transplanted with such cells to assess morphology, integration, and vitality of transplanted PRs. It is, however, unclear under which circumstances cell transplants integrate into the retina properly. As long as the retina is largely intact, the cells might lack an appropriate “niche” to engraft. On the other hand, a completely degenerated retina might suffer of secondary malformations, preventing correct connection to the optic nerve. Thus, transplantations in the retinae of USH1C pigs at different time points is planned to examine the therapeutic window and to assess the efficacy of retinal transplants.

Additionally, the nonsense mutation in exon 2 introduced in USH1C pigs allows the evaluation of translational read-through therapy. TRIDs were already assessed in cell culture and mice. NB30, NB54, and PTC124 were able to induce read-through of the stop mutation, even resulting in full-length harmonin to some extent (GOLDMANN et al., 2012).

In summary, the USH1C pig model is the first animal model to truly reflect all symptoms found in USH1 patients. It offers the possibility to better understand the pathophysiology of USH and will help to evaluate new treatment options.

VI. SUMMARY

Characterization of a pig model of Usher syndrome

Usher syndrome (USH) is an autosomal-recessive disorder leading to blindness, deafness, and vestibular dysfunction. USH is clinically and genetically heterogenous and divided into subgroups based on the affected gene, start of vision loss, severity of hearing loss, and occurrence of vestibular dysfunction. Within USH1, USH1C is characterized through congenital deafness, a beginning vision loss in the first decade of life and vestibular hypofunction caused by mutations in *USH1C,* leading to defective harmonin. Harmonin is presumably a scaffold protein that plays an important role in mechanoelectrical transduction in the ear by taking part in connecting hair cells in the inner ear and in regulating calcium influx in hair cells' synapses. Although the localization of harmonin in photoreceptors has been detected, less knowledge exists about the function of harmonin in vision loss. Similar applies to therapy. Deafness can be effectively treated with cochlear implants, but to date, no therapy exists for retinal degeneration. A major reason for this is that existing USH animal models only reflect the audiovestibular, but not the retinal phenotype of USH patients. Since pigs represent an excellent species for vision research, an USH1C pig model was generated, based on the human relevant R31X mutation in exon 2 of *USH1C*, obliterating harmonin.

The aim of this thesis was the characterization of the USH1C pig model and to evaluate if this model correctly mirrors the phenotype found in USH patients. Molecular biological analysis revealed that founder animals comprise a bi-allelic disruption of the *USH1C* gene, as one allele carried the humanized exon 2 with the desired R31X mutation, whereas the other allele apparently lacked exon 2 completely. As a result, founder animals expressed humanized transcripts and transcripts that lacked either exon 2 or exons 2-4. Heterozygous F1 offspring comprised one of these variants.

From a clinical perspective, USH1C pigs showed vestibular dysfunction. Newborn piglets exhibited a circling phenotype, which ceased around weaning and only occured under stressful situations later on. Occasionally, a nystagmus was observed and gait of USH1C pigs proved to be unsteady compared to WT

pigs. ABR tests demonstrated a severe hearing loss in USH1C pigs, as they did not show reactions to click stimuli of 100 db SPL. ERG recordings also revealed impaired vision in USH1C pigs, scotopic ffERG recordings showed 70% reduced rod-derived responses and photopic ffERG revealed 50% reduced cone-derived responses. OCT measurements displayed a reduced retinal thickness in USH1C pigs.

USH1C and WT pigs were evaluated in behavioral tests to assess their useful vision in a quantitative manner. USH1C pigs needed significantly longer to pass an obstacle course than WT pigs in the light, but not in the dark. Also, USH1C pigs were touching obstacles significantly more often than WT pigs. Trajectory analysis showed that movement of WT pigs was faster, smoother, and more bending. As they have a good overlook, they passed obstacles more effectively than USH1C pigs, which moved slower and less foreseeing. Moreover, the gait of USH1C pigs proved to be unsteady. In a barrier course, USH1C pigs seemed slower than WT pigs. In the dark, USH1C pigs sometimes hesitated to enter the course, collided frontally with barriers, and turned around before reaching the end, a behavior almost never observed in WT pigs. Furthermore, WT pigs moved more anticipatory whereas USH1C pigs walked closer up to barriers. Behavioral tests revealed an impaired vision and balance in USH1C pigs.

In conclusion, the USH1C pig reflects the situation found in patients. Thus, it presents an outstanding large animal model that truly mimics vision loss, hearing loss, and vestibular dysfunction. Hence, the USH1C pig offers the possibility to study the pathogenesis of Usher syndrome more closely and also helps in the development of new treatment options.

VII. ZUSAMMENFASSUNG

Charakterisierung eines Schweinemodells für das Usher Syndrom

Das Usher-Syndrom (USH) ist eine autosomal-rezessive Erbkrankheit, die durch Blindheit, Taubheit und vestibuläre Dysfunktion gekennzeichnet ist. USH ist klinisch und genetisch heterogen. Basierend auf dem betroffenen Gen, dem Beginn des Sehverlustes, dem Schweregrad des Hörverlustes und dem Vorhandensein einer vestibulären Dysfunktion wird es in Untergruppen eingeteilt. In der Klasse USH1 zeichnet sich USH1C durch eine angeborene Taubheit, einen beginnenden Sehverlust in der ersten Lebensdekade und einer vestibulären Unterfunktion aus, verursacht durch Mutationen in *USH1C*, die zu fehlerhaftem Harmonin führen. Harmonin ist ein Gerüstprotein, das eine wichtige Rolle in der mechanoelektrischen Transduktion im Ohr spielt, da es an der mechanischen Verbindung der Haarzellen im Innenohr und an der Regulierung des Kalziumeinstroms in den Synapsen der Haarzellen beteiligt ist. Obwohl die Lokalisation von Harmonin in Photorezeptoren bekannt ist, sind weniger Kenntnisse über die Rolle von Harmonin beim Sehverlust vorhanden. Ähnliches gilt für die Therapie. Taubheit kann erfolgreich mit Cochlea-Implantaten behandelt werden, aber für den Sehverlust gibt es bis heute keine Therapie. Dieser Umstand lässt sich auch darauf zurückführen, dass existierende USH Tiermodelle zwar den audiovestibulären, nicht aber den retinalen Phänotyp von USH-Patienten zeigen. Da Schweine sehr gut für die Sehforschung geeignet sind, wurde ein USH1C-Schweinemodell generiert, das auf der für den Menschen relevanten R31X-Mutation im Exon 2 von *USH1C* basiert und dazu führt, dass kein funktionsfähiges Harmonin gebildet wird.

Das Ziel dieser Arbeit war es, das USH1C-Schweinemodell zu charakterisieren und zu evaluieren, ob dieses Modell den Phänotyp, den USH-Patienten zeigen, widerspiegelt. Molekularbiologische Analysen ergaben, dass die Gründertiere eine Zerstörung des *USH1C*-Gens auf beiden Allelen aufweisen, da ein Allel das humanisierte Exon 2 mit der gewünschten R31X-Mutation trug, während dem anderen Allel das Exon 2 offenbar vollständig fehlte. Infolgedessen exprimierten Gründertiere humanisierte Transkripte und Transkripte, denen entweder Exon 2 oder die Exons 2-4 fehlten. Heterozygote F1-Nachkommen zeigten eine dieser

beiden Varianten.

Vom klinischen Befund weisen USH1C-Schweine eine vestibuläre Dysfunktion auf. Neugeborene Ferkel bewegen sich oft in Kreisen, dieses Verhalten lässt um das Absetzen nach und tritt später nur noch stressbedingt auf. Gelegentlich wurde ein Nystagmus beobachtet und der Gang der USH1C-Schweine erwies sich im Vergleich zu WT-Schweinen als unsicher. ABR-Tests bewiesen einen schweren Hörverlust bei USH1C-Schweinen, da sie keine Reaktionen auf Klickreize von 100 db SPL zeigten. ERG-Aufnahmen signalisierten zudem eine Beeinträchtigung des Sehvermögens bei USH1C-Schweinen, skotopische ffERG-Aufnahmen zeigten um 70% reduzierte Stäbchenantworten und photopische ffERG zeigten um 50% reduzierte Zapfenantworten. OCT-Messungen wiesen eine reduzierte Netzhautdicke bei USH1C-Schweinen nach.

Ein wesentlicher Teil meiner Arbeit war der Entwicklung von Verhaltenstests gewidmet, um das tatsächliche Sehvermögen von USH1C und WT Schweinen quantitativ zu beurteilen. Im Hellen, nicht aber im Dunkeln, brauchten USH1C-Schweine signifikant länger als WT-Schweine, um einen Hindernisparcours zu passieren. Außerdem berührten USH1C-Schweine Hindernisse signifikant häufiger als WT-Schweine. Eine Analyse der Laufbahnen zeigte, dass die Bewegung der WT-Schweine schneller, gleichmäßiger und gebogener ist. Da sie einen guten Überblick haben, passieren WT-Schweine die Hindernisse effektiver. Im Gegensatz dazu bewegen sich USH1C-Schweine langsamer, weniger vorausschauend und ihr Gang ist wackeliger. In einem zweiten Hindernisparcours brauchten USH1C-Schweine mehr Zeit als WT-Schweine, um den Parcours zu absolvieren. Im Dunklen zögerten USH1C-Schweine manchmal, den Parcours zu betreten, sie liefen frontal in die Barrieren und drehten um, bevor sie das Ende des Parcours erreichten - ein Verhalten, das bei WT-Schweinen fast nie beobachtet wurde. Darüber hinaus bewegten sich die WT-Schweine vorausschauender, während USH1C-Schweine näher an die Barrieren heranliefen. Verhaltenstests wiesen ein beeinträchtigtes Sehvermögen und Gleichgewicht bei USH1C-Schweinen nach.

Zusammenfassend lässt sich sagen, dass das USH1C-Schwein den Phänotyp widerspiegelt, den USH-Patienten aufweisen. Es stellt somit ein relevantes Großtiermodell dar, da es den Seh- und Hörverlust sowie die vestibuläre Dysfunktion nachahmt. Somit bietet das USH1C-Schwein die Möglichkeit, die

Pathogenese des Usher-Syndroms näher zu erforschen und hilft auch bei der Entwicklung neuer Behandlungsmethoden.

VIII. INDEX OF FIGURES

IX. INDEX OF TABLES

X. REFERENCES

Ahmed Z, Riazuddin S, Riazuddin S, Wilcox E. The molecular genetics of Usher syndrome. Clinical Genetics 2003; 63: 431-44.

Ahmed ZM, Smith TN, Riazuddin S, Makishima T, Ghosh M, Bokhari S, Menon PS, Deshmukh D, Griffith AJ, Riazuddin S. Nonsyndromic recessive deafness DFNB18 and Usher syndrome type IC are allelic mutations of USHIC. Human genetics 2002; 110: 527-31.

Aigner B, Renner S, Kessler B, Klymiuk N, Kurome M, Wünsch A, Wolf E. Transgenic pigs as models for translational biomedical research. Journal of molecular medicine 2010; 88: 653-64.

Aparisi MJ, Aller E, Fuster-García C, García-García G, Rodrigo R, Vázquez-Manrique RP, Blanco-Kelly F, Ayuso C, Roux AF, Jaijo T, Millán JM. Targeted next generation sequencing for molecular diagnosis of Usher syndrome. Orphanet Journal of Rare Diseases 2014; 9: 168-82.

Augsburger AS, Haag V, Leuillet S, Legrand JJ, Forster R. Recording of the full-field electroretinogram in minipigs. Veterinary Ophthalmology 2012; 15 Suppl 2: 84-93.

Barber AC, Hippert C, Duran Y, West EL, Bainbridge JW, Warre-Cornish K, Luhmann UF, Lakowski J, Sowden JC, Ali RR. Repair of the degenerate retina by photoreceptor transplantation. Proceedings of the National Academy of Sciences 2013; 110: 354-9.

Barbur J, Stockman A. Photopic, mesopic and scotopic vision and changes in visual performance. Encyclopedia of the Eye 2010; 3: 323-31.

Barone F, Nannoni E, Elmi A, Lambertini C, Scorpio DG, Ventrella D, Vitali M, Maya-Vetencourt JF, Martelli G, Benfenati F. Behavioral Assessment of Vision in Pigs. Journal of the American Association for Labaratory Animal Science 2018;

57: 350-6.

Bergua A (2017) Das menschliche Auge in Zahlen. Springer-Verlag

Britt W. Primate models: Pros and cons. In: Cytomegaloviruses: Molecular biology and Immunology. Reddehase MJ, ed. Norfolk: Caister Academic Press 2006: 561-606.

Brulé J, Lavoie M-P, Casanova C, Lachapelle P, Hébert M. Evidence of a possible impact of the menstrual cycle on the reproducibility of scotopic ERGs in women. Documenta ophthalmologica 2007; 114: 125-34.

Burkhardt K (2012) Generation of a tailored pig model of Duchenne muscular dystrophy. Dissertation, LMU München: Tierärztliche Fakultät

Chandler MJ, Smith PJ, Samuelson DA, MacKay EO. Photoreceptor density of the domestic pig retina. Veterinary Ophthalmology 1999; 2: 179-84.

Cheng J, Sohn EH, Jiao C, Adler KL, Kaalberg EE, Russell SR, Mullins RF, Stone EM, Tucker BA, Han IC. Correlation of optical coherence tomography and retinal histology in normal and Pro23His retinal degeneration pig. Translational Vision Science & Technology 2018; 7: 18.

Chuang AT, Margo CE, Greenberg PB. Retinal implants: a systematic review. British Journal of Ophthalmology 2014; 98: 852-6.

Chung DC, McCague S, Yu Z-F, Thill S, DiStefano-Pappas J, Bennett J, Cross D, Marshall K, Wellman J, High KA. Novel mobility test to assess functional vision in patients with inherited retinal dystrophies. Clinical & Experimental Ophthalmology 2018; 46: 247-59.

Colella P, Trapani I, Cesi G, Sommella A, Manfredi A, Puppo A, Iodice C, Rossi S, Simonelli F, Giunti M, Bacci ML, Auricchio A. Efficient gene delivery to the

cone-enriched pig retina by dual AAV vectors. Gene Ther 2014; 21: 450-6.

Cosgrove D, Zallocchi M. Usher protein functions in hair cells and photoreceptors. International Journal of Biochemistry & Cell Biolology 2014; 46: 80-9.

Croney CC, Adams KM, Washington CG, Stricklin WR. A note on visual, olfactory and spatial cue use in foraging behavior of pigs: indirectly assessing cognitive abilities. Applied Animal Behaviour Science 2003; 83: 303-8.

Croney CC, Boysen ST. Acquisition of a joystick-operated video task by pigs (Sus scrofa). Frontiers in Psychology 2021; 12: 631755.

Deligeorgis SG, Karalis K, Kanzouros G. The influence of drinker location and colour on drinking behaviour and water intake of newborn pigs under hot environments. Applied Animal Behaviour Science 2006; 96: 233-44.

Dell AI, Bender JA, Branson K, Couzin ID, de Polavieja GG, Noldus LP, Pérez-Escudero A, Perona P, Straw AD, Wikelski M. Automated image-based tracking and its application in ecology. Trends in ecology & evolution 2014; 29: 417-28.

Dinculescu A, Stupay RM, Deng W-T, Dyka FM, Min S-H, Boye SL, Chiodo VA, Abrahan CE, Zhu P, Li Q. AAV-Mediated Clarin-1 expression in the mouse retina: implications for USH3A gene therapy. PloS one 2016; 11: e0148874.

Dougherty JM, Carney M, Emmady PD. Vestibular Dysfunction. StatPearls [NCBI] 2020: https://www.ncbi.nlm.nih.gov/books/NBK558926/. Accessed February 16, 2021.

Dureau P, Jeanny J-C, Clerc B, Dufier J-L, Courtois Y. Long term light-induced retinal degeneration in the miniature pig. Molecular Vision 1996; 2: 7-14.

Edwards A, Fishman GA, Anderson RJ, Grover S, Derlacki DJ. Visual acuity and

visual field impairment in Usher syndrome. Archives of ophthalmology 1998; 116: 165-8.

Egerer S, Fiebig U, Kessler B, Zakhartchenko V, Kurome M, Reichart B, Kupatt C, Klymiuk N, Wolf E, Denner J, Bähr A. Early weaning completely eliminates porcine cytomegalovirus from a newly established pig donor facility for xenotransplantation. Xenotransplantation 2018; 25: e12449.

Eguchi Y, Tanida H, Tanaka T, Yoshimoto T. Color discrimination in wild boars. Journal of Ethology 1997; 15: 1-7.

El-Amraoui A, Petit C. The retinal phenotype of Usher syndrome: Pathophysiological insights from animal models. Comptes Rendus Biologies 2014; 337: 167-77.

Emptoz A, Michel V, Lelli A, Akil O, de Monvel JB, Lahlou G, Meyer A, Dupont T, Nouaille S, Ey E. Local gene therapy durably restores vestibular function in a mouse model of Usher syndrome type 1G. Proceedings of the National Academy of Sciences 2017; 114: 9695-700.

Ewbank R, Meese G, Cox J. Individual recognition and the dominance hierarchy in the domesticated pig. The role of sight. Animal Behaviour 1974; 22: 473-80.

Fernandez de Castro JP, Scott PA, Fransen JW, Demas J, DeMarco PJ, Kaplan HJ, McCall MA. Cone photoreceptors develop normally in the absence of functional rod photoreceptors in a transgenic swine model of retinitis pigmentosa. Investigative Ophthalmology & Visual Science 2014; 55: 2460-8.

Ferreira G, Keller M, Saint-Dizier H, Perrin G, Lévy F. Transfer between views of conspecific faces at different ages or in different orientations by sheep. Behavioural processes 2004; 67: 491-9.

Flores-Guevara R, Renault F, Loundon N, Marlin S, Pelosse B, Momtchilova M,

Auzoux-Chevé M, Vermersch AI, Richard P. Usher syndrome type 1: Early detection of electroretinographic changes. European Journal of Paediatric Neurology 2009; 13: 505-7.

Fujimoto JG, Pitris C, Boppart SA, Brezinski ME. Optical coherence tomography: an emerging technology for biomedical imaging and optical biopsy. Neoplasia (New York, N.Y.) 2000; 2: 9-25.

Fuster-García C, García-García G, González-Romero E, Jaijo T, Sequedo MD, Ayuso C, Vázquez-Manrique RP, Millán JM, Aller E. USH2A gene editing using the CRISPR system. Molecular Therapy-Nucleic Acids 2017; 8: 529-41.

García-Layana A, Pastor JC, Saornil MA, Gonzalez G. Porcine model of proliferative vitreoretinopathy with platelets. Current Eye Research 1997; 16: 556-63.

Ghosh F, Engelsberg K, English RV, Petters RM. Long-term neuroretinal full-thickness transplants in a large animal model of severe retinitis pigmentosa. Graefe's Archive for Clinical and Experimental Ophthalmology 2007; 245: 835-46.

Gibbs D, Kitamoto J, Williams DS. Abnormal phagocytosis by retinal pigmented epithelium that lacks myosin VIIa, the Usher syndrome 1B protein. Proceedings of the National Academy of Sciences 2003; 100: 6481-6.

Gieling ET, Musschenga MA, Nordquist RE, van der Staay FJ. Juvenile pigs use simple geometric 2D shapes but not portrait photographs of conspecifics as visual discriminative stimuli. Applied Animal Behaviour Science 2012; 142: 142-53.

Gillespie PG, Müller U. Mechanotransduction by hair cells: models, molecules, and mechanisms. Cell 2009; 139: 33-44.

Goldmann T, Overlack N, Moller F, Belakhov V, van Wyk M, Baasov T,

Wolfrum U, Nagel-Wolfrum K. A comparative evaluation of NB30, NB54 and PTC124 in translational read-through efficacy for treatment of an USH1C nonsense mutation. EMBO molecular medicine 2012; 4: 1186-99.

Graf R (1976) Das visuelle Orientierungsvermögen der Schweine in Abhängigkeit von der Beleuchtungsstärke. Rapport B-124, IVO, Zeist.

Gregory FD, Bryan KE, Pangršič T, Calin-Jageman IE, Moser T, Lee A. Harmonin inhibits presynaptic Cav1.3 Ca^{2+} channels in mouse inner hair cells. Nature neuroscience 2011; 14: 1109-11.

Gregory FD, Pangrsic T, Calin-Jageman IE, Moser T, Lee A. Harmonin enhances voltage-dependent facilitation of Cav1.3 channels and synchronous exocytosis in mouse inner hair cells. The Journal of Physiology 2013; 591: 3253-69.

Grillet N, Xiong W, Reynolds A, Kazmierczak P, Sato T, Lillo C, Dumont RA, Hintermann E, Sczaniecka A, Schwander M, Williams D, Kachar B, Gillespie PG, Muller U. Harmonin mutations cause mechanotransduction defects in cochlear hair cells. Neuron 2009; 62: 375-87.

György B, Meijer EJ, Ivanchenko MV, Tenneson K, Emond F, Hanlon KS, Indzhykulian AA, Volak A, Karavitaki KD, Tamvakologos PI. Gene transfer with AAV9-PHP. B rescues hearing in a mouse model of usher syndrome 3A and transduces hair cells in a non-human primate. Molecular Therapy-Methods & Clinical Development 2019; 13: 1-13.

Hartong DT, Berson EL, Dryja TP. Retinitis pigmentosa. The Lancet 2006; 368: 1795-809.

Hastings ML, Brigande JV. Fetal gene therapy and pharmacotherapy to treat congenital hearing loss and vestibular dysfunction. Hearing Research 2020; 394: 107931.

Hendrickson A, Hicks D. Distribution and Density of Medium- and Short-wavelength Selective Cones in the Domestic Pig Retina. Experimental Eye Research 2002; 74: 435-44.

Hood DC, Bach M, Brigell M, Keating D, Kondo M, Lyons JS, Marmor MF, McCulloch DL, Palmowski-Wolfe AM. ISCEV standard for clinical multifocal electroretinography (mfERG) (2011 edition). Documenta ophthalmologica 2012; 124: 1-13.

Huang D, Swanson EA, Lin CP, Schuman JS, Stinson WG, Chang W, Hee MR, Flotte T, Gregory K, Puliafito CA. Optical coherence tomography. Science 1991; 254: 1178-81.

Huckenpahler AL, Carroll J, Salmon AE, Sajdak BS, Mastey RR, Allen KP, Kaplan HJ, McCall MA. Noninvasive imaging and correlative histology of cone photoreceptor structure in the pig retina. Translational Vison Science & Technology 2019; 8: 38.

Isgrig K, Shteamer JW, Belyantseva IA, Drummond MC, Fitzgerald TS, Vijayakumar S, Jones SM, Griffith AJ, Friedman TB, Cunningham LL. Gene therapy restores balance and auditory functions in a mouse model of Usher syndrome. Molecular therapy 2017; 25: 780-91.

Jatana KR, Thomas D, Weber L, Mets MB, Silverman JB, Young NM. Usher syndrome: characteristics and outcomes of pediatric cochlear implant recipients. Otology & Neurotology 2013; 34: 484-9.

Johnson KR, Gagnon LH, Webb LS, Peters LL, Hawes NL, Chang B, Zheng QY. Mouse models of USH1C and DFNB18: phenotypic and molecular analyses of two new spontaneous mutations of the Ush1c gene. Human Molecular Genetics 2003; 12: 3075-86.

Klocek C, Nowicki J, Brudzisz B, Pabiańczyk M. Colour preferences in pigs. Scientific Annals of Polish Society of Animal Production 2016; 12: 123-9.

Kostic C, Lillico SG, Crippa SV, Grandchamp N, Pilet H, Philippe S, Lu Z, King TJ, Mallet J, Sarkis C. Rapid cohort generation and analysis of disease spectrum of large animal model of cone dystrophy. PloS one 2013; 8: e71363.

Kostic C, Arsenijevic Y. Animal modelling for inherited central vision loss. Journal of Pathology 2016; 238: 300-10.

Krawitz PM, Schiska D, Krüger U, Appelt S, Heinrich V, Parkhomchuk D, Timmermann B, Millan JM, Robinson PN, Mundlos S, Hecht J, Gross M. Screening for single nucleotide variants, small indels and exon deletions with a next-generation sequencing based gene panel approach for Usher syndrome. Molecular Genetics & Genomic Medicine 2014; 2: 393-401.

Kurome M, Kessler B, Wuensch A, Nagashima H, Wolf E. Nuclear transfer and transgenesis in the pig. In: Nuclear Reprogramming: Methods and Protocols. Beaujean N, Jammes H, Jouneau A, eds. New York, NY: Springer New York 2015: 37-59.

Lassota N, Kiilgaard JF, Prause JU, Qvortrup K, Scherfig E, la Cour M. Surgical induction of choroidal neovascularization in a porcine model. Graefe's Archive for Clinical and Experimental Ophthalmology 2007; 245: 1189-98.

Lefèvre G, Michel V, Weil D, Lepelletier L, Bizard E, Wolfrum U, Hardelin J-P, Petit C. A core cochlear phenotype in USH1 mouse mutants implicates fibrous links of the hair bundle in its cohesion, orientation and differential growth. Development 2008; 135: 1427-37.

LeMasurier M, Gillespie PG. Hair-cell mechanotransduction and cochlear amplification. Neuron 2005; 48: 403-15.

Lenassi E, Saihan Z, Cipriani V, Stabej PLQ, Moore AT, Luxon LM, Bitner-Glindzicz M, Webster AR. Natural history and retinal structure in patients with Usher syndrome type 1 owing to MYO7A mutation. Ophthalmology 2014; 121: 580-7.

Lentz JJ, Gordon WC, Farris HE, MacDonald GH, Cunningham DE, Robbins CA, Tempel BL, Bazan NG, Rubel EW, Oesterle EC. Deafness and retinal degeneration in a novel USH1C knock-in mouse model. Developmental neurobiology 2010; 70: 253-67.

Li SY, Yin ZQ, Chen SJ, Chen LF, Liu Y. Rescue from light-induced retinal degeneration by human fetal retinal transplantation in minipigs. Current Eye Research 2009; 34: 523-35.

Li ZY, Wong F, Chang JH, Possin DE, Hao Y, Petters RM, Milam AH. Rhodopsin transgenic pigs as a model for human retinitis pigmentosa. Investigative Ophthalmolgy & Visual Science 1998; 39: 808-19.

Lind NM, Vinther M, Hemmingsen RP, Hansen AK. Validation of a digital video tracking system for recording pig locomotor behaviour. Journal of Neuroscience Methods 2005; 143: 123-32.

Liu X, Ondek B, Williams DS. Mutant myosin VIIa causes defective melanosome distribution in the RPE of shaker-1 mice. Nature Genetics 1998; 19: 117-8.

Liu X, Bulgakov OV, Darrow KN, Pawlyk B, Adamian M, Liberman MC, Li T. Usherin is required for maintenance of retinal photoreceptors and normal development of cochlear hair cells. Proceedings of the National Academy of Sciences 2007; 104: 4413-8.

Lonborg-Moller H, Subhi Y, Kessel L. Living with Usher Syndrome: Patient and Physician Perspectives. Ophthalmology & Therapy 2020; 9: 1-6.

Lopes VS, Gibbs D, Libby RT, Aleman TS, Welch DL, Lillo C, Jacobson SG, Radu RA, Steel KP, Williams DS. The Usher 1B protein, MYO7A, is required for normal localization and function of the visual retinoid cycle enzyme, RPE65. Human Molecular Genetics 2011; 20: 2560-70.

Lopes VS, Boye SE, Louie CM, Boye S, Dyka F, Chiodo V, Fofo H, Hauswirth WW, Williams DS. Retinal gene therapy with a large MYO7A cDNA using adeno-associated virus. Gene therapy 2013; 20: 824-33.

Luo J, Ying K, Bai J. Savitzky–Golay smoothing and differentiation filter for even number data. Signal processing 2005; 85: 1429-34.

Maguire AM, Russell S, Wellman JA, Chung DC, Yu Z-F, Tillman A, Wittes J, Pappas J, Elci O, Marshall KA, McCague S, Reichert H, Davis M, Simonelli F, Leroy BP, Wright JF, High KA, Bennett J. Efficacy, safety, and durability of Voretigene Neparvovec-rzyl in RPE65 mutation–associated inherited retinal dystrophy: results of phase 1 and 3 trials. Ophthalmology 2019; 126: 1273-85.

Mahmoud TH, McCuen BW, Hao Y, Moon SJ, Tatebayashi M, Stinnett S, Petters RM, Wong F. Lensectomy and vitrectomy decrease the rate of photoreceptor loss in rhodopsin P347L transgenic pigs. Graefe's Archive for Clinical and Experimental Ophthalmology 2003; 241: 298-308.

Marmor MF, Hood DC, Keating D, Kondo M, Seeliger MW, Miyake Y. Guidelines for basic multifocal electroretinography (mfERG). Documenta ophthalmologica 2003; 106: 105-15.

Mathur P, Yang J. Usher syndrome: hearing loss, retinal degeneration and associated abnormalities. Biochimica et Biophysica Acta - Molecular Basis of Disease 2015; 1852: 406-20.

May-Simera H, Nagel-Wolfrum K, Wolfrum U. Cilia - The sensory antennae in the eye. Progress in Retinal and Eye Research 2017; 60: 144-80.

McCulloch DL, Marmor MF, Brigell MG, Hamilton R, Holder GE, Tzekov R, Bach M. ISCEV Standard for full-field clinical electroretinography (2015 update). Documenta ophthalmologica 2015; 130: 1-12.

McGill TJ, Wilson DJ, Stoddard J, Renner LM, Neuringer M. Cell transplantation for retinal degeneration: transition from rodent to nonhuman primate models. Advances in Experimental Medicine and Biology 2018; 1074: 641-7.

McLean DJ, Skowron Volponi MA. trajr: An R package for characterisation of animal trajectories. Ethology 2018; 124: 440-8.

McLeman MA, Mendl MT, Jones RB, Wathes CM. Social discrimination of familiar conspecifics by juvenile pigs, Sus scrofa: Development of a non-invasive method to study the transmission of unimodal and bimodal cues between live stimuli. Applied Animal Behaviour Science 2008; 115: 123-37.

Michalski N, Michel V, Caberlotto E, Lefèvre GM, van Aken AF, Tinevez JY, Bizard E, Houbron C, Weil D, Hardelin JP, Richardson GP, Kros CJ, Martin P, Petit C. Harmonin-b, an actin-binding scaffold protein, is involved in the adaptation of mechanoelectrical transduction by sensory hair cells. Pflugers Archive - European Journal of Physiology 2009; 459: 115-30.

Middleton S. Porcine ophthalmology. Veterinary Clinics of North America: Food Animal Practice 2010; 26: 557-72.

Moller CG, Kimberling WJ, Davenport SL, Priluck I, White V, Biscone-Halterman K, Odkvist LM, Brookhouser PE, Lund G, Grissom TJ. Usher syndrome: an otoneurologic study. Laryngoscope 1989; 99: 73-9.

Mönck HJ, Jörg A, von Falkenhausen T, Tanke J, Wild B, Dormagen D, Piotrowski J, Winklmayr C, Bierbach D, Landgraf T. BioTracker: An open-source computer vision framework for visual animal tracking. arXiv e-prints 2018: arXiv: 1803.07985.

Monés J, Leiva M, Peña T, Martínez G, Biarnés M, Garcia M, Serrano A, Fernandez E. A swine model of selective geographic atrophy of outer retinal layers mimicking atrophic AMD: A phase I escalating dose of subretinal sodium iodate. Investigative Ophthalmology & Visual Science 2016; 57: 3974-83.

NCBI. N-terminal protein-binding module of harmonin and similar domains, also known as HHD (harmonin homology domain). Conserved Domain Database: https://www.ncbi.nlm.nih.gov/Structure/cdd/cddsrv.cgi?uid=259818. Accessed March 3, 2021.

NCBI. USH1 protein network component harmonin [Homo sapiens (human)]. GenBank: https://www.ncbi.nlm.nih.gov/gene/10083. Accessed March 3, 2021.

Neitz J, Jacobs GH. Spectral sensitivity of cones in an ungulate. Visual neuroscience 1989; 2: 97-100.

Noel JM, Fernandez de Castro JP, Demarco PJ, Jr., Franco LM, Wang W, Vukmanic EV, Peng X, Sandell JH, Scott PA, Kaplan HJ, McCall MA. Iodoacetic acid, but not sodium iodate, creates an inducible swine model of photoreceptor damage. Experimental Eye Research 2012; 97: 137-47.

Noell WK. Experimentally induced toxic effects on structure and function of visual cells and pigment epithelium. American Journal of Ophthalmology 1953; 36: 103-16.

Noldus LPJJ, Spink AJ, Tegelenbosch RAJ. EthoVision: A versatile video tracking system for automation of behavioral experiments. Behavior Research Methods, Instruments, & Computers 2001; 33: 398-414.

Ollivier FJ, Samuelson DA, Brooks DE, Lewis PA, Kallberg ME, Komáromy AM. Comparative morphology of the tapetum lucidum (among selected species). Veterinary Ophthalmology 2004; 7: 11-22.

OMIM Johns Hopkins University B, MD. USH1 protein network component harmonin; USH1C. June 6, 2020: https://omim.org/entry/605242?search=harmonin&highlight=harmonin. Accessed March 3, 2021.

Ouyang XM, Yan D, Du LL, Hejtmancik JF, Jacobson SG, Nance WE, Li AR, Angeli S, Kaiser M, Newton V. Characterization of Usher syndrome type I gene mutations in an Usher syndrome patient population. Human genetics 2005; 116: 292-9.

Overlack N, Goldmann T, Wolfrum U, Nagel-Wolfrum K. Gene repair of an Usher syndrome causing mutation by zinc-finger nuclease mediated homologous recombination. Investigative Ophthalmology & Visual Science 2012; 53: 4140-6.

Pan B, Askew C, Galvin A, Heman-Ackah S, Asai Y, Indzhykulian AA, Jodelka FM, Hastings ML, Lentz JJ, Vandenberghe LH. Gene therapy restores auditory and vestibular function in a mouse model of Usher syndrome type 1c. Nature biotechnology 2017; 35: 264.

Patel N, Urias M, Ebrahimi A, He C, Gehlbach P, Iordachita I. Sclera force evaluation during vitreoretinal surgeries in ex vivo porcine eye model. Proceedings of IEEE Sensors 2019; 2019: 1-4.

Pearson R, Barber A, Rizzi M, Hippert C, Xue T, West E, Duran Y, Smith A, Chuang J, Azam S. Restoration of vision after transplantation of photoreceptors. Nature 2012; 485: 99-103.

Peng YW, Zallocchi M, Wang WM, Delimont D, Cosgrove D. Moderate light-induced degeneration of rod photoreceptors with delayed transducin translocation in shaker1 mice. Investigative Ophthalmology & Visual Science 2011; 52: 6421-7.

Perleberg C, Kind A, Schnieke A. Genetically engineered pigs as models for human disease. Disease models & mechanisms 2018; 11: 1-12.

Petters RM, Alexander CA, Wells KD, Collins EB, Sommer JR, Blanton MR, Rojas G, Hao Y, Flowers WL, Banin E, Cideciyan AV, Jacobson SG, Wong F. Genetically engineered large animal model for studying cone photoreceptor survival and degeneration in retinitis pigmentosa. Nature biotechnology 1997; 15:

965-70.

Phillips JB, Blanco-Sanchez B, Lentz JJ, Tallafuss A, Khanobdee K, Sampath S, Jacobs ZG, Han PF, Mishra M, Titus TA. Harmonin (Ush1c) is required in zebrafish Müller glial cells for photoreceptor synaptic development and function. Disease models & mechanisms 2011; 4: 786-800.

Pietola L, Aarnisalo AA, Abdel-Rahman A, Västinsalo H, Isosomppi J, Löppönen H, Kentala E, Johansson R, Valtonen H, Vasama J-P, Sankila E-M, Jero J. Speech recognition and communication outcomes with cochlear implantation in Usher syndrome type 3. Otology & Neurotology 2012; 33: 38-41.

Plog S, Klymiuk N, Binder S, Van Hook MJ, Thoreson WB, Gruber AD, Mundhenk L. Naturally occurring deletion mutants of the pig-specific, intestinal crypt epithelial cell protein CLCA4b without apparent phenotype. PloS one 2015; 10: e0140050.

Reiners J, van Wijk E, Märker T, Zimmermann U, Jürgens K, te Brinke H, Overlack N, Roepman R, Knipper M, Kremer H, Wolfrum U. Scaffold protein harmonin (USH1C) provides molecular links between Usher syndrome type 1 and type 2. Human Molecular Genetics 2005; 14: 3933-43.

Reiners J, Nagel-Wolfrum K, Jürgens K, Märker T, Wolfrum U. Molecular basis of human Usher syndrome: Deciphering the meshes of the Usher protein network provides insights into the pathomechanisms of the Usher disease. Experimental Eye Research 2006; 83: 97-119.

Richter A, Kurome M, Kessler B, Zakhartchenko V, Klymiuk N, Nagashima H, Wolf E, Wuensch A. Potential of primary kidney cells for somatic cell nuclear transfer mediated transgenesis in pig. BMC Biotechnology 2012; 12: 1-14.

Roborel de Climens A, Tugaut B, Piscopo A, Arnould B, Buggage R, Brun-Strang C. Living with type I Usher syndrome: insights from patients and their parents. Ophthalmic Genetics 2020; 41: 240-51.

Rosolen SG, Rigaudiere F, Saint-Macary G, Lachapelle P. Recording the photopic electroretinogram from conscious adult Yucatan micropigs. Documenta ophthalmologica 1999; 98: 197-205.

Ross JW, Fernandez de Castro JP, Zhao J, Samuel M, Walters E, Rios C, Bray-Ward P, Jones BW, Marc RE, Wang W, Zhou L, Noel JM, McCall MA, DeMarco PJ, Prather RS, Kaplan HJ. Generation of an inbred miniature pig model of retinitis pigmentosa. Investigative Ophthalmology & Visual Science 2012; 53: 501-7.

Ruiz-Ederra J, García M, Hernández M, Urcola H, Hernández-Barbáchano E, Araiz J, Vecino E. The pig eye as a novel model of glaucoma. Experimental Eye Research 2005; 81: 561-9.

Sadeghi AM, Eriksson K, Kimberling WJ, Sjöström A, Möller C. Longterm visual prognosis in Usher syndrome types 1 and 2. Acta Ophthalmologica Scandinavica 2006; 84: 537-44.

Sahly I, Dufour E, Schietroma C, Michel V, Bahloul A, Perfettini I, Pepermans E, Estivalet A, Carette D, Aghaie A. Localization of Usher 1 proteins to the photoreceptor calyceal processes, which are absent from mice. Journal of Cell Biology 2012; 199: 381-99.

Sanchez I, Martin R, Ussa F, Fernandez-Bueno I. The parameters of the porcine eyeball. Graefe's Archive for Clinical and Experimental Ophthalmology 2011; 249: 475-82.

Savitzky A, Golay MJ. Smoothing and differentiation of data by simplified least squares procedures. Analytical chemistry 1964; 36: 1627-39.

Scanlan MJ, Williamson B, Jungbluth A, Stockert E, Arden KC, Viars CS, Gure AO, Gordan JD, Chen Y-T, Old LJ. Isoforms of the human PDZ-73 protein exhibit differential tissue expression. Biochimica et Biophysica Acta 1999; 1445: 39-52.

Schietroma C, Parain K, Estivalet A, Aghaie A, Boutet de Monvel J, Picaud S, Sahel J-A, Perron M, El-Amraoui A, Petit C. Usher syndrome type 1–associated cadherins shape the photoreceptor outer segment. Journal of Cell Biology 2017; 216: 1849-64.

Schramke S, Schuldenzucker V, Schubert R, Frank F, Wirsig M, Ott S, Motlik J, Fels M, Kemper N, Hölzner E. Behavioral phenotyping of minipigs transgenic for the Huntington gene. Journal of Neuroscience Methods 2016; 265: 34-45.

Schuldenzucker V, Schubert R, Muratori LM, Freisfeld F, Rieke L, Matheis T, Schramke S, Motlik J, Kemper N, Radespiel U. Behavioral testing of minipigs transgenic for the Huntington gene - A three-year observational study. PloS one 2017; 12: e0185970.

Scott PA, Kaplan HJ, Sandell JH. Anatomical evidence of photoreceptor degeneration induced by iodoacetic acid in the porcine eye. Experimental Eye Research 2011; 93: 513-27.

Seeliger M, Pfister M, Gendo K, Paasch S, Apfelstedt-Sylla E, Plinkert P, Zenner H-P, Zrenner E. Comparative study of visual, auditory, and olfactory function in Usher syndrome. Graefe's Archive for Clinical and Experimental Ophthalmology 1999; 237: 301-7.

Seeliger MW, Fischer MD, Pfister M. Usher syndrome: clinical features, diagnostic options, and therapeutic prospects. Der Ophthalmologe 2009; 106: 505-11.

Sommer JR, Estrada JL, Collins EB, Bedell M, Alexander CA, Yang Z, Hughes G, Mir B, Gilger BC, Grob S, Wei X, Piedrahita JA, Shaw PX, Petters RM, Zhang K. Production of ELOVL4 transgenic pigs: a large animal model for Stargardt-like macular degeneration. British Journal of Ophthalmology 2011; 95: 1749-54.

Sridhar VH, Roche DG, Gingins S. Tracktor: Image-based automated tracking of animal movement and behaviour. Methods in Ecology and Evolution 2019; 10:

815-20.

Stingl K, Kurtenbach A, Hahn G, Kernstock C, Hipp S, Zobor D, Kohl S, Bonnet C, Mohand-Saïd S, Audo I. Full-field electroretinography, visual acuity and visual fields in Usher syndrome: a multicentre European study. Documenta ophthalmologica 2019; 139: 151-60.

Sugiura T, Kurosaka D, Uezuki Y, Eguchi S, Obata H, Takahashi T. Creating cataract in a pig eye. Journal of Cataract & Refractive Surgery 1999; 25: 615-21.

Szlyk JP, Fishman GA, Alexander KR, Revelins BI, Derlacki DJ, Anderson RJ. Relationship between difficulty in performing daily activities and clinical measures of visual function in patients with retinitis pigmentosa. Archives of ophthalmology 1997; 115: 53-9.

Tanaka T, Murayama Y, Eguchi Y, Yoshimoto T. Studies on the visual acuity of pigs using shape discrimination learning. Animal Science and Technology (Japan) 1998; 69: 260-6.

Tanida H, Senda K, Suzuki S, Tanaka T, Yoshimoto T, Gakkaiho NC. Color Discrimination in Weanling Pigs. Animal Science and Technology (Japan) 1991; 62: 1029-34.

Tanskanen P, Kylmä T, Kommonen B, Karhunen U. Propofol influences the electroretinogram to a lesser degree than thiopentone. Acta anaesthesiologica scandinavica 1996; 40: 480-5.

Terrell D, Comander J. Current stem-cell approaches for the treatment of inherited retinal degenerations. Seminars in Ophthalmology 2019; 34: 287-92.

Tian C, Liu XZ, Han F, Yu H, Longo-Guess C, Yang B, Lu C, Yan D, Zheng QY. Ush1c gene expression levels in the ear and eye suggest different roles for Ush1c in neurosensory organs in a new Ush1c knockout mouse. Brain Research 2010;

1328: 57-70.

Tian M, Wang W, Delimont D, Cheung L, Zallocchi M, Cosgrove D, Peng YW. Photoreceptors in whirler mice show defective transducin translocation and are susceptible to short-term light/dark changes-induced degeneration. Experimental Eye Research 2014; 118: 145-53.

Toms M, Bitner-Glindzicz M, Webster A, Moosajee M. Usher syndrome: a review of the clinical phenotype, genes and therapeutic strategies. Expert Review of Ophthalmology 2015; 10: 241-56.

Toms M, Pagarkar W, Moosajee M. Usher syndrome: clinical features, molecular genetics and advancing therapeutics. Therapeutic Advances in Ophthalmology 2020a; 12: 2515841420952194.

Toms M, Dubis AM, de Vrieze E, Tracey-White D, Mitsios A, Hayes M, Broekman S, Baxendale S, Utoomprurkporn N, Bamiou D, Bitner-Glindzicz M, Webster AR, Van Wijk E, Moosajee M. Clinical and preclinical therapeutic outcome metrics for USH2A-related disease. Human Molecular Genetics 2020b; 29: 1882-99.

Tran J, Craven C, Wabner K, Schmit J, Matter B, Kompella U, Grossniklaus HE, Olsen TW. A pharmacodynamic analysis of choroidal veovascularization in a porcine model using three targeted drugs. Investigative Ophthalmology & Visual Science 2017; 58: 3732-40.

Trapani I, Perota A, Tiberi P, Colecchi L, Lagutina I, Duchi R, Lazzari G, Gesualdo C, Rossi S, Testa F, Simonelli F, Auricchio A, Galli C. Somatic or germline ABCA4 editing to generate a pig model of Stargardt disease type 1. Investigative Ophthalmology & Visual Science 2019; 60: 4230.

Tsang SH, Sharma T. Optical coherence tomography. In: Atlas of Inherited Retinal Diseases. Advances in Experimental Medicine and Biology, vol 1085. Tsang SH, Sharma T, eds. Cham: Springer 2018a: 11-3.

Tsang SH, Sharma T. Electroretinography. In: Atlas of Inherited Retinal Diseases. Advances in Experimental Medicine and Biology, vol 1085. Tsang SH, Sharma T, eds. Cham: Springer 2018b: 17-20.

Usher CH. On the inheritance of retinitis pigmentosa; with note of cases. The Royal London Opthalmic Hospital Reports 1914; 19: 130-236.

v. Graefe A. Vereinzelte Beobachtungen und Bemerkungen. Archiv für Ophthalmologie 1858; 4: 211-76.

Verpy E, Leibovici M, Zwaenepoel I, Liu X-Z, Gal A, Salem N, Mansour A, Blanchard S, Kobayashi I, Keats BJB, Slim R, Petit C. A defect in harmonin, a PDZ domain-containing protein expressed in the inner ear sensory hair cells, underlies Usher syndrome type 1C. Nature Genetics 2000; 26: 51-5.

Vochozkova P, Simmet K, Jemiller E-M, Wünsch A, Klymiuk N. Gene Editing in Primary Cells of Cattle and Pig. In: CRISPR Gene Editing. Methods in Molecular Biology, vol 1961. Luo Y, ed. New York, NY: Springer 2019: 271-89.

Voss Kyhn M, Kiilgaard JF, Lopez AG, Scherfig E, Prause JU, La Cour M. The multifocal electroretinogram (mfERG) in the pig. Acta Ophthalmologica Scandinavica 2007; 85: 438-44.

Wang L, Kempton JB, Jiang H, Jodelka FM, Brigande AM, Dumont RA, Rigo F, Lentz JJ, Hastings ML, Brigande JV. Fetal antisense oligonucleotide therapy for congenital deafness and vestibular dysfunction. Nucleic Acids Research 2020; 48: 5065-80.

Wang W, Fernandez de Castro J, Vukmanic E, Zhou L, Emery D, Demarco PJ, Kaplan HJ, Dean DC. Selective rod degeneration and partial cone inactivation characterize an iodoacetic acid model of Swine retinal degeneration. Investigative Ophthalmology & Visual Science 2011; 52: 7917-23.

Williams DS. Usher syndrome: Animal models, retinal function of Usher proteins, and prospects for gene therapy. Vision research 2008; 48: 433-41.

Winkler BS, Sauer MW, Starnes CA. Modulation of the Pasteur effect in retinal cells: implications for understanding compensatory metabolic mechanisms. Experimental Eye Research 2003; 76: 715-23.

Wondrak M, Conzelmann E, Veit A, Huber L. Pigs (Sus scrofa domesticus) categorize pictures of human heads. Applied Animal Behaviour Science 2018; 205: 19-27.

Yu-Wai-Man P, Newman NJ, Carelli V, Moster ML, Biousse V, Sadun AA, Klopstock T, Vignal-Clermont C, Sergott RC, Rudolph G. Bilateral visual improvement with unilateral gene therapy injection for Leber hereditary optic neuropathy. Science translational medicine 2020; 12: eaaz7423.

Yu W, Wu Z. Ocular delivery of CRISPR/Cas genome editing components for treatment of eye diseases. Advanced Drug Delivery Reviews 2020; 168: 181-95.

Zallocchi M, Binley K, Lad Y, Ellis S, Widdowson P, Iqball S, Scripps V, Kelleher M, Loader J, Miskin J. EIAV-based retinal gene therapy in the shaker1 mouse model for usher syndrome type 1B: development of UshStat. PloS one 2014; 9: e94272.

Zonderland JJ, Cornelissen L, Wolthuis-Fillerup M, Spoolder H. Visual acuity of pigs at different light intensities. Applied Animal Behaviour Science 2008; 111: 28-37.

Zou J, Luo L, Shen Z, Chiodo VA, Ambati BK, Hauswirth WW, Yang J. Whirlin replacement restores the formation of the USH2 protein complex in whirlin knockout photoreceptors. Investigative Ophthalmology & Visual Science 2011; 52: 2343-51.

Zuker M. Mfold web server for nucleic acid folding and hybridization prediction. Nucleic Acids Research 2003; 31: 3406-15.

Zwaenepoel I, Verpy E, Blanchard S, Meins M, Apfelstedt-Sylla E, Gal A, Petit C. Identification of three novel mutations in the USH1C gene and detection of thirty-one polymorphisms used for haplotype analysis. Human mutation 2001; 17: 34-41.

XI. APPENDIX

a	WT					USH1C				
pig	1	2	3	4	5	6	7	8	9	10
time light	11.3	12.5	11.0	13.3	12.4	18.4	17.9	13.0	19.9	14.6
time dark	14.8	12.8	16.1	11.4	13.9	16.8	17.6	12.1	14.3	15.1

b

test day	course setup	WT light	USH1C light
1	1	11.9	13.7
2	1	13.6	18.3
3	1	10.9	16.4
4	2	13.4	16.4
5	3	12.1	18.5
6	4	9.5	27.8
7	5	10.0	23.6
8	6	8.6	11.9
9	7	6.7	11.9
10	8	9.4	13.9
11	9	15.4	21.1
12	10	17.4	21.6
13	10	12.5	15.0
15	12	17.5	12.1
16	13	15.0	16.3
17	14	12.1	17.8
20	17	11.7	14.4
22	19	11.3	11.3
23	20	12.9	21.6
24	21	10.6	12.0
26	21	13.4	9.7
28	21	9.7	11.3

c

test day	course setup	WT dark	USH1C dark
14	11	21.9	24.3
18	15	11.8	13.0
19	16	9.0	14.3
21	18	15.0	12.4
25	21	13.8	10.1
27	21	10.0	12.2

Supplementary Table 1: Mean time. Mean time in seconds of each pig averaged over all test days in light and dark condition (a), mean time in seconds of each test day averaged over all pigs in one group in light condition (b), mean time in seconds of each test day averaged over all pigs in one group in dark condition (c).

a	WT					USH1C				
pig	1	2	3	4	5	6	7	8	9	10
contacts light	1.33	1.26	0.74	0.95	1.33	3.47	3.53	1.68	2.94	2.19
contacts dark	1.80	1.50	1.40	0.67	1.33	2.17	3.25	1.67	2.17	2.00

b

test day	course setup	WT light	USH1C light
1	1	0.50	1.33
2	1	0.40	2.75
3	1	0.80	1.75
4	2	1.40	3.40
5	3	2.00	1.25
6	4	1.25	4.00
7	5	1.40	5.60
8	6	0.00	0.60
9	7	0.20	2.25
10	8	0.75	2.80
11	9	1.50	5.25
12	10	1.00	2.75
13	10	1.00	2.00
15	12	2.60	2.40
16	13	2.40	4.40
17	14	1.60	2.20
20	17	1.00	2.25
22	19	0.75	2.00
23	20	2.00	3.67
24	21	1.20	2.67
26	21	0.40	1.50
28	21	0.25	0.33

c

test day	course setup	WT dark	USH1C dark
14	11	3.40	3.80
18	15	1.20	1.80
19	16	0.80	2.60
21	18	0.80	1.00
25	21	0.75	1.67
27	21	0.75	1.67

Supplementary Table 2: Mean contacts. Mean snout contacts of each pig averaged over all test days and all obstacles in light and dark conditions (a), mean snout contacts of each test day averaged over all obstacles and all pigs of one group in light condition (b), mean snout contacts of each test day averaged over all obstacles and all pigs of one group in dark condition (c).

a

contacts in total		obstacle 1 (contacts counted singly)	obstacle 1 (actual contacts)	obstacle 1 (worst case contacts)	obstacle 1 (0 contacts)	obstacle 1 (1 contact)	obstacle 1 (2 contacts)	obstacle 1 (3 contacts)	obstacle 1 (4 contacts)
WT	light	18	20	91	73	16	2	0	0
USH1C	light	45	66	80	35	27	15	3	0
WT	dark	8	9	28	20	7	1	0	0
USH1C	dark	18	21	25	7	15	3	0	0

b

contacts in total		obstacle 2 (contacts counted singly)	obstacle 2 (actual contacts)	obstacle 2 (worst case contacts)	obstacle 2 (0 contacts)	obstacle 2 (1 contact)	obstacle 2 (2 contacts)	obstacle 2 (3 contacts)	obstacle 2 (4 contacts)
WT	light	28	28	91	63	28	0	0	0
USH1C	light	36	50	80	44	24	10	2	0
WT	dark	9	12	28	19	6	3	0	0
USH1C	dark	14	21	25	11	8	5	1	0

c

contacts in total		obstacle 3 (contacts counted singly)	obstacle 3 (actual contacts)	obstacle 3 (worst case contacts)	obstacle 3 (0 contacts)	obstacle 3 (1 contact)	obstacle 3 (2 contacts)	obstacle 3 (3 contacts)	obstacle 3 (4 contacts)
WT	light	24	34	56	32	17	5	1	1
USH1C	light	29	48	44	15	16	7	6	0
WT	dark	7	8	23	16	6	1	0	0
USH1C	dark	4	5	20	16	3	1	0	0

d

contacts in total		obstacle 4 (contacts counted singly)	obstacle 4 (actual contacts)	obstacle 4 (worst case contacts)	obstacle 4 (0 contacts)	obstacle 4 (1 contact)	obstacle 4 (2 contacts)	obstacle 4 (3 contacts)	obstacle 4 (4 contacts)
WT	light	3	3	74	71	3	0	0	0
USH1C	light	15	16	70	55	14	1	0	0
WT	dark	0	0	10	10	0	0	0	0
USH1C	dark	0	0	9	9	0	0	0	0

e

contacts in total		obstacle 5 (contacts counted singly)	obstacle 5 (actual contacts)	obstacle 5 (worst case contacts)	obstacle 5 (0 contacts)	obstacle 5 (1 contact)	obstacle 5 (2 contacts)	obstacle 5 (3 contacts)	obstacle 5 (4 contacts)
WT	light	5	5	5	0	5	0	0	0
USH1C	light	1	1	4	3	1	0	0	0
WT	dark			0					
USH1C	dark			0					

f

contacts in total		obstacle 6 (contacts counted singly)	obstacle 6 (actual contacts)	obstacle 6 (worst case contacts)	obstacle 6 (0 contacts)	obstacle 6 (1 contact)	obstacle 5 (2 contacts)	obstacle 6 (3 contacts)	obstacle 6 (4 contacts)
WT	light	4	4	4	0	4	0	0	0
USH1C	light	5	9	5	0	1	4	0	0
WT	dark			0					
USH1C	dark			0					

g

contacts in total		obstacle 7 (contacts counted singly)	obstacle 7 (actual contacts)	obstacle 7 (worst case contacts)	obstacle 7 (0 contacts)	obstacle 7 (1 contact)	obstacle 7 (2 contacts)	obstacle 7 (3 contacts)	obstacle 7 (4 contacts)
WT	light	4	5	51	47	3	1	0	0
USH1C	light	13	13	44	31	13	0	0	0
WT	dark	8	8	28	20	8	0	0	0
USH1C	dark	5	5	26	21	5	0	0	0

h

contacts in total		obstacle 8 (contacts counted singly)	obstacle 8 (actual contacts)	obstacle 8 (worst case contacts)	obstacle 8 (0 contacts)	obstacle 8 (1 contact)	obstacle 8 (2 contacts)	obstacle 8 (3 contacts)	obstacle 8 (4 contacts)
WT	light	6	6	14	8	6	0	0	0
USH1C	light	11	14	15	4	9	1	1	0
WT	dark			0					
USH1C	dark			0					

i

contacts in total		obstacle 9 (contacts counted singly)	obstacle 9 (actual contacts)	obstacle 9 (worst case contacts)	obstacle 9 (0 contacts)	obstacle 9 (1 contact)	obstacle 9 (2 contacts)	obstacle 9 (3 contacts)	obstacle 9 (4 contacts)
WT	light	0	0	5	5	0	0	0	0
USH1C	light	1	1	5	4	1	0	0	0
WT	dark			0					
USH1C	dark			0					

j

contacts in total		obstacle 10 (contacts counted singly)	obstacle 10 (actual contacts)	obstacle 10 (worst case contacts)	obstacle 10 (0 contacts)	obstacle 10 (1 contact)	obstacle 10 (2 contacts)	obstacle 10 (3 contacts)	obstacle 10 (4 contacts)
WT	light	0	0	5	5	0	0	0	0
USH1C	light	3	3	4	1	3	0	0	0
WT	dark			0					
USH1C	dark			0					

k

contacts in total		obstacle 11 (contacts counted singly)	obstacle 11 (actual contacts)	obstacle 11 (worst case contacts)	obstacle 11 (0 contacts)	obstacle 11 (1 contact)	obstacle 11 (2 contacts)	obstacle 11 (3 contacts)	obstacle 11 (4 contacts)
WT	light	1	1	5	4	1	0	0	0
USH1C	light	4	6	4	0	2	2	0	0
WT	dark			0					
USH1C	dark			0					

l

contacts in total		wall (contacts counted singly)	wall (actual contacts)	wall (worst case contacts)	wall (0 contacts)	wall (1 contact)	wall (2 contacts)	wall (3 contacts)	wall (4 contacts)
WT	light	8	8	101	93	8	0	0	0
USH1C	light	12	14	89	77	10	2	0	0
WT	dark	0	0	28	28	0	0	0	0
USH1C	dark	2	3	25	23	1	1	0	0

m

obstacle		1	2	3	4	5	6
WT	light	0.22	0.31	0.61	0.04	1.00	1.00
USH1C	light	0.83	0.63	1.09	0.23	0.25	1.80
WT	dark	0.32	0.43	0.35	0.00		
USH1C	dark	0.84	0.84	0.25	0.00		

obstacle		7	8	9	10	11	wall
WT	light	0.10	0.43	0.00	0.00	0.20	0.08
USH1C	light	0.30	0.93	0.20	0.75	1.50	0.16
WT	dark	0.29					0.00
USH1C	dark	0.19					0.12

Supplementary Table 3: Contacts in detail for every used obstacle. Sometimes a pig touched one obstacle more than once. Tables show how often each obstacle has been touched not at all (“0 contacts“), once (“1 contact“), twice (“2 contacts“), three times (“3 contacts“) or four times (“4 contacts“) in total. The contacts of all test days and all pigs of one group were added up. The number “contacts counted

singly“ tells how often the obstacle has been touched ignoring repeated touches, e.g. if one pig has touched the obstacle three times, this is just counted as one touch. The number “actual contacts“ tells how often an obstacle has been actually touched, e.g. if one pig has touched the obstacle three times, this is also counted as three touches. The number “worst case touches“ tells how often an obstacle could have been touched, if every pig would have touched every obstacle once every test day (a – l). Table shows the relation actual contacts – worst case contacts (m).

XII. ACKNOWLEDGEMENTS

First, I would like to thank Prof. Dr. Eckhard Wolf for the opportunity to do my doctoral thesis at the Chair of Molecular Animal Breeding and Biotechnology, LMU Munich.

Next, sincerest thanks to my mentor Prof. Dr. Nikolai Klymiuk, for his patient support, scientific suggestions, and excellent guidance.

I also want to thank Prof. Jan Motlik and his team of IAPG Libechov for scientific exchange and successfully breeding first USH1C pigs. Thank you also to Prof. Dr. Uwe Wolfrum, Prof. Dr. Dominik Fischer, Prof. Dr. Andrea Fischer, PD Dr. Andreas Parzefall, and Dr. Andrea Bähr for collaboration on the Usher pig project.

Thank you to Prof. Dr. Michael Erhard, PD Dr. Dorothea Döring, and Dr. Dorian Patzkéwitsch of Institute for Animal Welfare, Ethology and Animal Hygiene, LMU, for their advice with behavioral tests. I am also thankful to Dr. Gianluca Santamaria and PD Dr. Wolfgang Hitzl for supporting data evaluation.

A big thank you to all colleagues and personnel working at Moorversuchsgut. Special thanks to Georg, Barbara, Arne, Simone, and Silja for their help to conduct the obstacle course, to animal caretakers for their help in the stable and to technical assistants for their help in lab. Thank you also to my fellow doctoral students, Steffi, Melli, Lina, Flo, Petra, Claudi, Michi, Andreas, Lisa, Nadja, and Jessica for all your help, discussions and nice coffee breaks. I especially want to thank Hannah, I really enjoyed working on the Usher pig project with you, thanks for your help and for listening to my problems.

Finally, I want to thank all my friends and family for always being there for me.